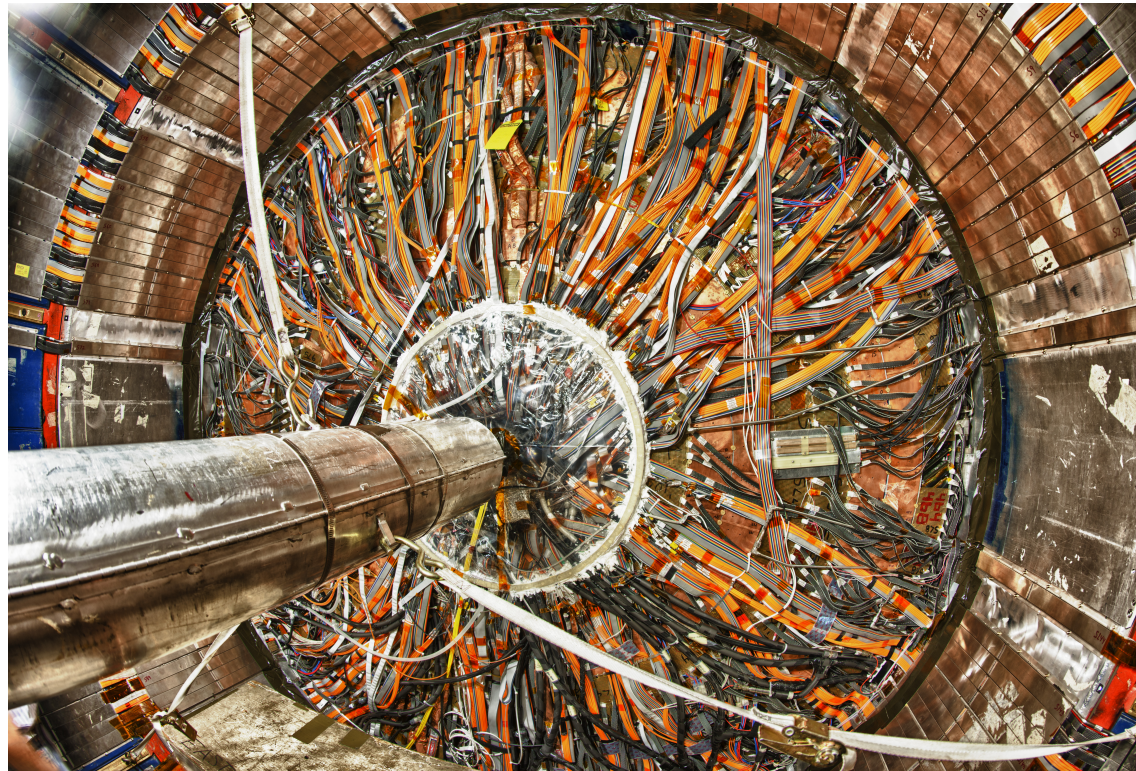# High-Precision Measurement of the
W Boson Mass with the CDF II Detector

Ashutosh Kotwal
Duke University

For the CDF Collaboration

Joint Theoretical-Experimental Physics Seminar
Fermilab, April 8, 2022

Outline

- Motivation

- Analysis Strategy

- Experimental Apparatus and Data Samples

- Analysis Techniques

- GEANT Detector Studies

- Custom Simulation and Fitting

- Studies and calibrations with data

- Results and Systematic Uncertainties

- Conclusions

Motivation for Precision Measurements

- The electroweak gauge sector of the standard model is constrained by precisely known parameters

  - $\alpha_{EM}(M_Z) = 1 / 127.918(18)$

  - $G_F = 1.16637\,(1) \times 10^{-5}\ GeV^{-2}$

  - $M_Z = 91.1876\,(21)\ GeV$

  - $m_{top} = 172.89\,(59)\ GeV$

  - $M_H = 125.25\,(17)\ GeV$

- At tree-level, these parameters are related to M_W

  - $M_W^2 = \pi \alpha_{EM} / \sqrt{2} G_F \sin^2\vartheta_W$

    - Where ϑ_W is the Weinberg mixing angle, defined by

      $$\cos\vartheta_W = M_W/M_Z$$

Motivation for Precision Measurements

- Radiative corrections due to heavy quark and Higgs loops and (potentially) undiscovered particles
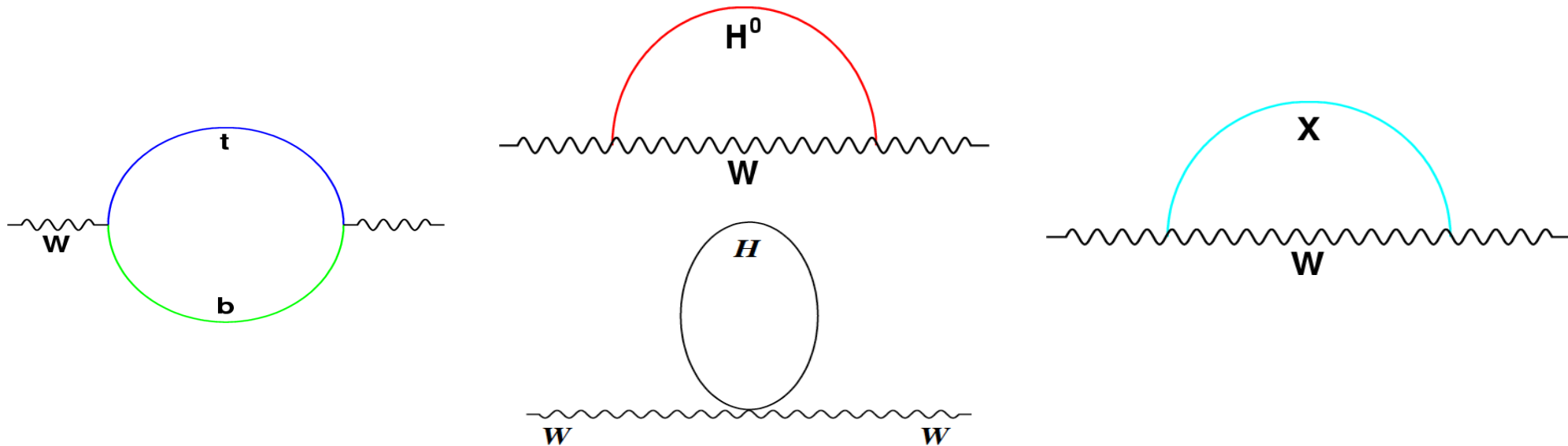
Motivate the introduction of the ρ parameter: $M_W^2 = \rho \, [M_W(\text{tree})]^2$
with the predictions $\Delta\rho = (\rho-1) \sim M_{\text{top}}^2$ and $\Delta\rho \sim \ln M_H$

Motivation for Precision Measurements

- The mass of the W boson is tightly constrained by the symmetries of the standard model, in conjunction with M_{top} and M_{Higgs}

    - The Higgs boson was the last missing component of the model

    - Following the observation of the Higgs boson, a measurement of the W-boson mass provides a stringent test of the model

- The W boson mass is presently constrained by SM global fits to a relative precision of 0.01%

    - provides a strong motivation to test the SM by measuring the mass to the same level of precision

    - SM expectation $M_W = 80{,}357 \pm 4_{inputs} \pm 4_{theory}$ MeV

    - Inputs include Z- and Higgs boson and top-quark masses, EM coupling and muon lifetime measurements

Beyond-SM Modifications to Expected M_W

- Hypotheses to provide a deeper explanation of the Higgs field, its potential and the Higgs boson, include

  - Supersymmetry

  - Compositeness

  - New strong interactions

  - Extended Higgs sector

- Hypothetical sources of particulate dark matter
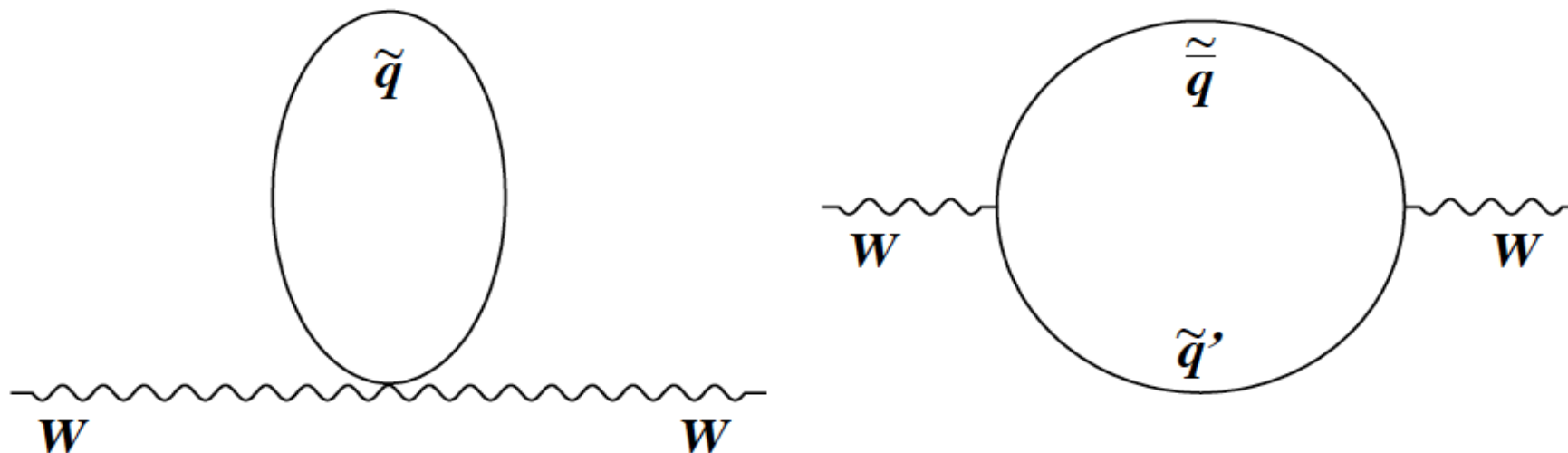
- Extended gauge sector

Single Scalar Extension of Higgs Sector

Inclusion of an additional scalar particle with no SM charges, which mixes with the Higgs boson
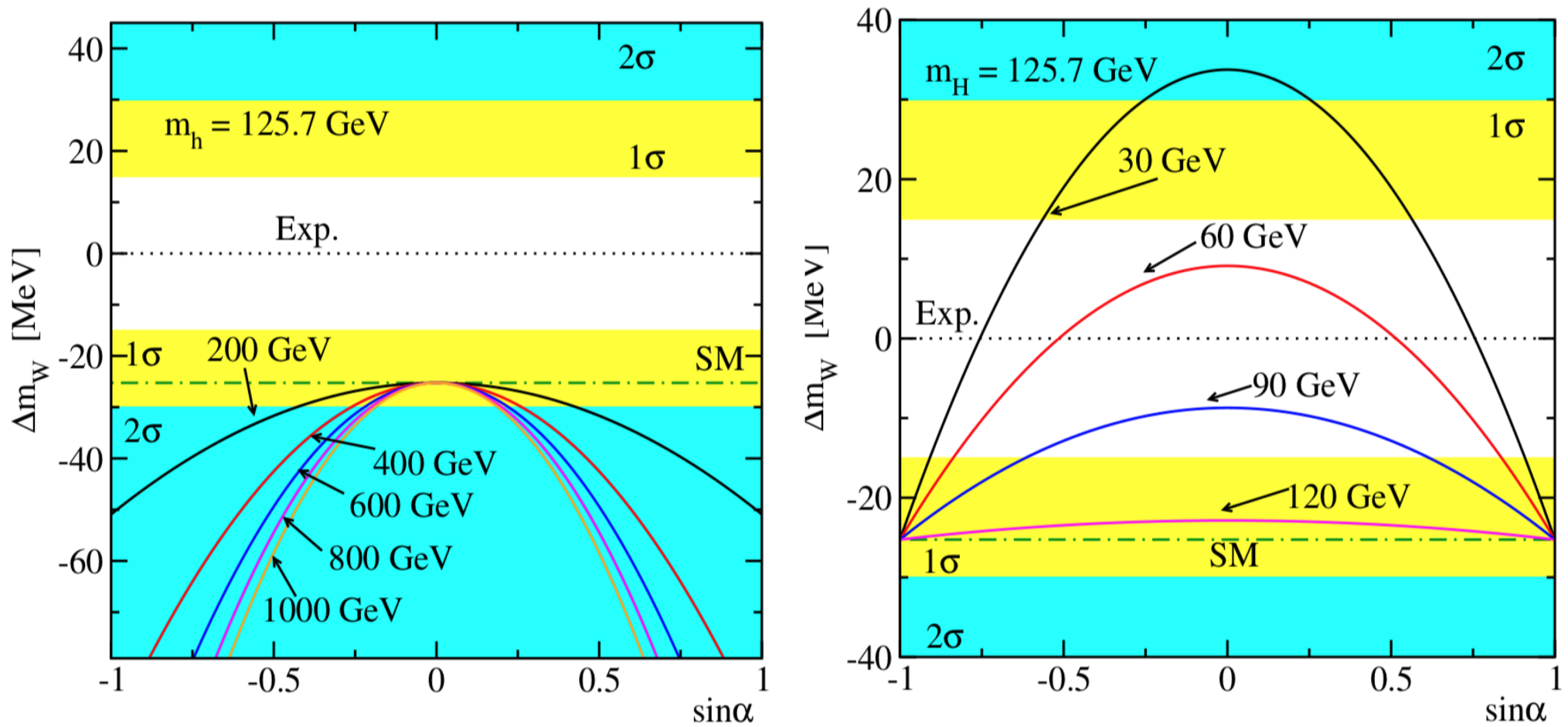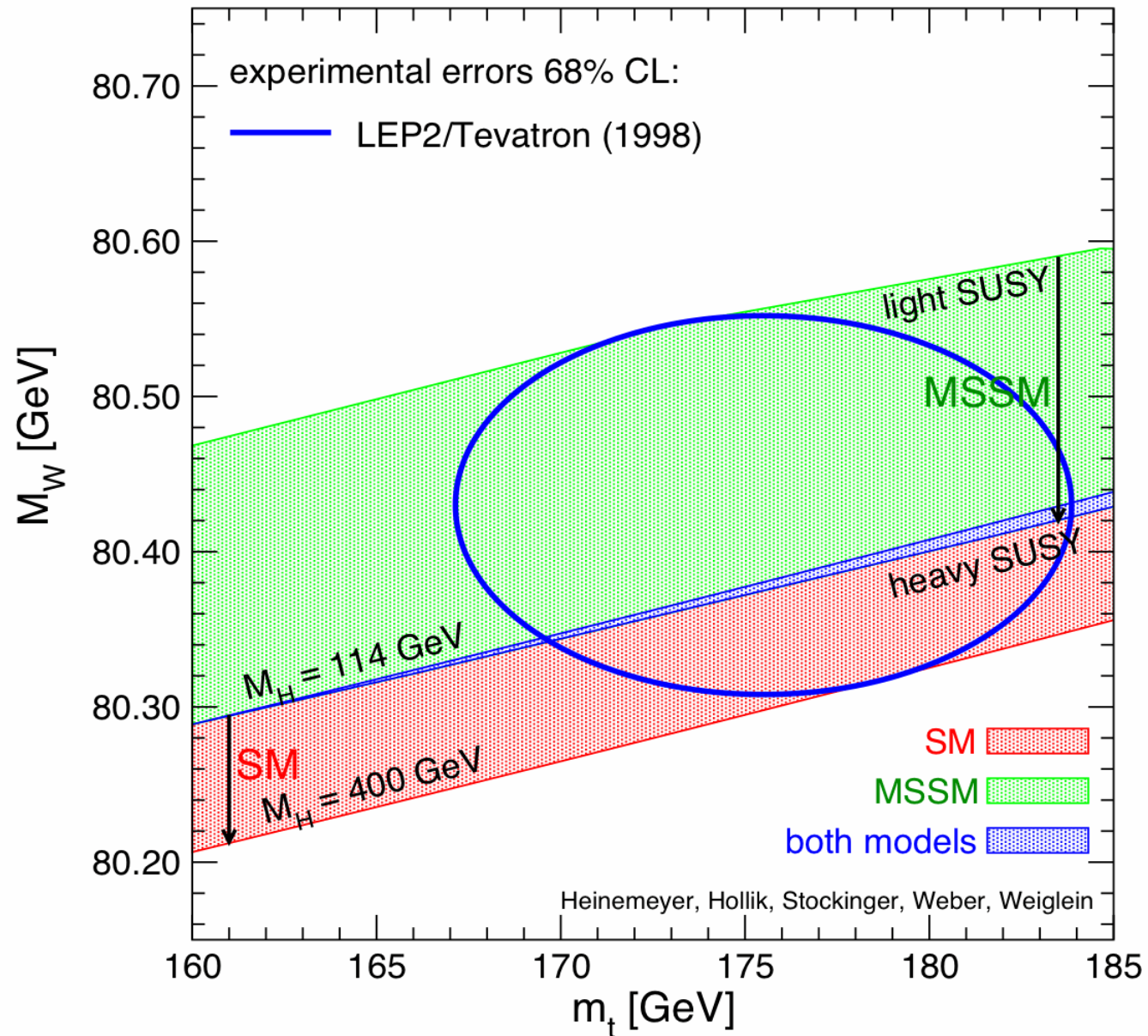

D. López-Val and T. Robens, Phys. Rev. D 90, 114018 (2014)

Contributions from Supersymmetric Particles

- Radiative correction depends on mass splitting (Δm^2) between squarks in SU(2) doublet

- SUSY loops can contribute tens of MeV to M_W
    - Multi-dimensional parameter space with significant exclusions from LHC

1998 Status of M_W *vs* M_{top}

- Generic parameterization of new physics contributing to W and *Z* boson self-energies: *S, T, U* parameters

U=0 assumed
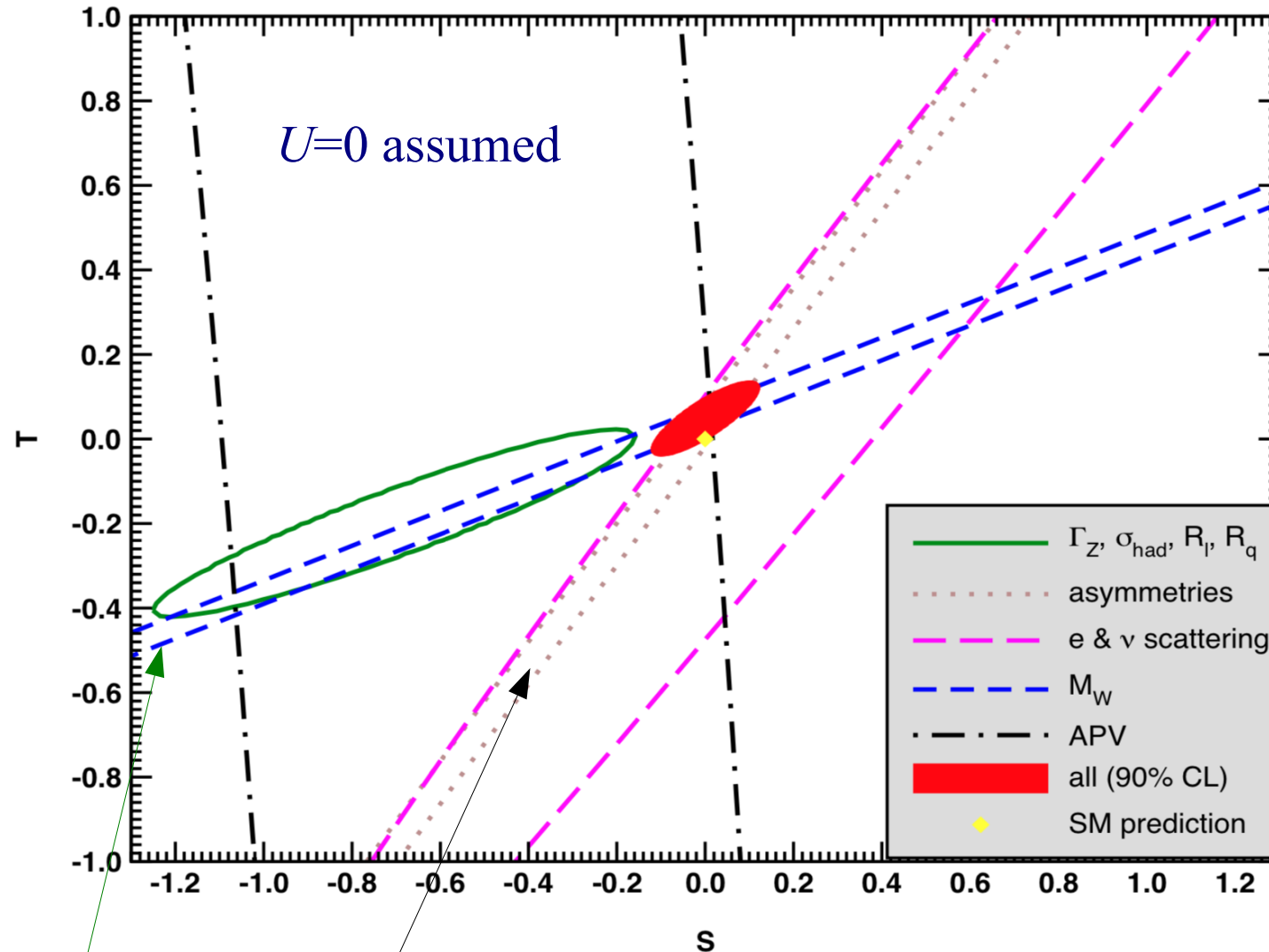
Additionally, M_W is the only measurement which constrains *U*

(From PDG 2021)

M_W and Asymmetries are the most powerful observables

Legend in figure:
- Γ_Z, σ_{had}, R_l, R_q
- asymmetries
- e & ν scattering
- M_W
- APV
- all (90% CL)
- SM prediction

Previous CDF Result (2.2 fb^{-1}) Transverse Mass Fit Uncertainties (MeV)

(CDF, PRL 108 (2012) 151803;   Phys. Rev. D 89 (2014) 7, 072003)
Total uncertainty of 19 MeV on W boson mass

	electrons	muons	common
W statistics	19	16	0
Lepton energy scale	10	7	5
Lepton resolution	4	1	0
Recoil energy scale	5	5	5
Recoil energy resolution	7	7	7
Selection bias	0	0	0
Lepton removal	3	2	2
Backgrounds	4	3	0
pT(W) model	3	3	3
Parton dist. Functions	10	10	10
QED rad. Corrections	4	4	4
Total	23	26	15

Systematic uncertainties shown in green: statistics-limited by control data samples

W Boson Production at the Tevatron
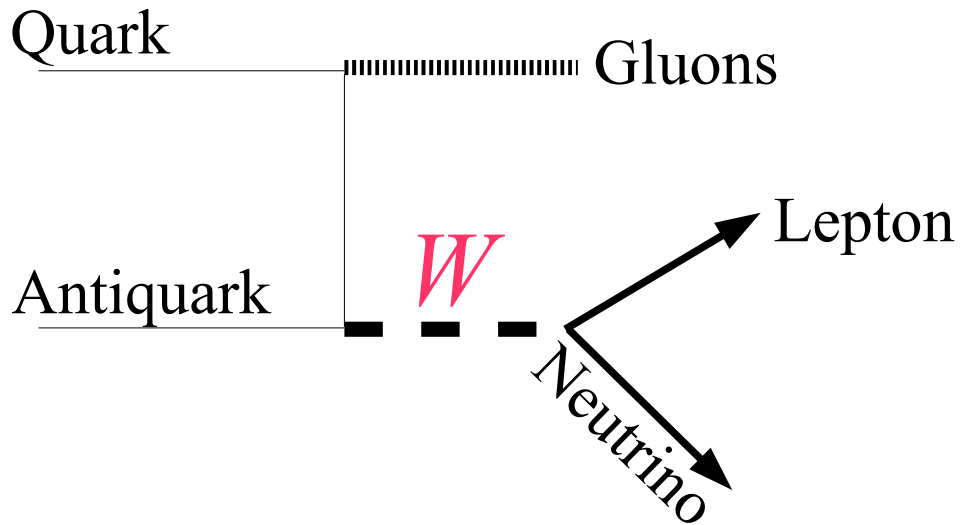
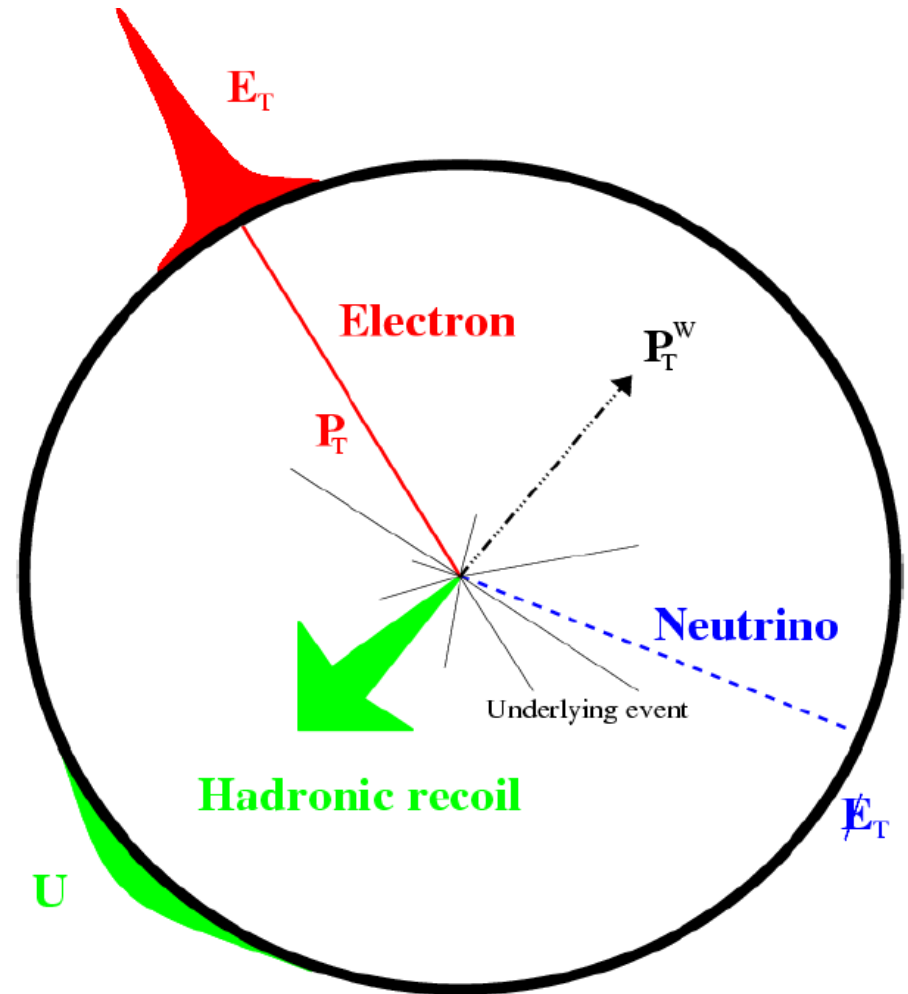Quark ⸻ Gluons

Antiquark ⸻ W → Lepton / Neutrino
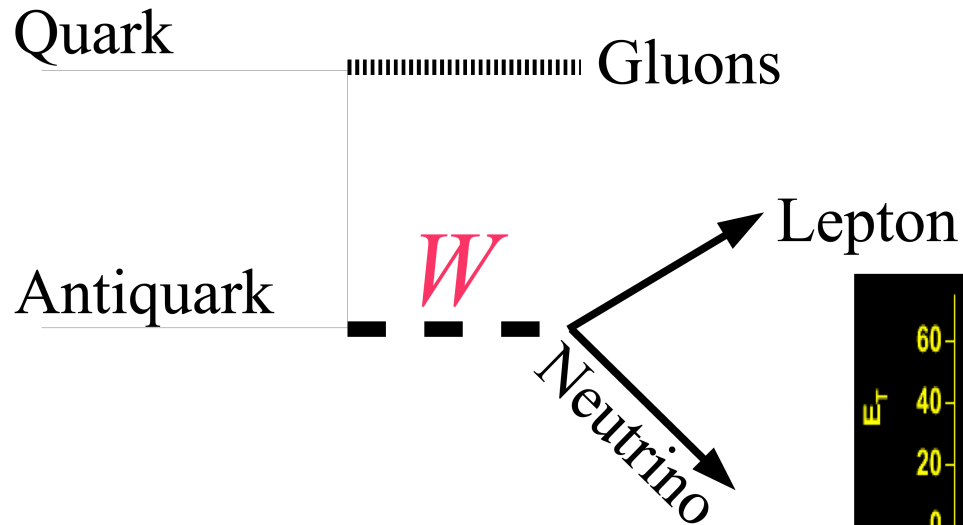
Quark-antiquark annihilation dominates (80%)

Lepton p_T carries most of W mass information, can be measured precisely (achieved 0.004%)

Initial state QCD radiation is $O(10\ \mathrm{GeV})$, measure as soft 'hadronic recoil' in calorimeter (calibrated to ~0.2%) dilutes W mass information, fortunately $p_T(W) \ll M_W$

W Boson Production at the Tevatron

Quark ———————— Gluons
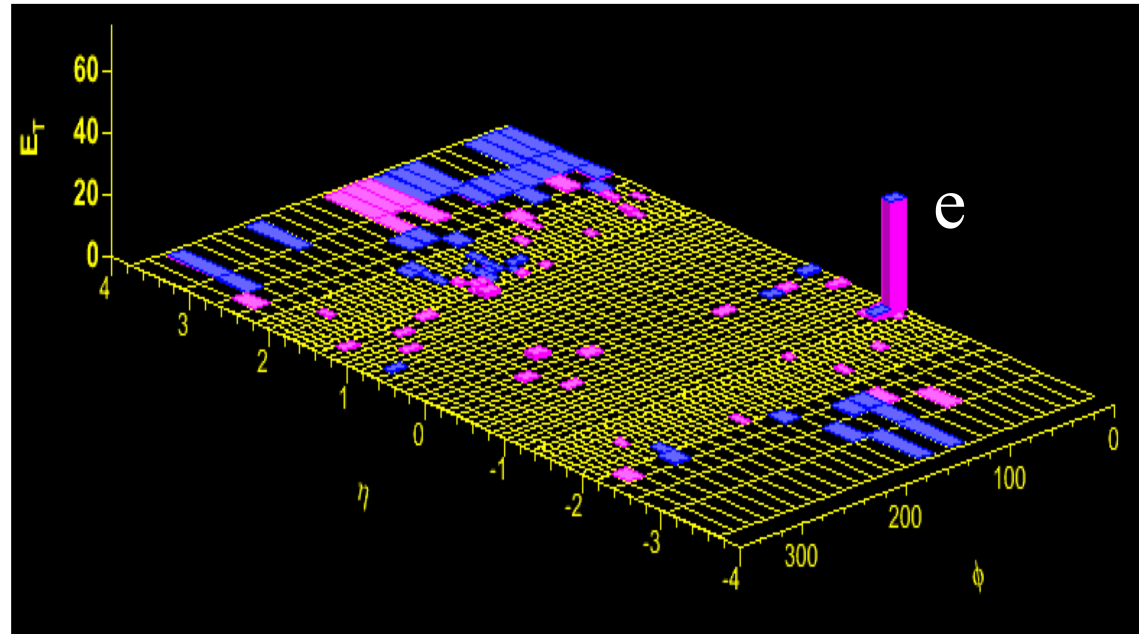
Antiquark — W — → Lepton

Neutrino

Quark-antiquark annihilation
dominates (80%)

Lepton p_T carries most of W mass
information, can be measured precisely (achieved 0.004%)

Initial state QCD radiation is O(10 GeV), measure as soft 'hadronic recoil' in
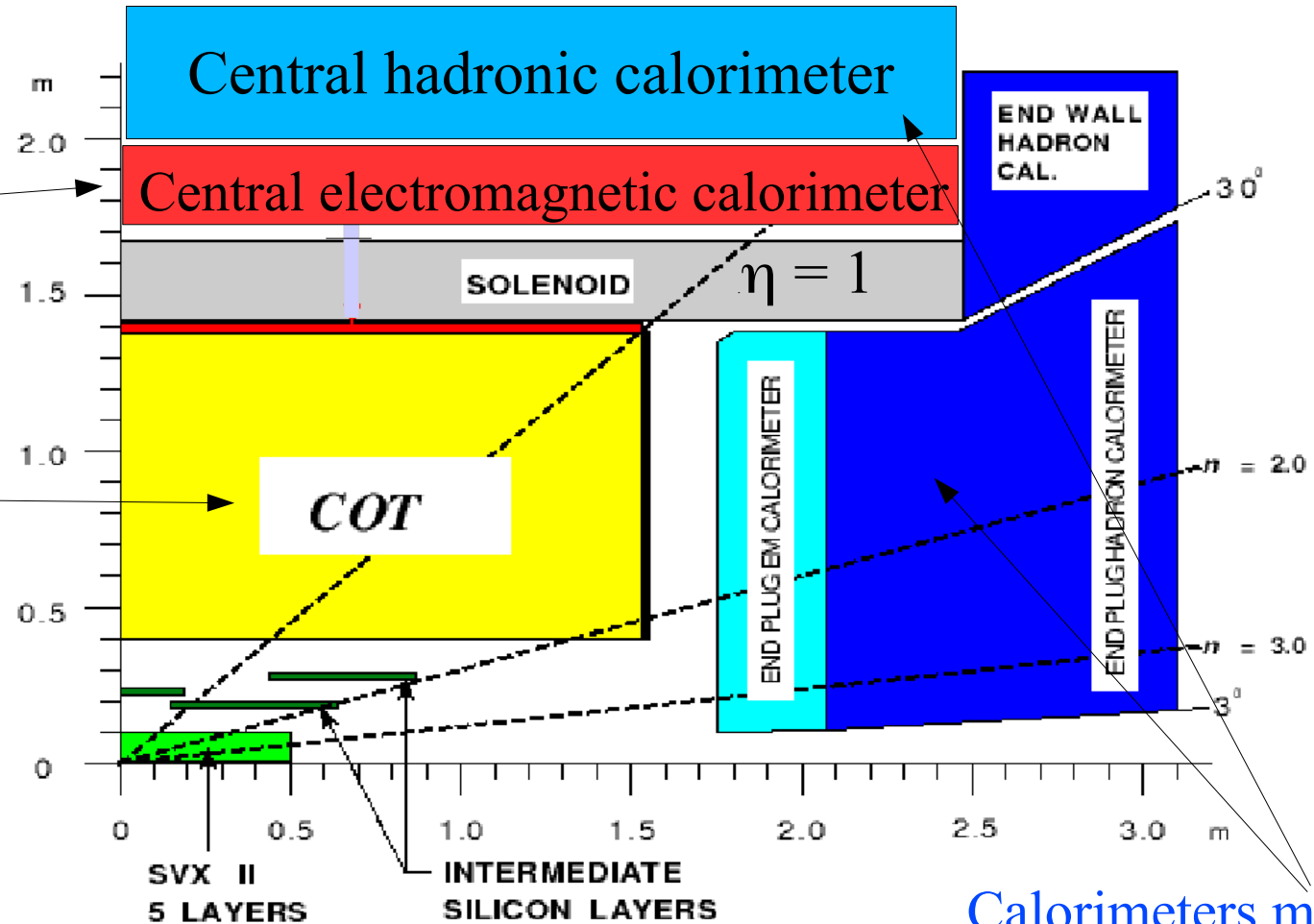calorimeter (calibrated to ~0.2%)
dilutes W mass information, fortunately $p_T(W) << M_W$

Quadrant of Collider Detector at Fermilab (CDF)

EM calorimeter provides precise electron energy measurement

COT provides precise lepton track momentum measurement

Central hadronic calorimeter

Central electromagnetic calorimeter

END WALL HADRON CAL.

SOLENOID

$\eta = 1$

30^0

m

2.0

1.5

1.0

0.5

0

COT

END PLUG EM CALORIMETER

END PLUG HADRON CALORIMETER

$\eta = 2.0$

$\eta = 3.0$

3^0

0   0.5   1.0   1.5   2.0   2.5   3.0   m

SVX II
5 LAYERS

INTERMEDIATE
SILICON LAYERS

Calorimeters measure hadronic recoil particles

Select W and Z bosons with central ($|\eta| < 1$) leptons

Collider Detector at Fermilab (CDF)

Muon detector

Central hadronic calorimeter

Central EM calorimeter

Central outer tracker (COT)
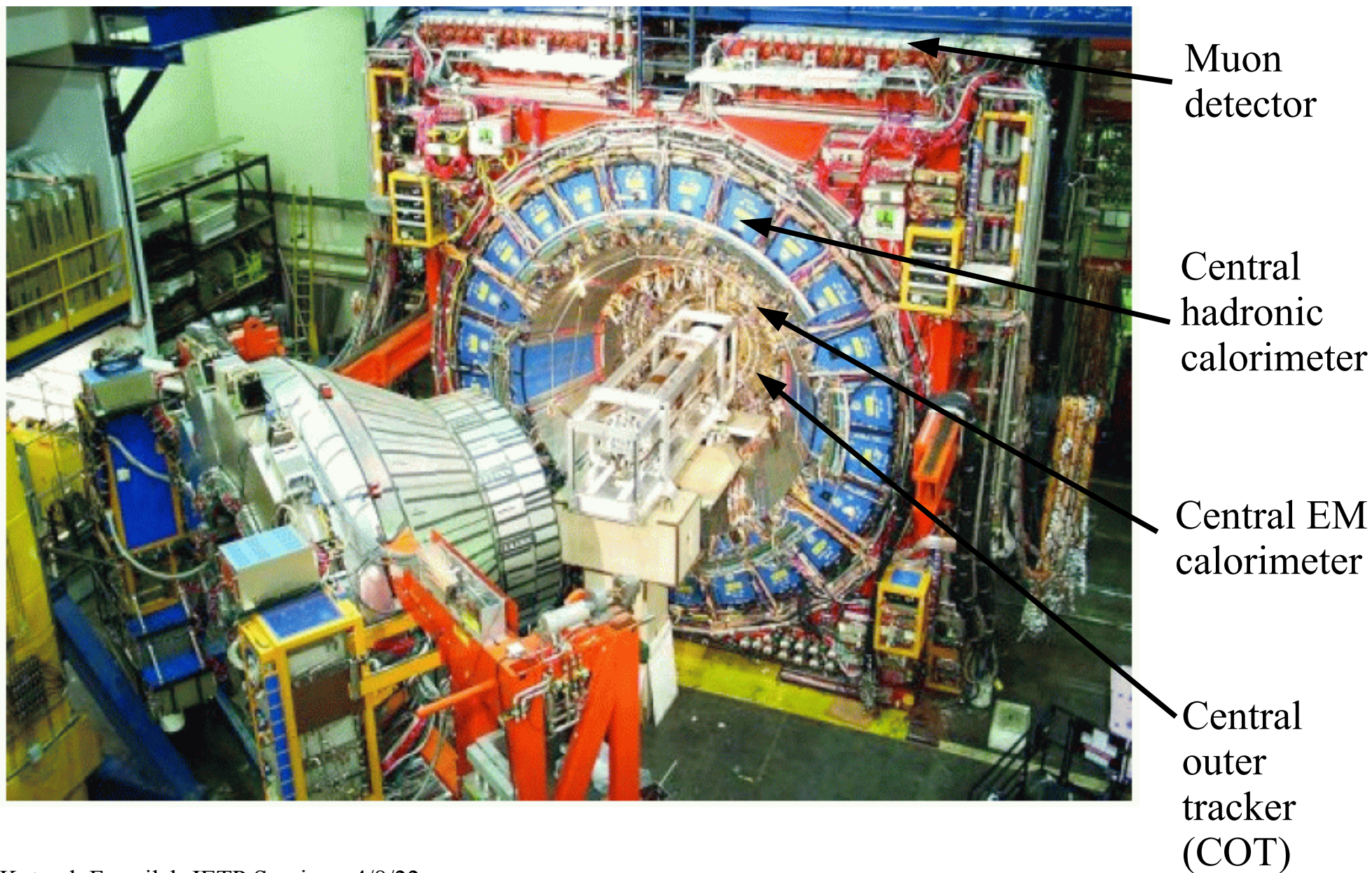
Event Selection

- Goal: Select events with high p_T leptons and small hadronic recoil activity

  - to maximize W mass information content and minimize backgrounds

- Inclusive lepton triggers: loose lepton track and muon stub / calorimeter cluster requirements, with lepton $p_T > 18$ GeV

  - Kinematic efficiency of trigger ~100% for offline selection

- Offline selection requirements:

  - Electron cluster $E_T > 30$ GeV, track $p_T > 18$ GeV

  - Muon track $p_T > 30$ GeV

  - Loose identification requirements to minimize selection bias

- W boson event selection: one selected lepton, $|u| < 15$ GeV & $p_T(\nu) > 30$ GeV

  - Z boson event selection: two selected leptons

W & Z Data Samples

Sample	Candidates
W → electron	1 811 700
Z → electrons	66 180
W → muon	2 424 486
Z → muons	238 534

- Integrated Luminosity (collected between February 2002 – September 2011):

  – Electron and muon channels: $L = 8.8 \text{ fb}^{-1}$

  – Identical running conditions for both channels, guarantees cross-calibration

- Event selection gives fairly clean samples

  – Mis-identification backgrounds ~ 0.5%

Analysis Strategy

Strategy

Maximize the number of internal constraints and cross-checks

Driven by three goals:

1) Robustness: constrain the same parameters in as many different ways as possible

2) Precision: combine independent measurements after showing consistency

3) minimize bias: blinded measurements of M_Z and M_W

Outline of Analysis

Energy scale measurements drive the W mass measurement

- **Tracker Calibration**

    - alignment of the COT (2,520 cells; 30,240 sense wires) using cosmic rays

    - COT momentum scale and tracker non-linearity constrained using J/ψ ⟶ μμ and Υ ⟶ μμ mass fits

    - Confirmed using Z ⟶ μμ mass fit

- **EM Calorimeter Calibration**

    - COT momentum scale transferred to EM calorimeter using a fit to the peak of the E/p spectrum, around E/p ~ 1

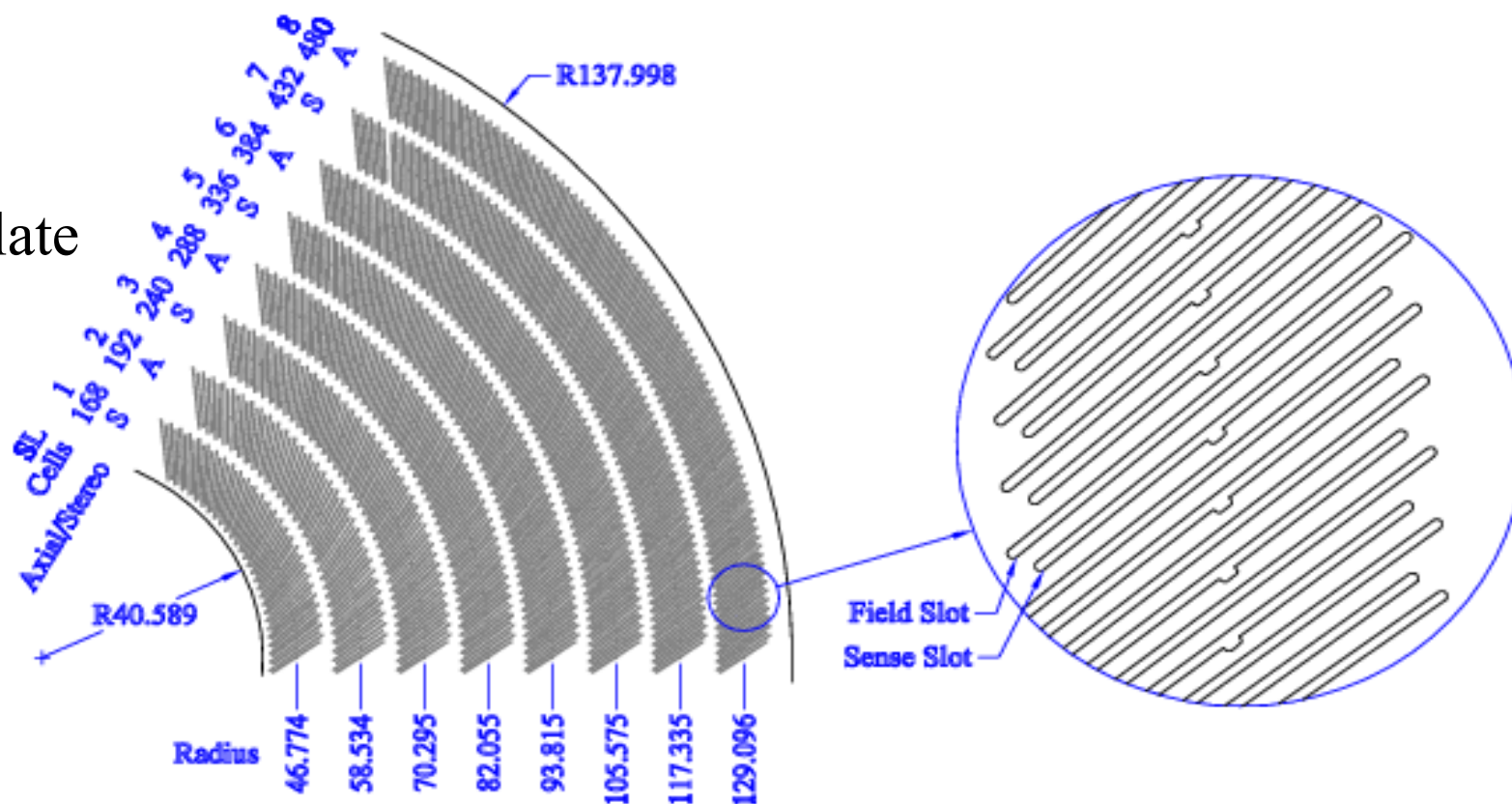   - Calorimeter energy scale confirmed using Z ⟶ ee mass fit

- **Tracker and EM Calorimeter resolutions**

- **Hadronic recoil modeling**

    - Characterized using p_T-balance in Z ⟶ *ll* events

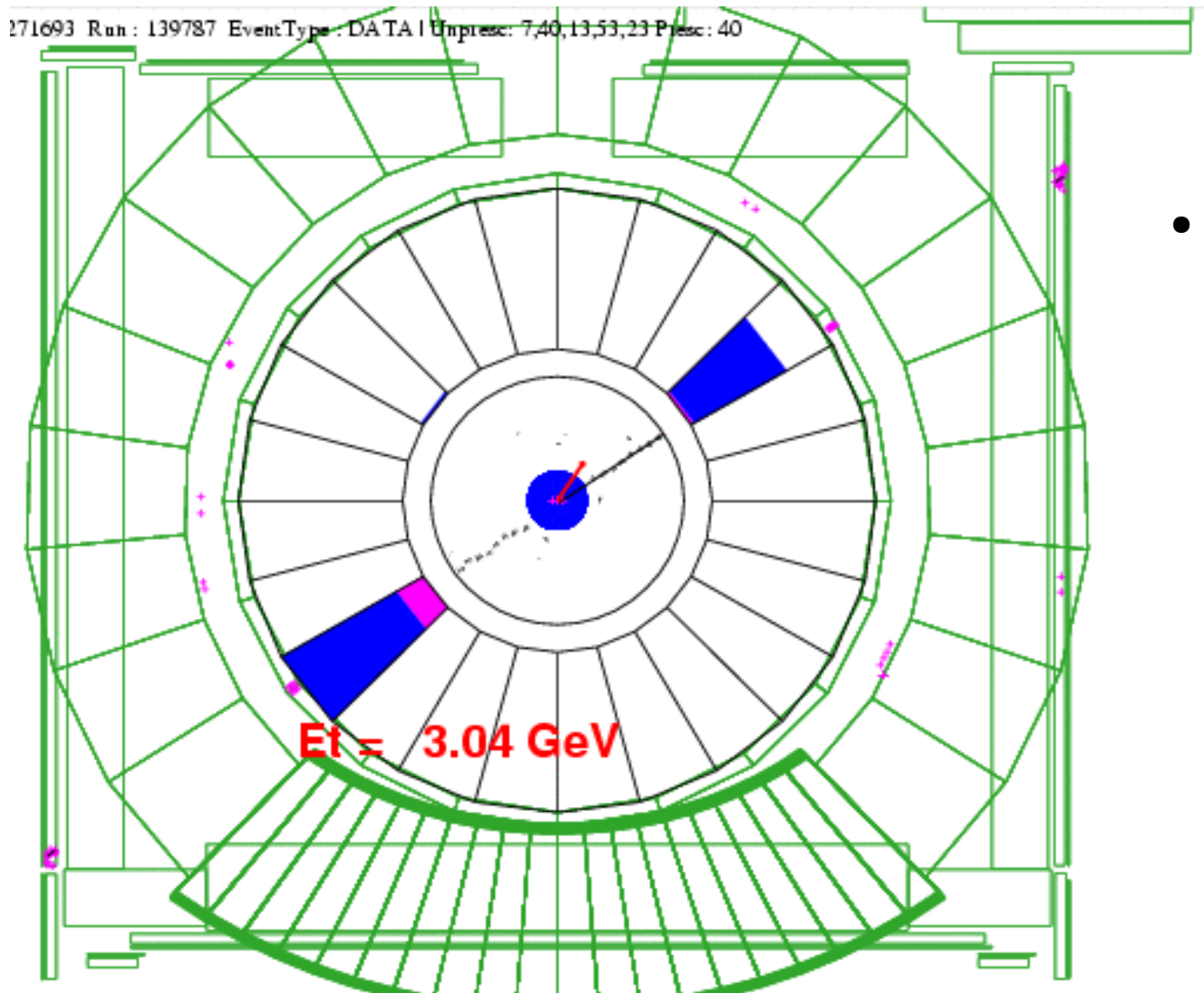# Drift Chamber (COT) Alignment

COT endplate
geometry

Internal Alignment of COT

- Use a clean sample of ~480k cosmic rays for cell-by-cell internal alignment

271693 Run : 139787 EventType : DATA I Unpres: 7,40,13,53,23 Presc : 40

Et = 3.04 GeV

- Fit COT hits on both sides simultaneously to a single helix (AVK, H. Gerberich and C. Hays, NIMA 506, 110 (2003))

  - Time of incidence is a floated parameter in this 'di-cosmic fit'

Residuals of COT cells after alignment

before alignment

after alignment
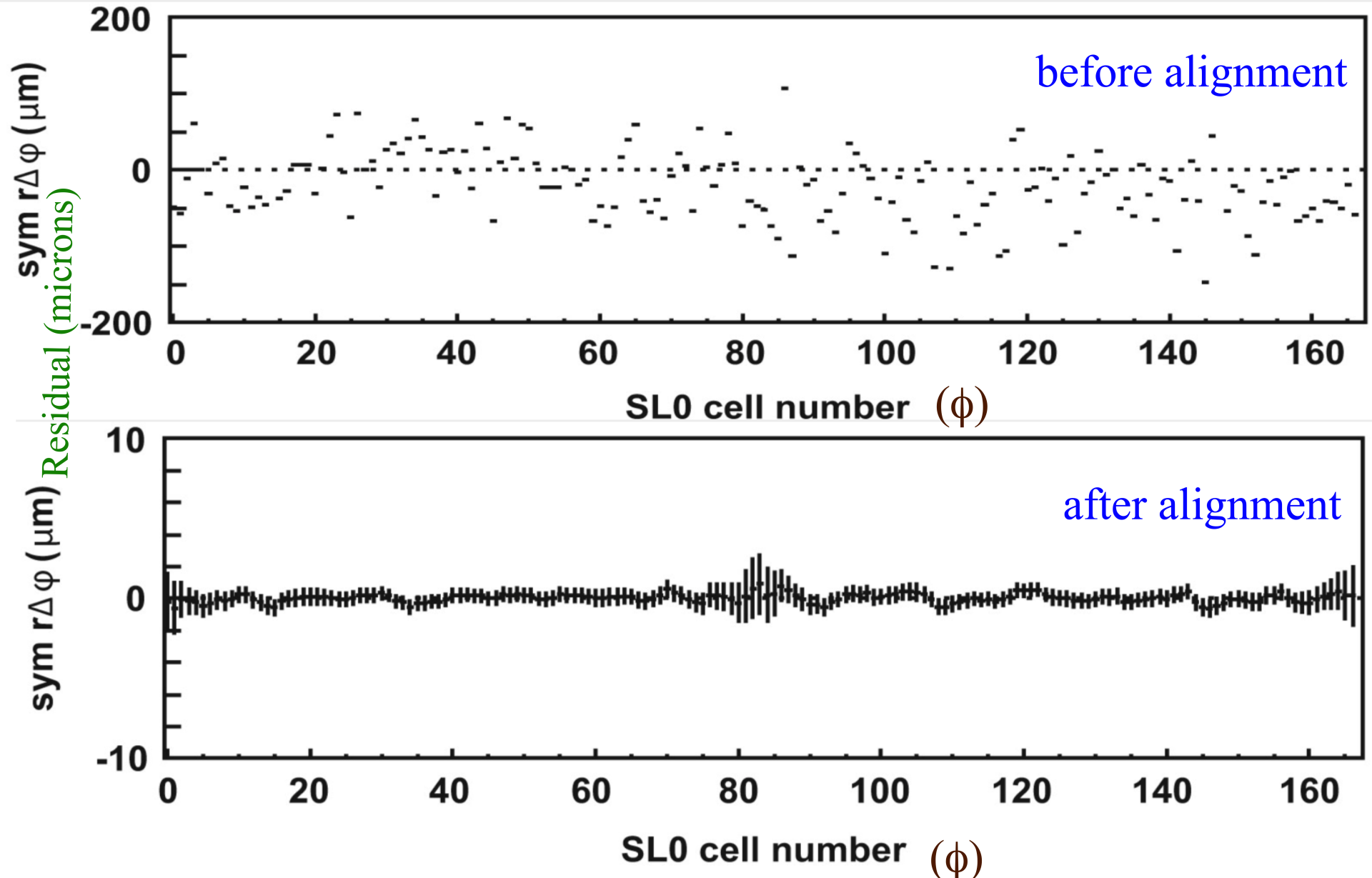
Final relative alignment of cells ~1 μm (initial alignment ~50 μm)

Consistency check of COT alignment procedure
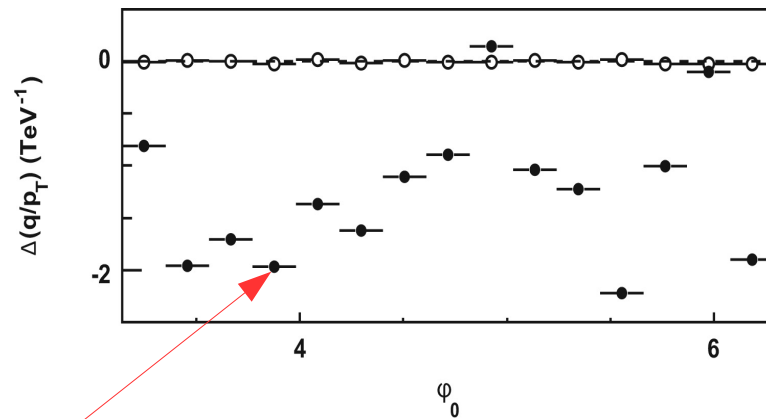
Fit separate helices to cosmic ray tracks

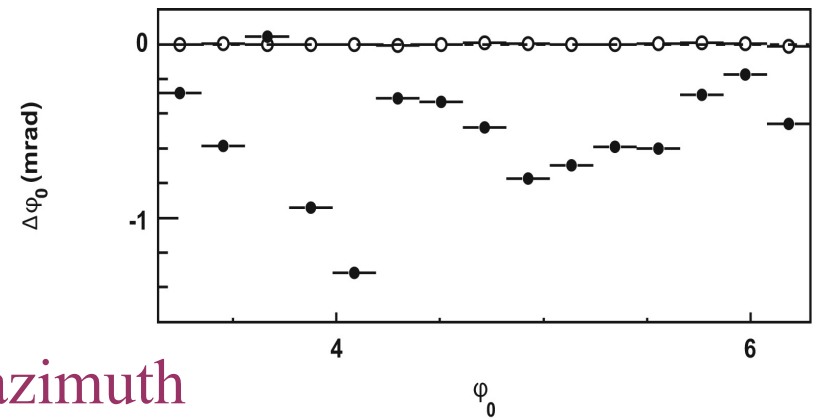**Compare track parameters of the two tracks: a measure of track parameter bias**
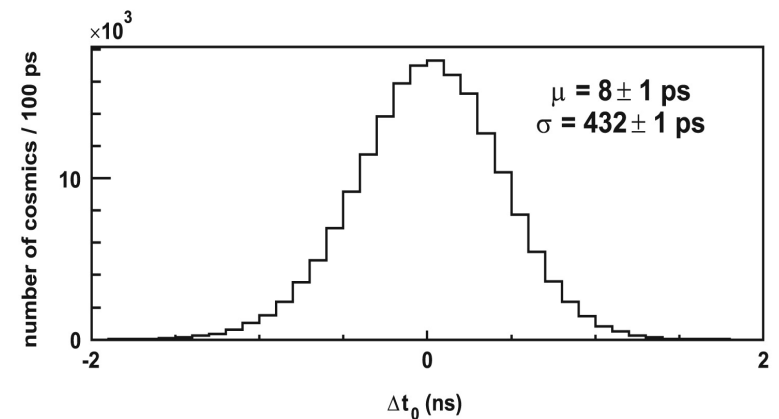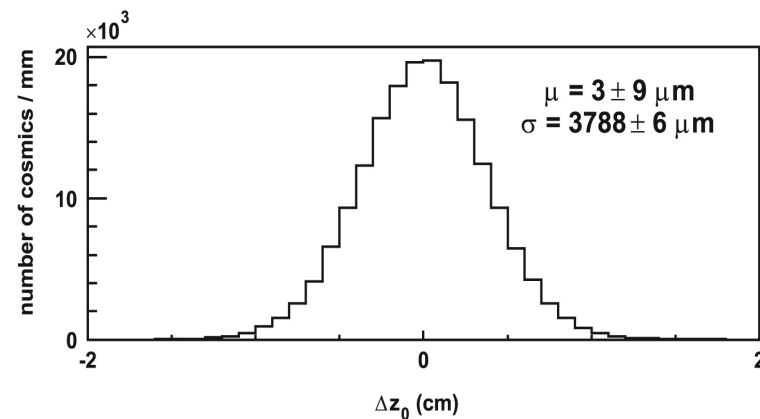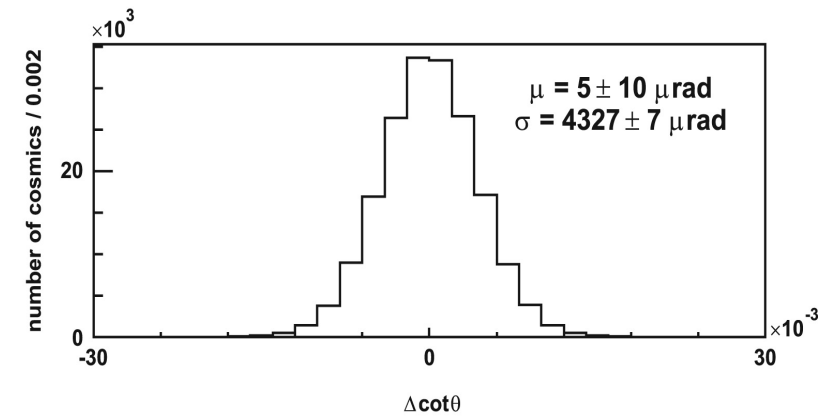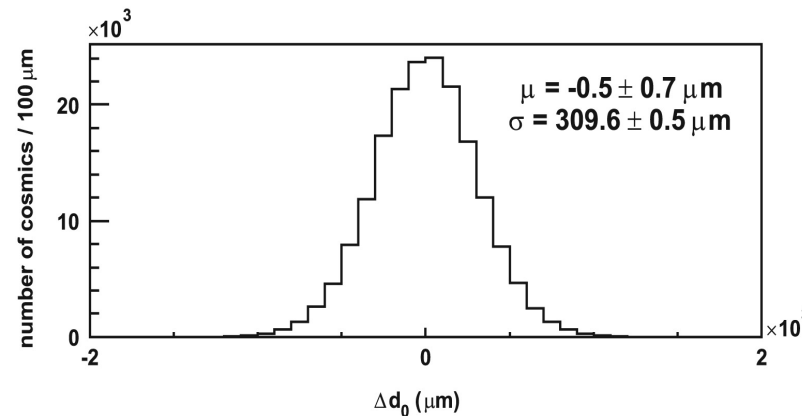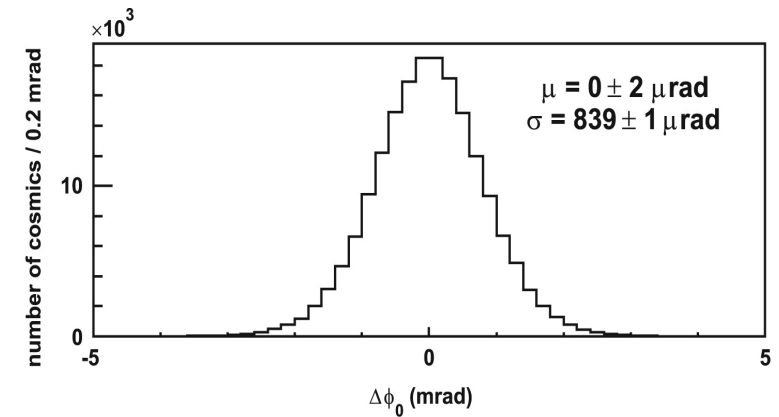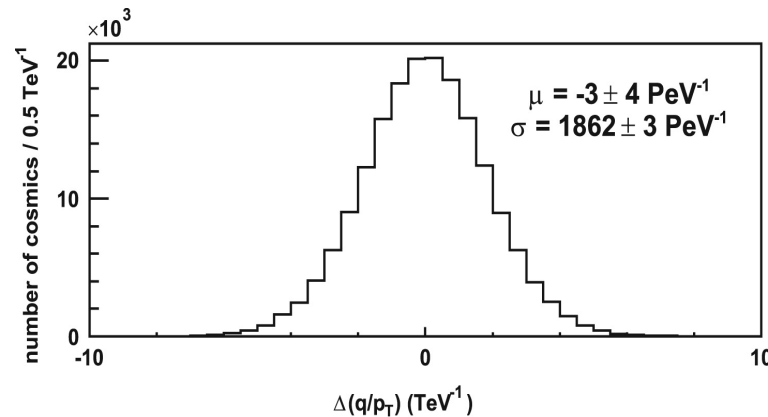
Consistency check of COT alignment procedure

track parameter
bias versus
azimuth

solid = before
alignment
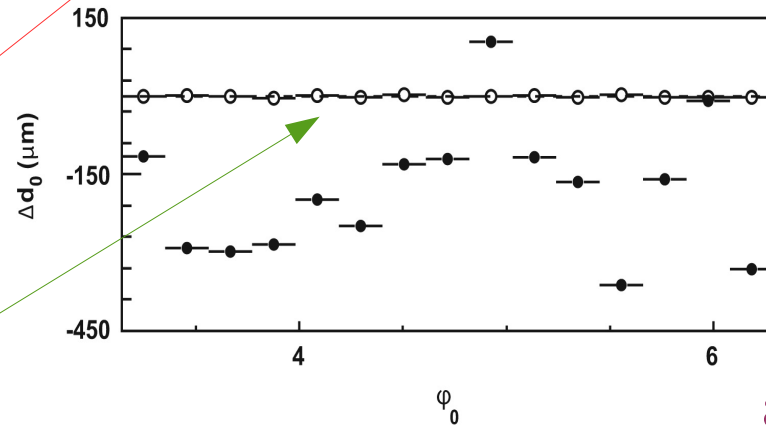
open = after
alignment
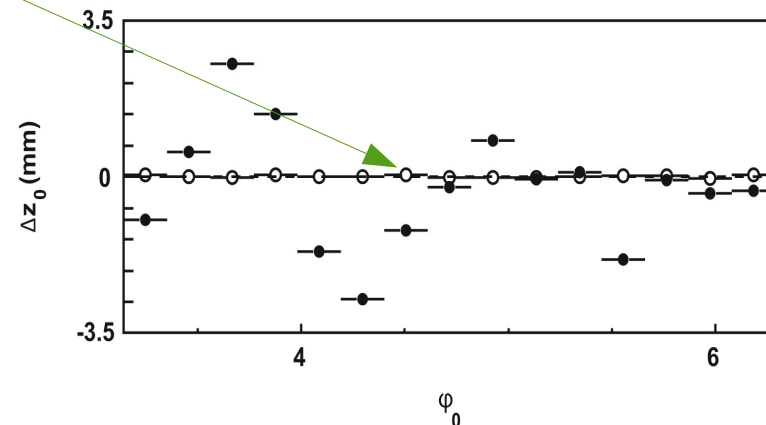
azimuth

azimuth

azimuth
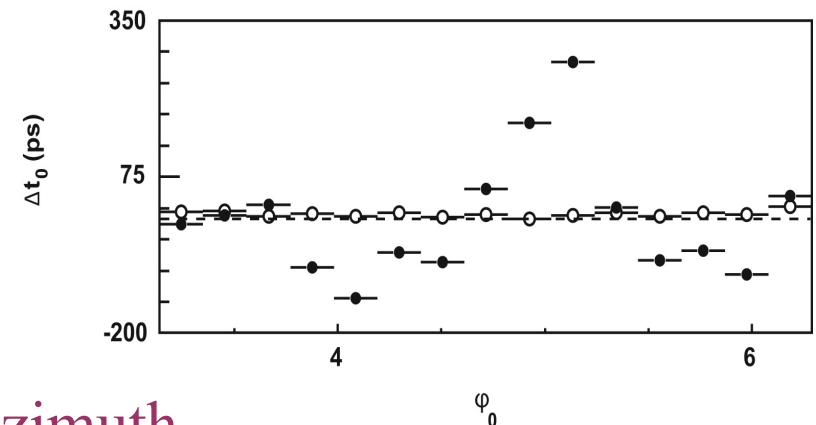
Cross-check of COT alignment

- Cosmic ray alignment removes most deformation degrees of freedom, but "weakly constrained modes" remain

- Final cross-check and correction to beam-constrained track curvature based on difference of $<E/p>$ for positrons *vs* electrons

- Smooth ad-hoc curvature corrections as a function of polar and azimuthal angle: statistical errors => $\Delta M_W = 1$ MeV

q/p_T (measured) =

$c_0 + c_1\, q/p_T + c_2\, (q/p_T)^2$

+ …

c_1 measures momentum scale
c_2 includes energy loss

$\times 10^{-3}$

$\Delta <E/p>\ (e^+ - e^-)$

$c_0 = 0$

Fig. S6

cot θ
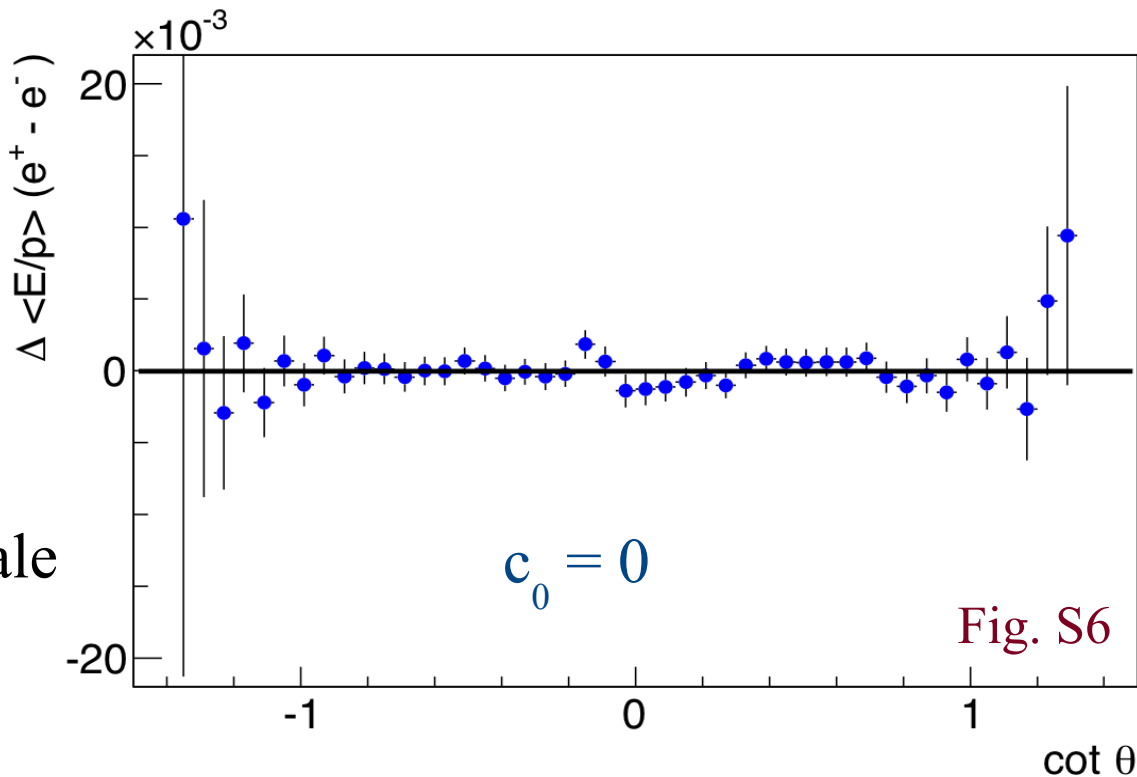
Signal Simulation and Fitting

Signal Simulation and Template Fitting

- **All signals simulated using a Custom Monte Carlo**

  - Generate finely-spaced templates as a function of the fit variable

  - perform binned maximum-likelihood fits to the data

- **Custom fast Monte Carlo makes smooth, high statistics templates**

  - And provides analysis control over key components of the simulation

M_W = 81 GeV
Monte Carlo template

M_W = 80 GeV
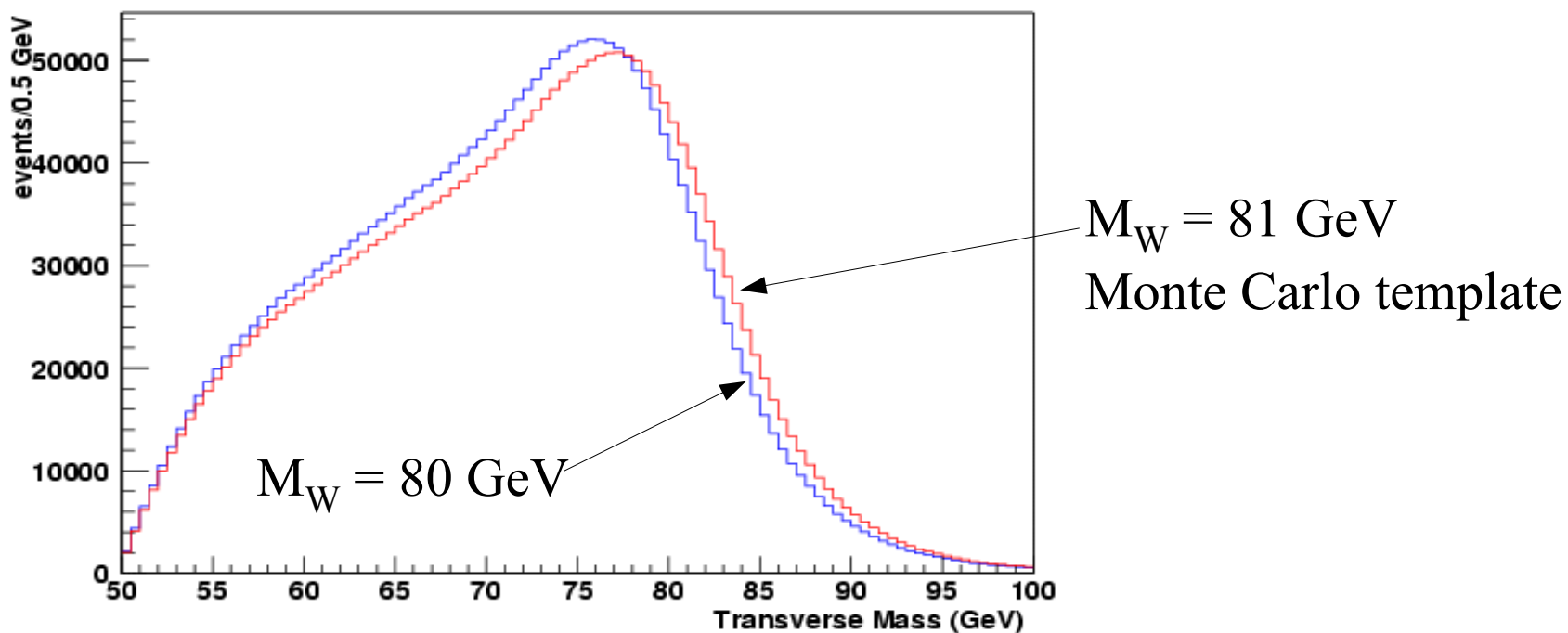
- We will extract the W mass from six kinematic distributions: Transverse mass, charged lepton p_T and missing E_T using both electron and muon channels

Generator-level Signal Simulation
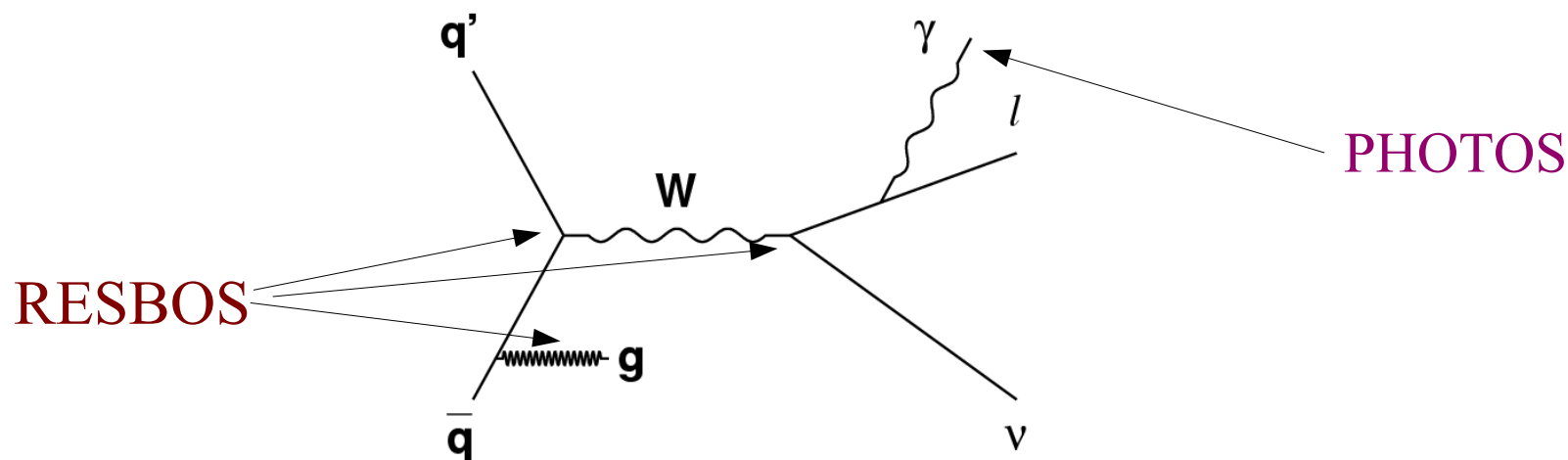
- Generator-level input for W & Z simulation provided by RESBOS
  (C. Balazs & C.-P. Yuan, PRD56, 5558 (1997) and references therein), which

  - Calculates triple-differential production cross section, and p_T-dependent double-differential decay angular distribution

  - calculates boson p_T spectrum reliably over the relevant p_T range: includes tunable parameters in the non-perturbative regime at low p_T

- Multiple radiative photons generated according to PHOTOS
  (P. Golonka and Z. Was, Eur. J. Phys. C 45, 97 (2006) and references therein)

Validation of QED Calculations

- Extensive comparisons between PHOTOS and HORACE (C.M. Carloni Calame, G. Montagna, O. Nicrosini and A. Vicini, JHEP 0710:109,2007) programs

  - Comparing multi-photon final state radiation algorithms

  - Including multi-photon radiation from all charged lines (HORACE), and consistency with exact one-photon calculation

AVK & BJ, Adv. High Energy Phys. (2016) 1615081
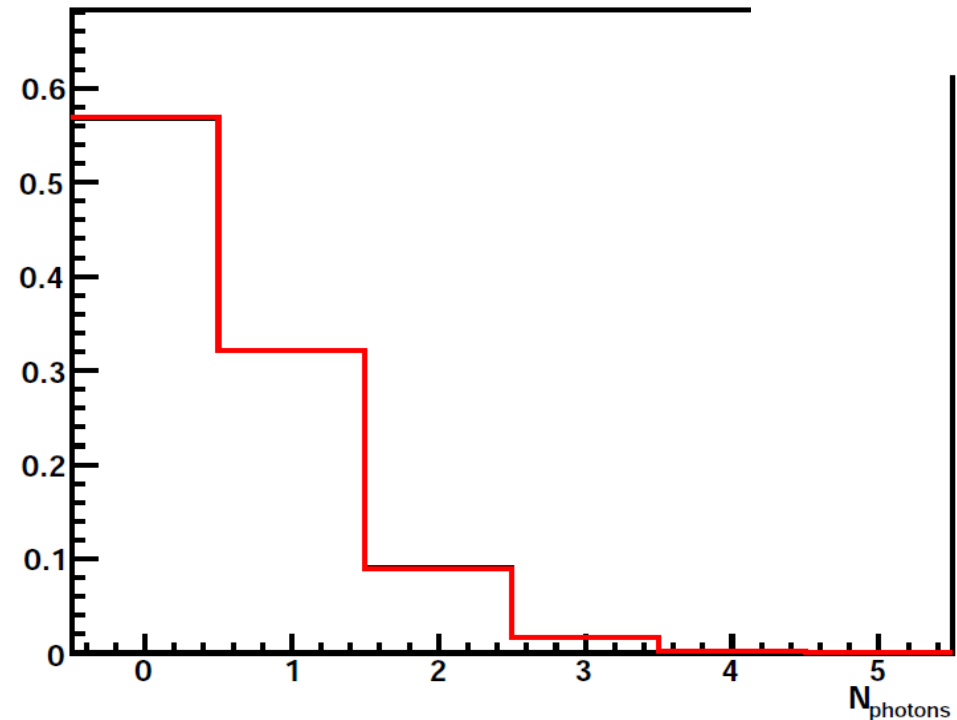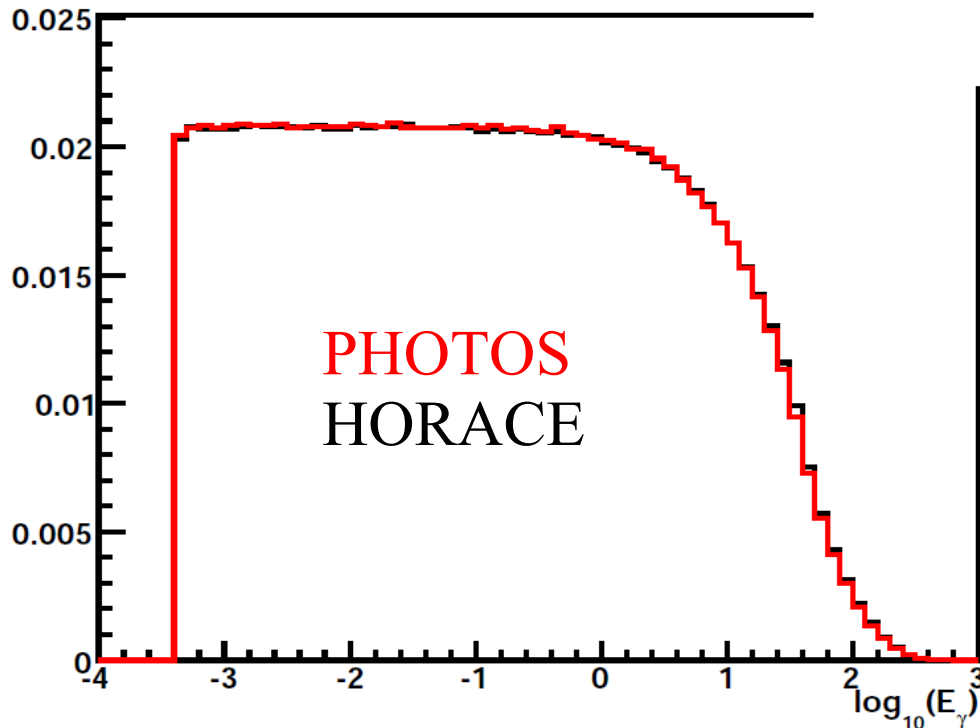
Validations confirm systematic uncertainty due to QED radiation of 3 MeV

Uncertainties in QED Calculations

- Extensive studies performed on uncertainties arising from

  - leading logarithm approximation

  - Multi-photon calculation

  - higher order soft and virtual corrections

  - Electron-positron pair creation (included at LO)

  - QED/QCD interference

  - dependence on electroweak parameters/scheme

- Total systematic uncertainty due to QED radiation of 3 MeV on W mass

Constraining Boson p_T Spectrum

- Fit the non-perturbative parameter g_2 and QCD coupling α_s in RESBOS to $p_T(ll)$ spectra:

$$\Delta M_W = 1.8 \text{ MeV}$$

Position of peak in boson p_T spectrum depends on g_2
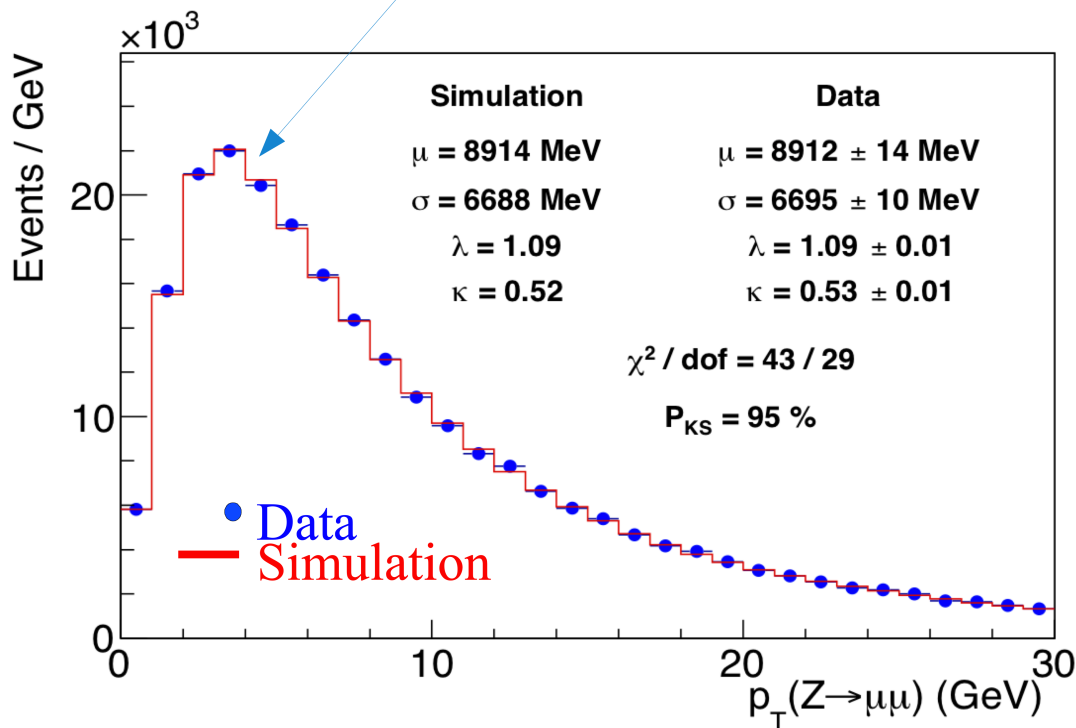
Tail to peak ratio depends on α_s

Simulation	Data
μ = 8914 MeV	μ = 8912 ± 14 MeV
σ = 6688 MeV	σ = 6695 ± 10 MeV
λ = 1.09	λ = 1.09 ± 0.01
κ = 0.52	κ = 0.53 ± 0.01

χ^2 / dof = 43 / 29

P_{KS} = 95 %

Data
Simulation

Simulation	Data
μ = 8940 MeV	μ = 8868 ± 26 MeV
σ = 6751 MeV	σ = 6715 ± 18 MeV
λ = 1.07	λ = 1.08 ± 0.01
κ = 0.46	κ = 0.51 ± 0.02

χ^2 / dof = 26 / 29

P_{KS} = 11 %
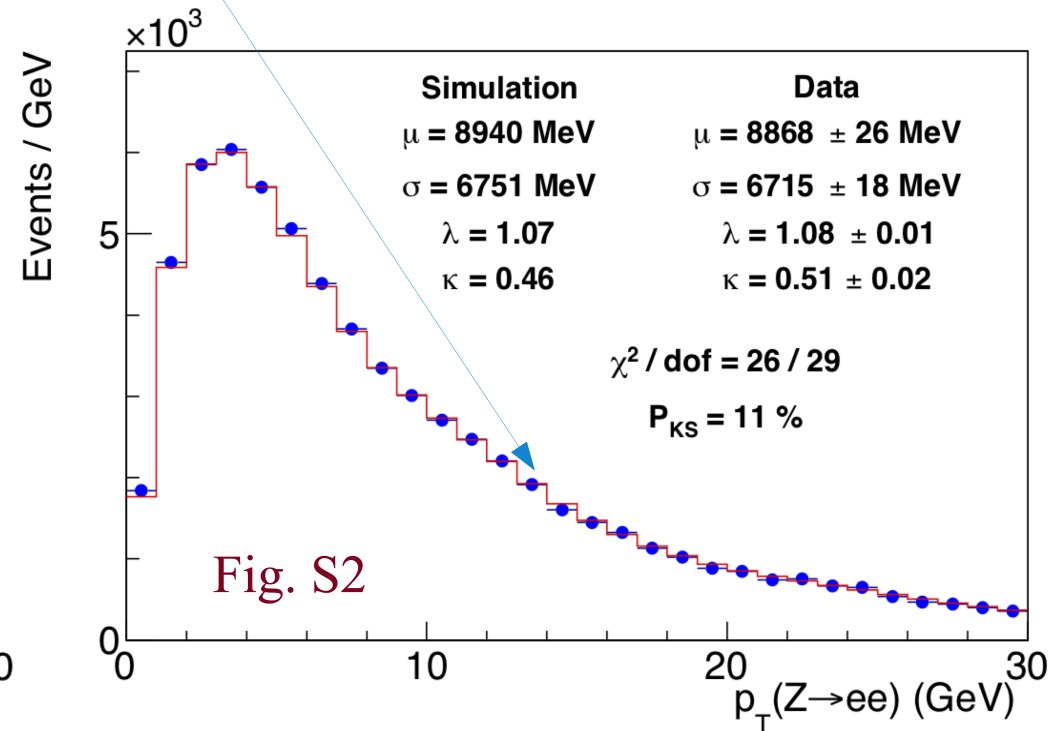
Fig. S2

Constraining Boson p$_T$ Spectrum

- NEW: Use azimuthal opening angle between leptons as a check of the p$_T$(*ll*) spectrum modeling:

$$\phi_\eta^* = \tan\left(\frac{\pi - \Delta\phi^{\ell\ell}}{2}\right) \text{sech}\left(\frac{\eta^- - \eta^+}{2}\right)$$

Acceptance effect modeled in simulation
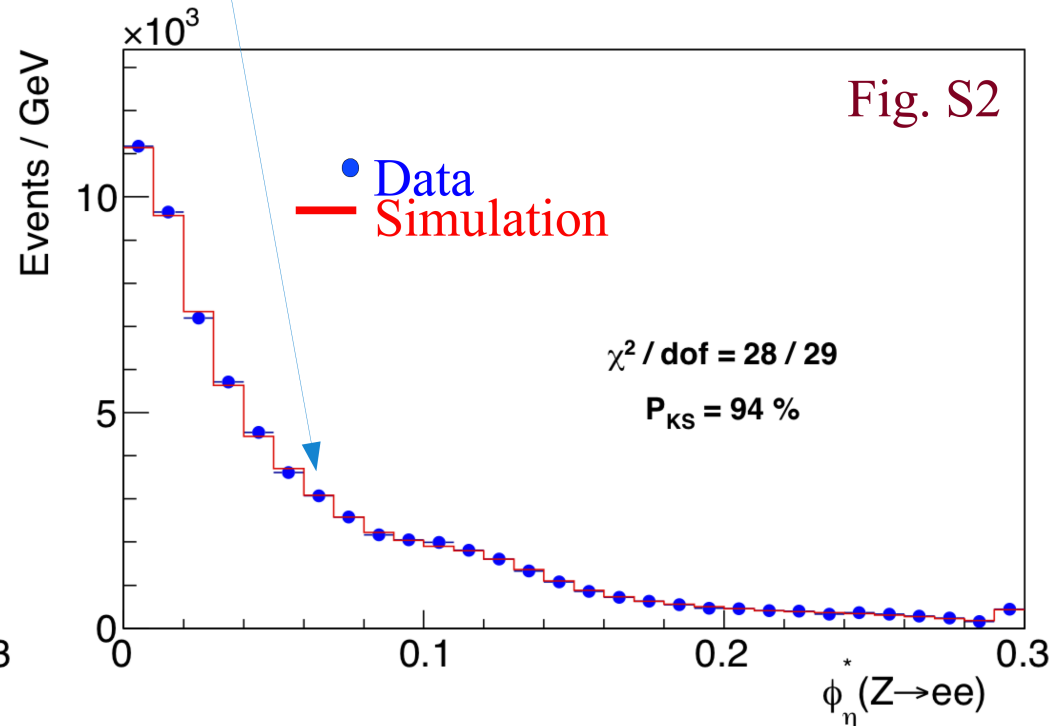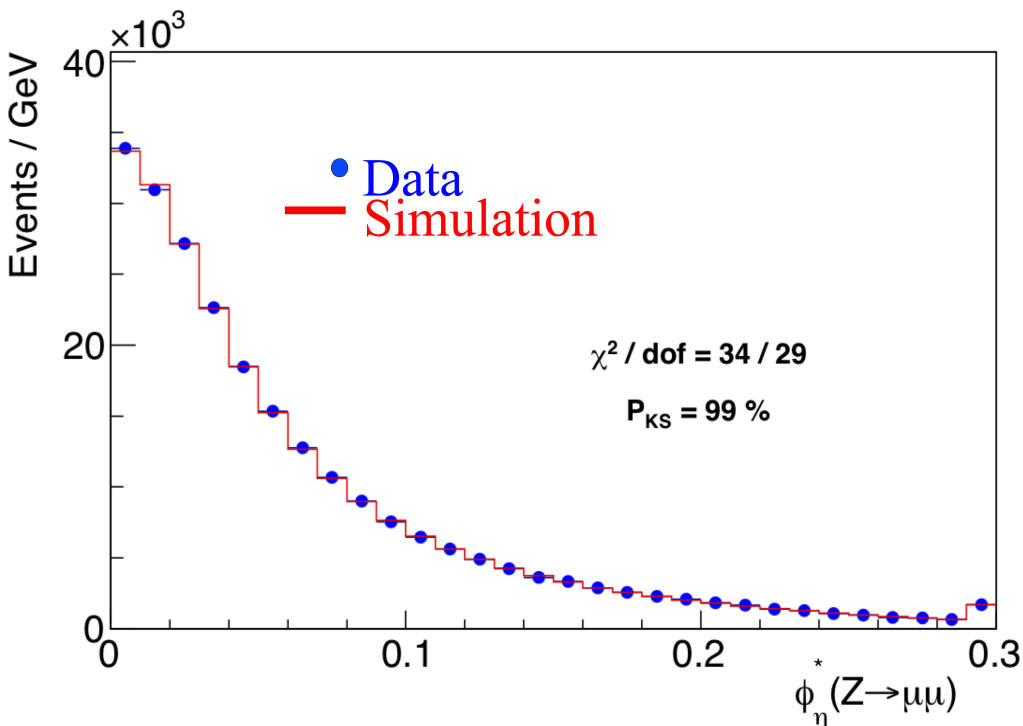
Fig. S2

Outline of Analysis

Energy scale measurements drive the W mass measurement

- Tracker Calibration

    - alignment of the COT (~2400 cells, ~30k sense wires) using cosmic rays

    - COT momentum scale and tracker non-linearity constrained using $J/\psi \longrightarrow \mu\mu$ and $\Upsilon \longrightarrow \mu\mu$ mass fits

    - Confirmed using $Z \longrightarrow \mu\mu$ mass fit

- EM Calorimeter Calibration

    - COT momentum scale transferred to EM calorimeter using a fit to the peak of the E/p spectrum, around E/p ~ 1

    - Calorimeter energy scale confirmed using $Z \longrightarrow ee$ mass fit

- Tracker and EM Calorimeter resolutions

- Hadronic recoil modeling

    - Characterized using p_T-balance in $Z \longrightarrow ll$ events

Custom Monte Carlo Detector Simulation

- A complete detector simulation of all quantities measured in the data

- First-principles simulation of tracking

  - Tracks and photons propagated through a high-resolution 3-D lookup table of material properties for silicon detector and COT

  - At each material interaction, calculate

    - Ionization energy loss according to detailed formulae and Landau distribution

    - Generate bremsstrahlung photons down to 0.4 MeV, using detailed cross section and spectrum calculations

    - Simulate photon conversion and Compton scattering

    - Propagate bremsstrahlung photons and conversion electrons

    - Simulate multiple Coulomb scattering, including non-Gaussian tail

  - Deposit and smear hits on COT wires, perform full helix fit including optional beam-constraint

Custom Monte Carlo Detector Simulation

- A complete detector simulation of all quantities measured in the data

- First-principles simulation of tracking

  - Tracks and photons propagated through a high-resolution 3-D lookup table of material properties for silicon detector and COT

e^+

e^-

e^-

e^-

!

Calorimeter
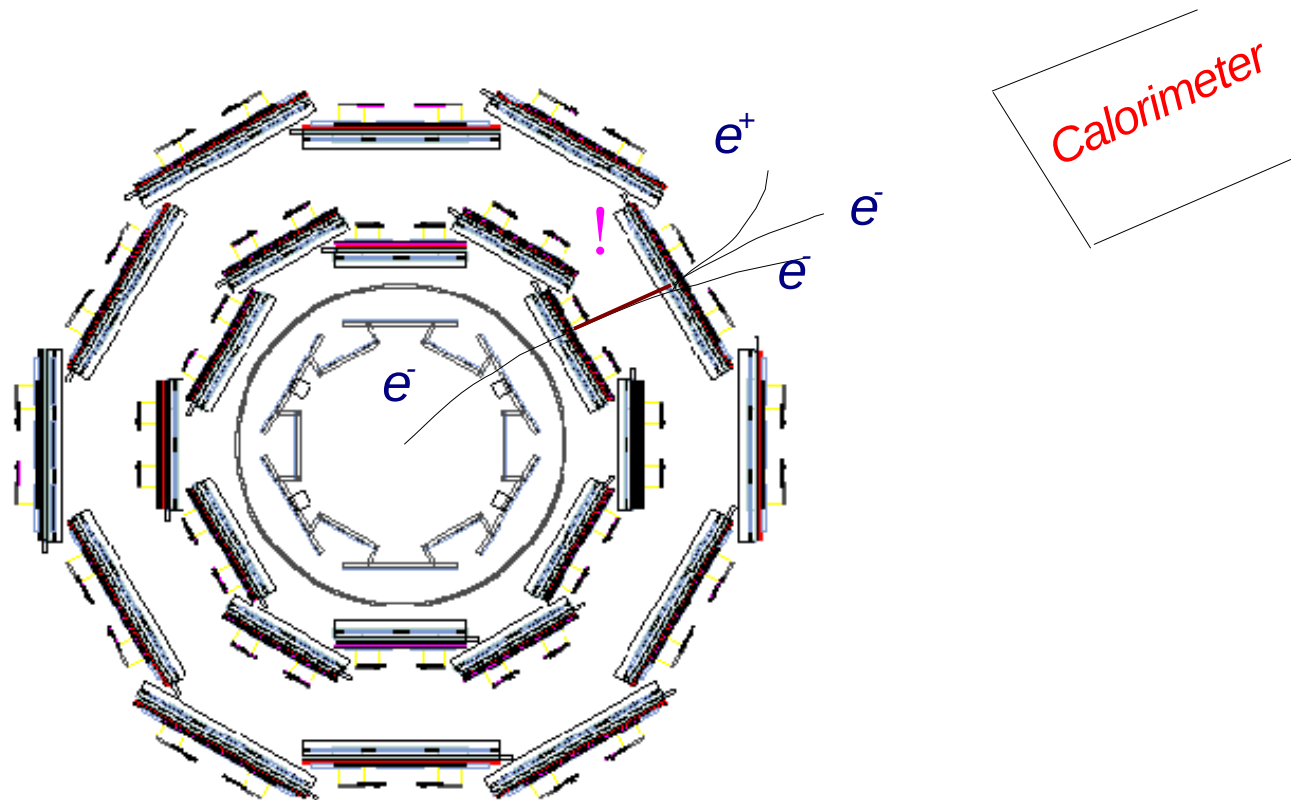
3-D Material Map in Simulation

- Built from detailed construction-level knowledge of inner tracker: silicon ladders, bulkheads, port-cards etc.

- Tuned based on studies of inclusive photon conversions

ϕ

- Radiation lengths *vs* (ϕ,z) at different radii shows localized nature of material distribution

Radius 4.09-4.54 cm

$\longleftarrow$ Z (cm) $\longrightarrow$

- Include dependence on type of material via Landau-Pomeranchuk-Migdal suppression of soft bremsstrahlung
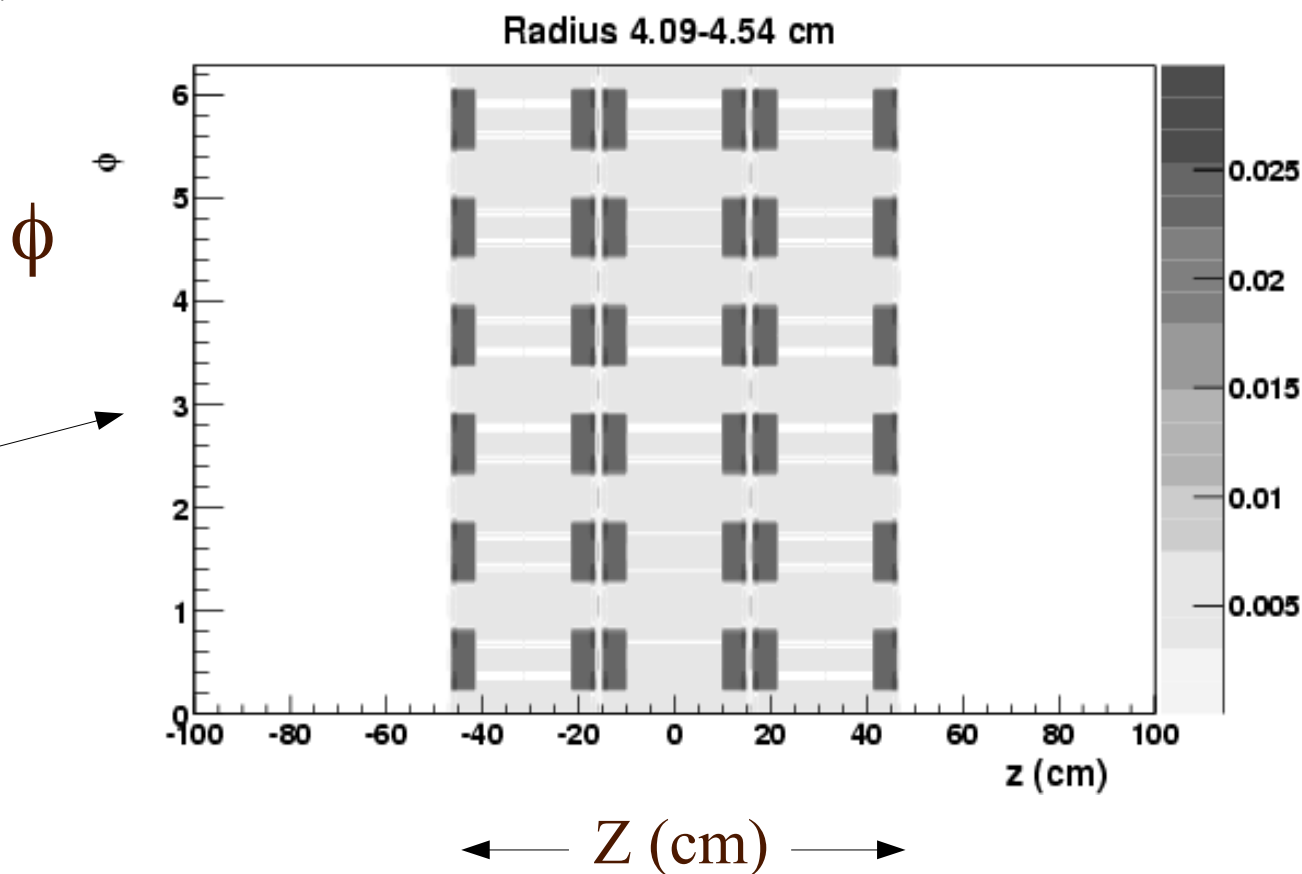
Tracking Momentum Scale

Tracking Momentum Scale

Set using J/ψ ⟶ μμ and ϒ ⟶ μμ resonance and Z ⟶ μμ masses

- Extracted by fitting J/ψ mass in bins of $1/p_T(\mu)$, and extrapolating momentum scale to zero curvature

- J/ψ ⟶ μμ mass independent of $p_T(\mu)$ after 2.6% tuning of energy loss

Fig. 2

J/ψ ⟶ μμ mass fit (bin 8)

$\chi^2/dof = 106 / 108$

Fig. S9
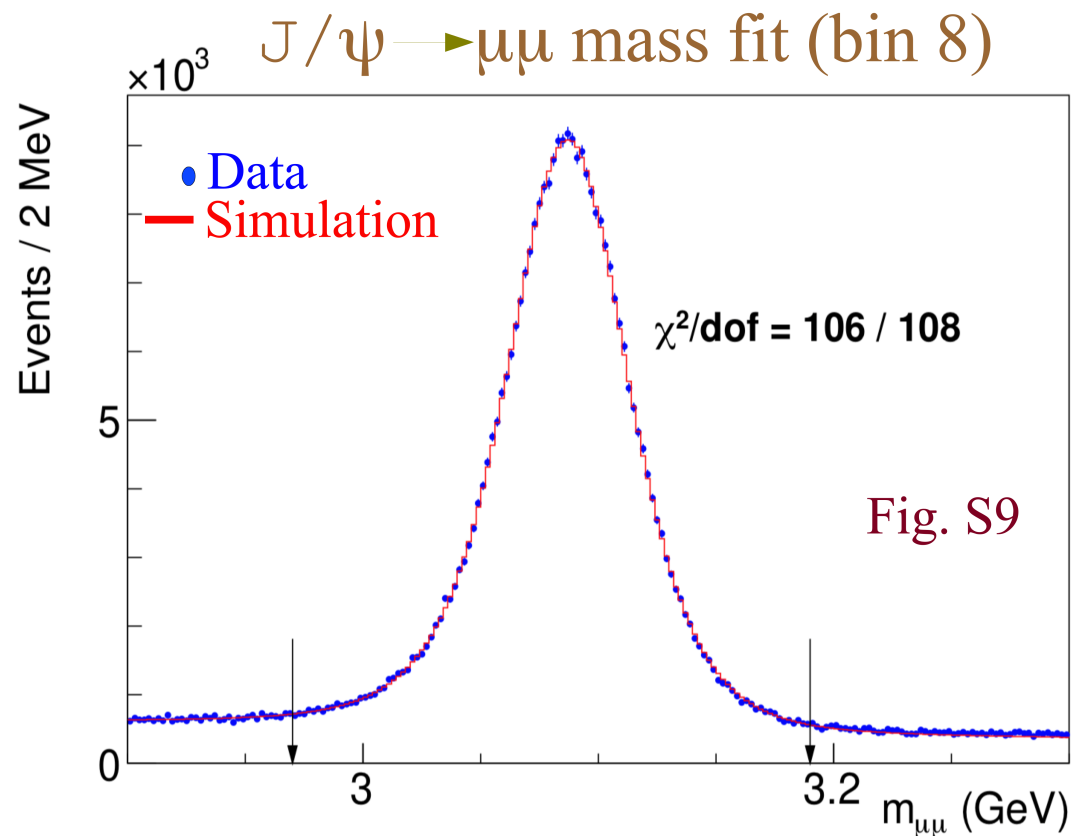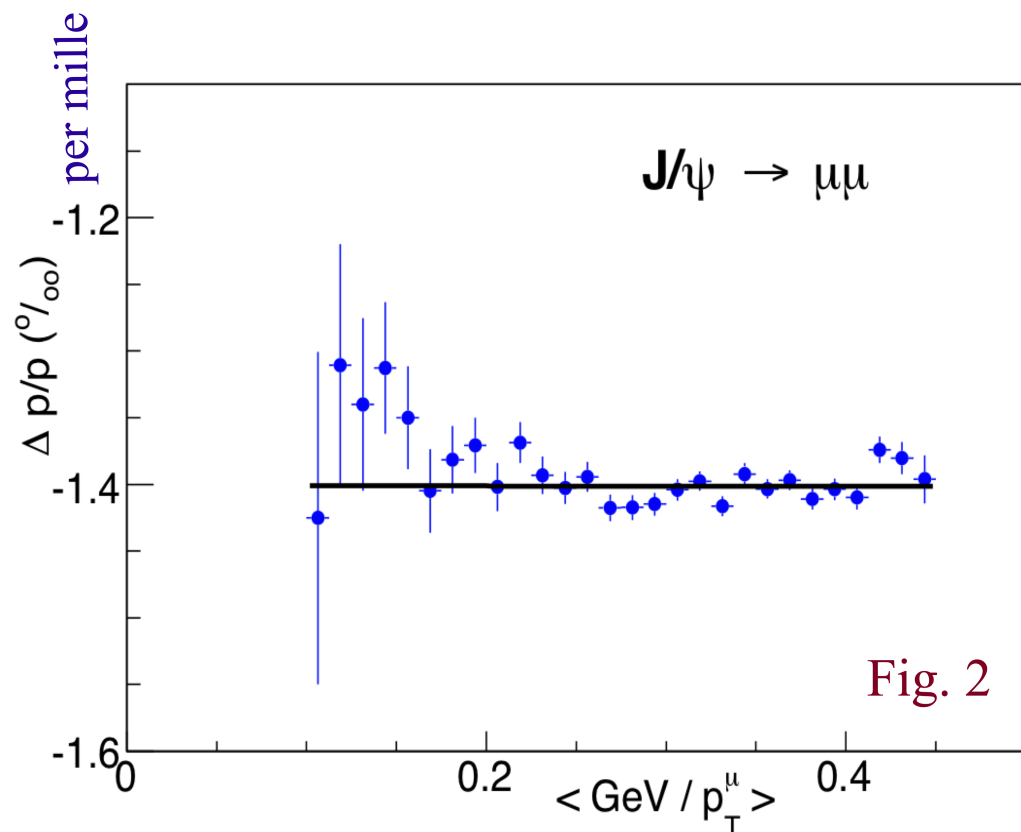
Tracking Momentum Scale

$\Upsilon \longrightarrow \mu\mu$ resonance provides

- Momentum scale measurement at higher p_T
- Validation of beam-constaining procedure (upsilons are promptly produced)
- Cross-check of non-beam-constrained (NBC) and beam-constrained (BC) fits

Fig. S12

$\Delta p/p = (-1371 \pm 13_{stat})$ ppm

$\chi^2/dof = 52 / 70$
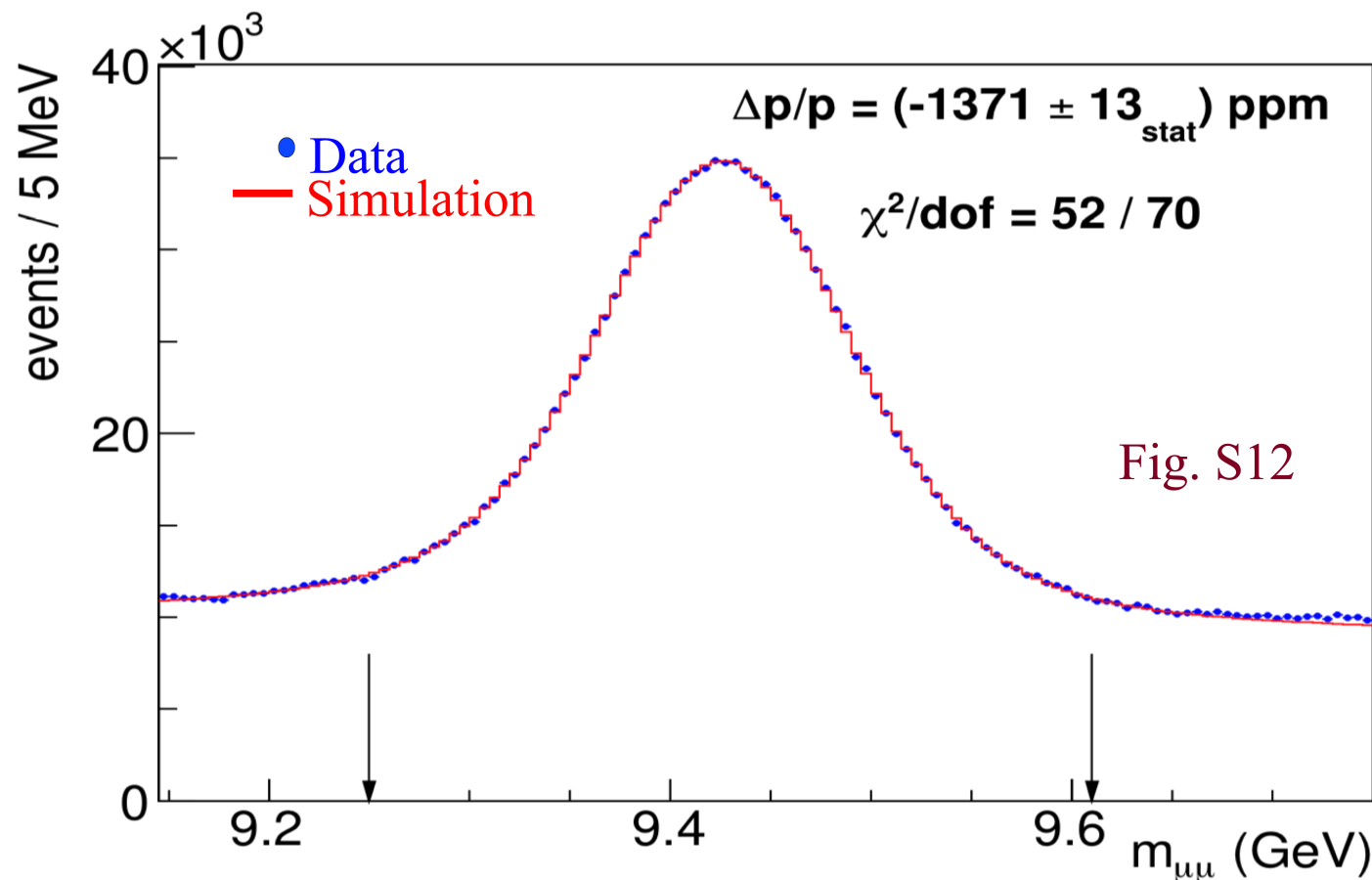
NBC $\Upsilon \longrightarrow \mu\mu$ mass fit

Tracking Momentum Scale

Υ ⟶ μμ resonance provides

– Cross-check of non-beam-constrained (NBC) and beam-constrained (BC) fits

– Consistent measurements after incorporating silicon detector passive energy loss in extrapolator code of track reconstruction

Fig. S12

BC Υ ⟶ μμ mass fit

Tracking Momentum Scale Systematics

Systematic uncertainties on momentum scale (parts per million)

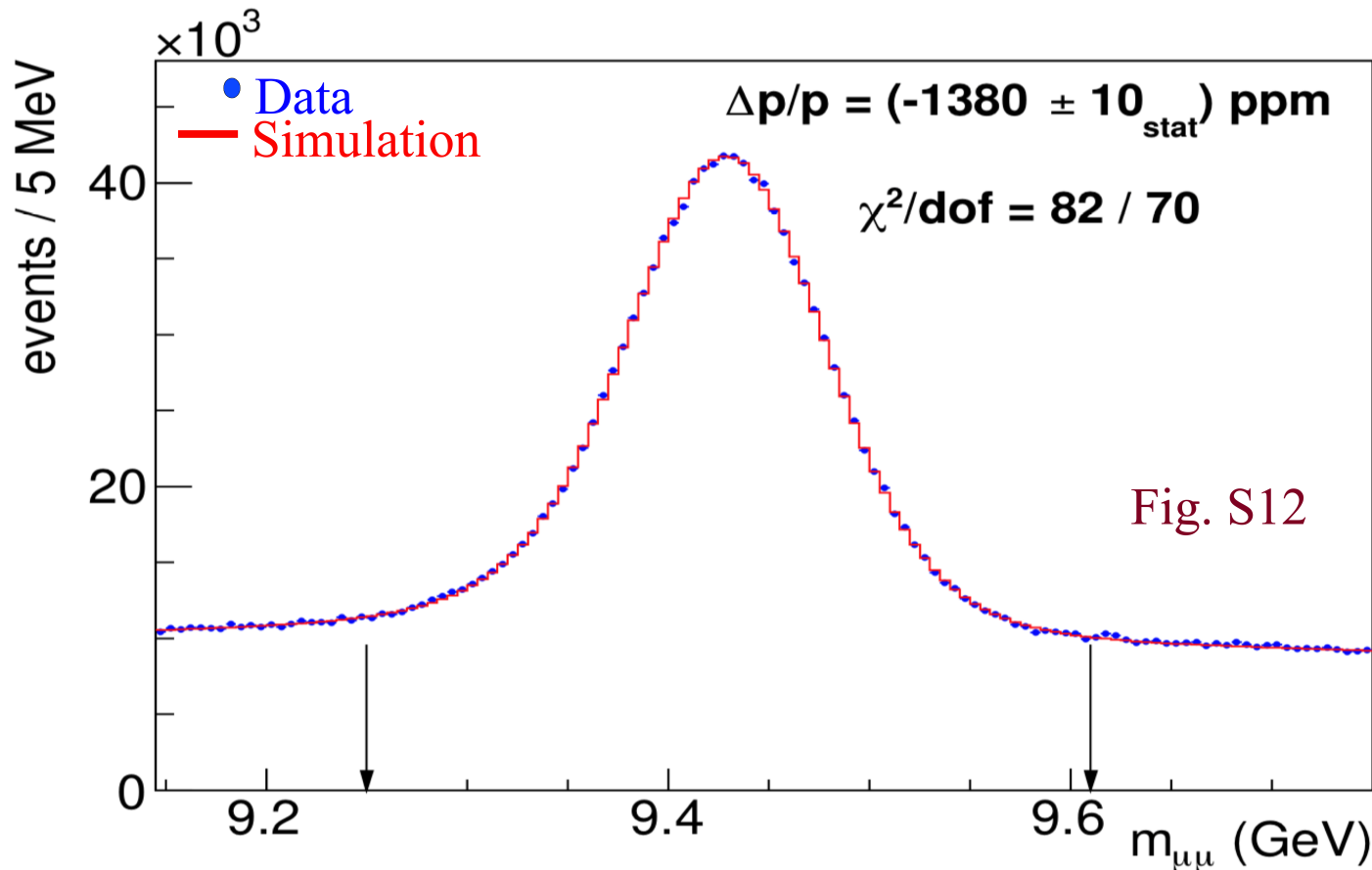| Source	J/ψ (ppm)	Υ (ppm)	Correlation (%)
QED	1	1	100
Magnetic field non-uniformity	13	13	100
Ionizing material correction	11	8	100
Resolution model	10	1	100
Background model	7	6	0
COT alignment correction	4	8	0
Trigger efficiency	18	9	100
Fit range	2	1	100
$\Delta p/p$ step size	2	2	0
World-average mass value	4	27	0
Total systematic	29	34	16 ppm
Statistical NBC (BC)	2	13(10)	0
Total	29	36	16 ppm

Table S2

$\Delta M_{W,Z} = 2$ MeV

Uncertainty dominated by magnetic field non-uniformity, passive material energy loss, low p_T modeling and Υ mass world average

$Z \rightarrow \mu\mu$ Mass Cross-check & Combination

- Using the J/ψ and Υ momentum scale, performed "blinded" measurement of Z boson mass

  – Z mass consistent with PDG value (91188 MeV) (0.7σ statistical)

  – $M_Z = 91192.0 \pm 6.4_{stat} \pm 2.3_{momentum} \pm 3.1_{QED} \pm 1_{alignment}$ MeV

Fig. 3

$M(\mu\mu)$ (GeV)
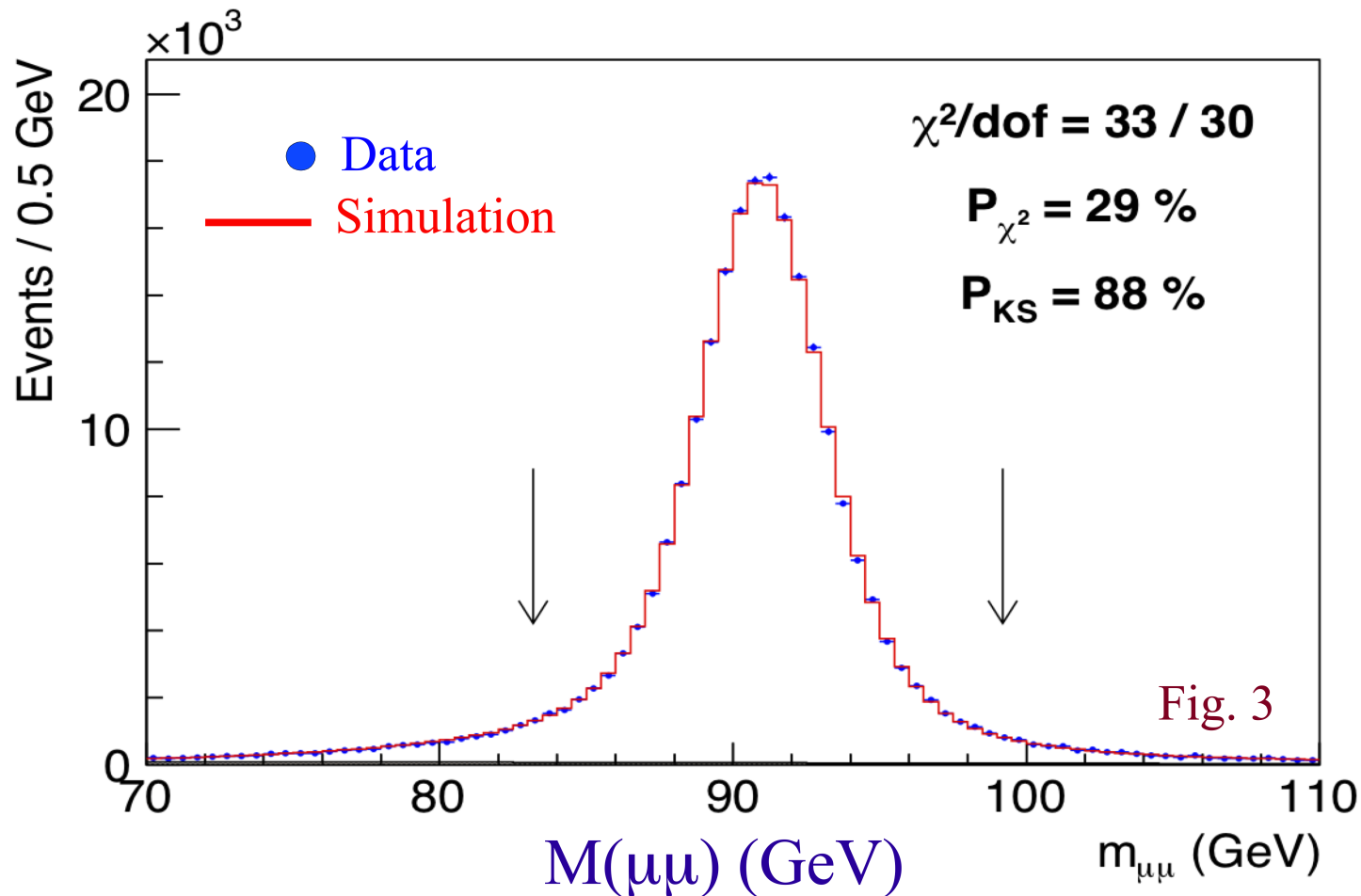
Tracker Linearity Cross-check & Combination

- Final calibration using the J/ψ, ϒ and Z bosons for calibration

- Combined momentum scale correction :

$$\Delta p/p = (-1389 \pm 25_{syst})\ \text{parts per million}$$
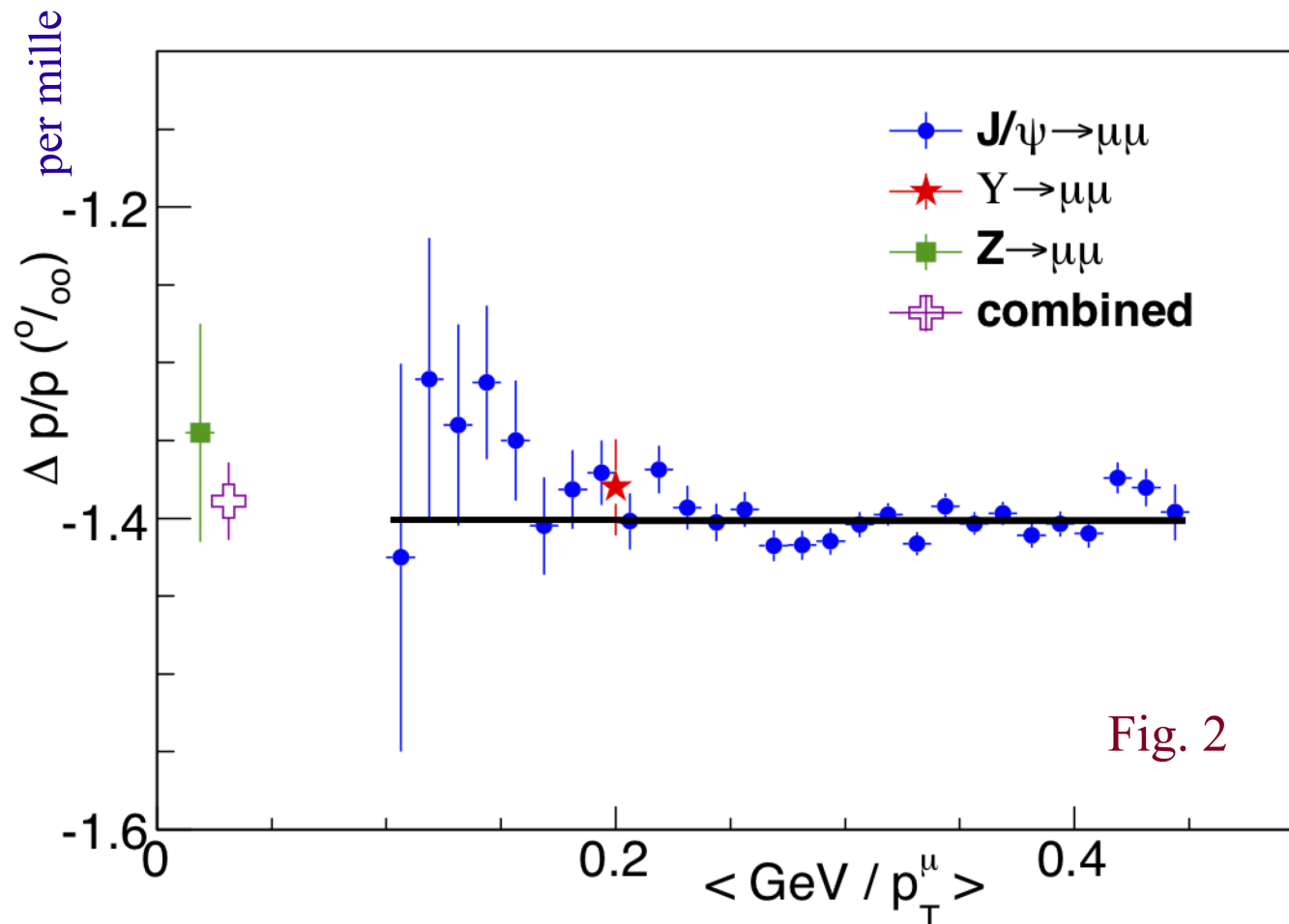
$$\Delta M_W = 2\ \text{MeV}$$

Fig. 2

EM Calorimeter Response

Calorimeter Simulation for Electrons and Photons

- Distributions of lost energy calculated using detailed GEANT4 simulation of calorimeter, tuned on data

    – Leakage into hadronic calorimeter

    – Absorption in the coil

    – Dependence on incident angle and E_T

  (AVK & CH, *NIM A* 729 (2013) pp 25-35)
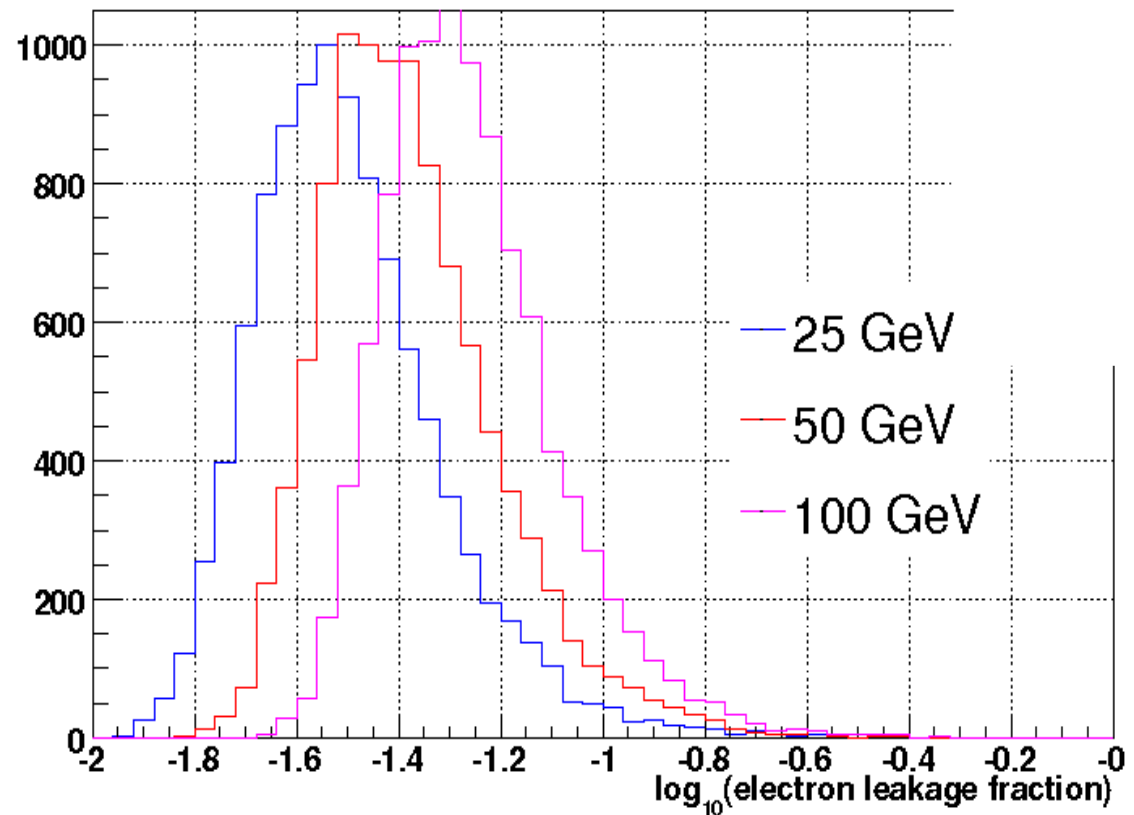
- Energy-dependent gain (non-linearity) parameterized and fit from data

- Energy resolution: fixed sampling term and tunable constant term

    – Constant terms are fit from the width of E/p peak and Z→ee mass peak

EM Calorimeter Scale

- E/p peak from $W \rightarrow e\upsilon$ decays provides measurements of EM calorimeter scale and its (E_T-dependent) non-linearity

$$\Delta S_E = (43_{stat} \pm 30_{non-linearity} \pm 34_{X0} \pm 45_{Tracker}) \texttt{ parts per million}$$

Setting S_E to 1 using E/p calibration from combined $W \rightarrow e\upsilon$ and $Z \rightarrow ee$ samples

$\Delta M_W = 6$ MeV

$\Delta S_E = 12 \pm 43_{stat}$ ppm

$\chi^2/dof = 39 / 33$

$P_{\chi^2} = 21 \%$

$P_{KS} = 69 \%$

● Data

— Simulation

Low tail used for tuning calorimeter thickness

Fig. 2

High tail of used for tuning model of radiative material

E_{CAL} / p_{track}
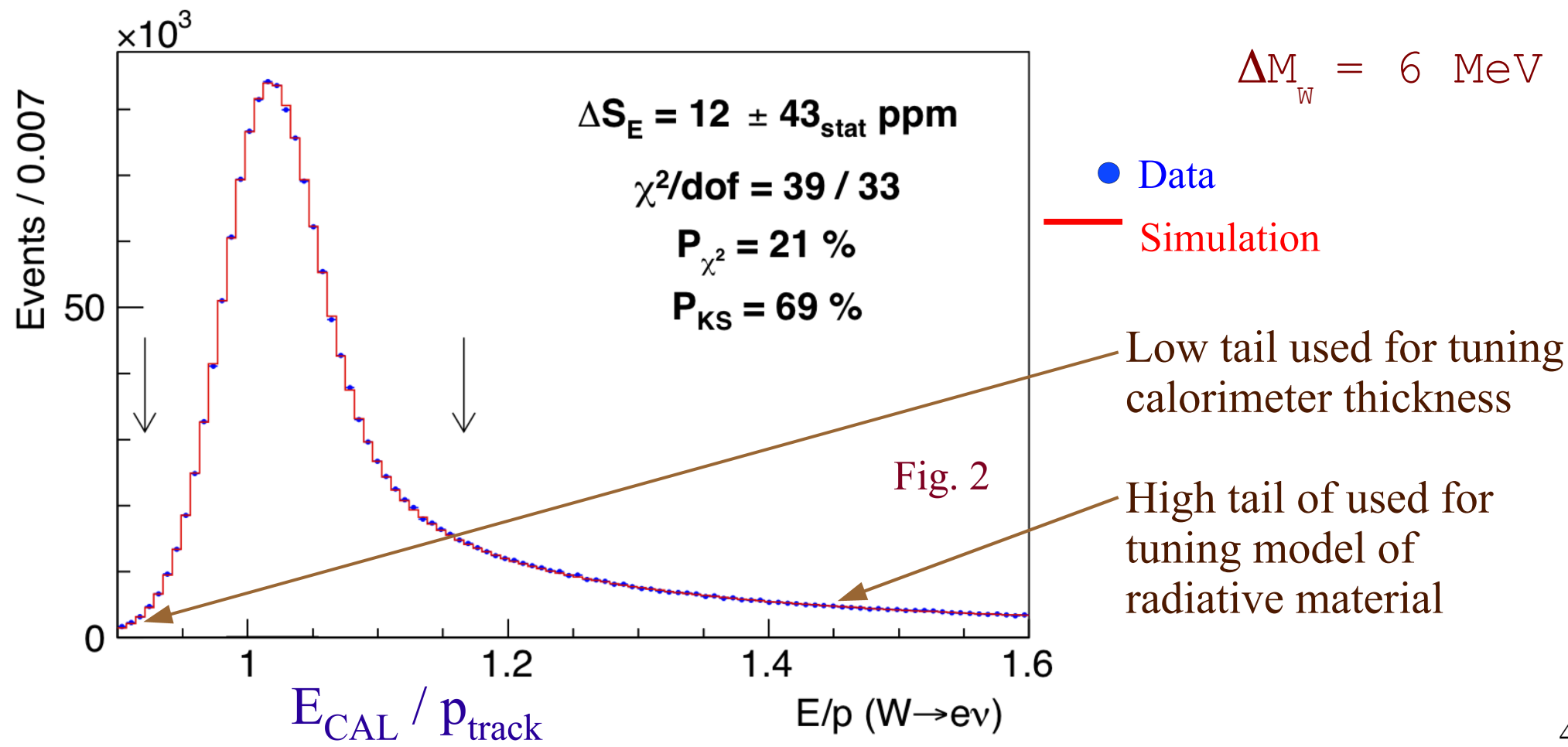
Consistency of Radiative Material Model

- Excellent description of E/p spectrum tail

- radiative material tune factor: $S_{X0} = 1.049 \pm 0.002$ achieves consistency with E/p spectrum tail

$$\Delta S_{mat} = 0.05 \pm 0.16_{stat} \%$$

$$\chi^2/dof = 3.1 / 2$$

$$P_{\chi^2} = 20 \%$$

Default energy loss * 1.049

Fig. S14

Data
— Simulation

E_{CAL} / p_{track}

$E/p \ (W \rightarrow e\nu)$
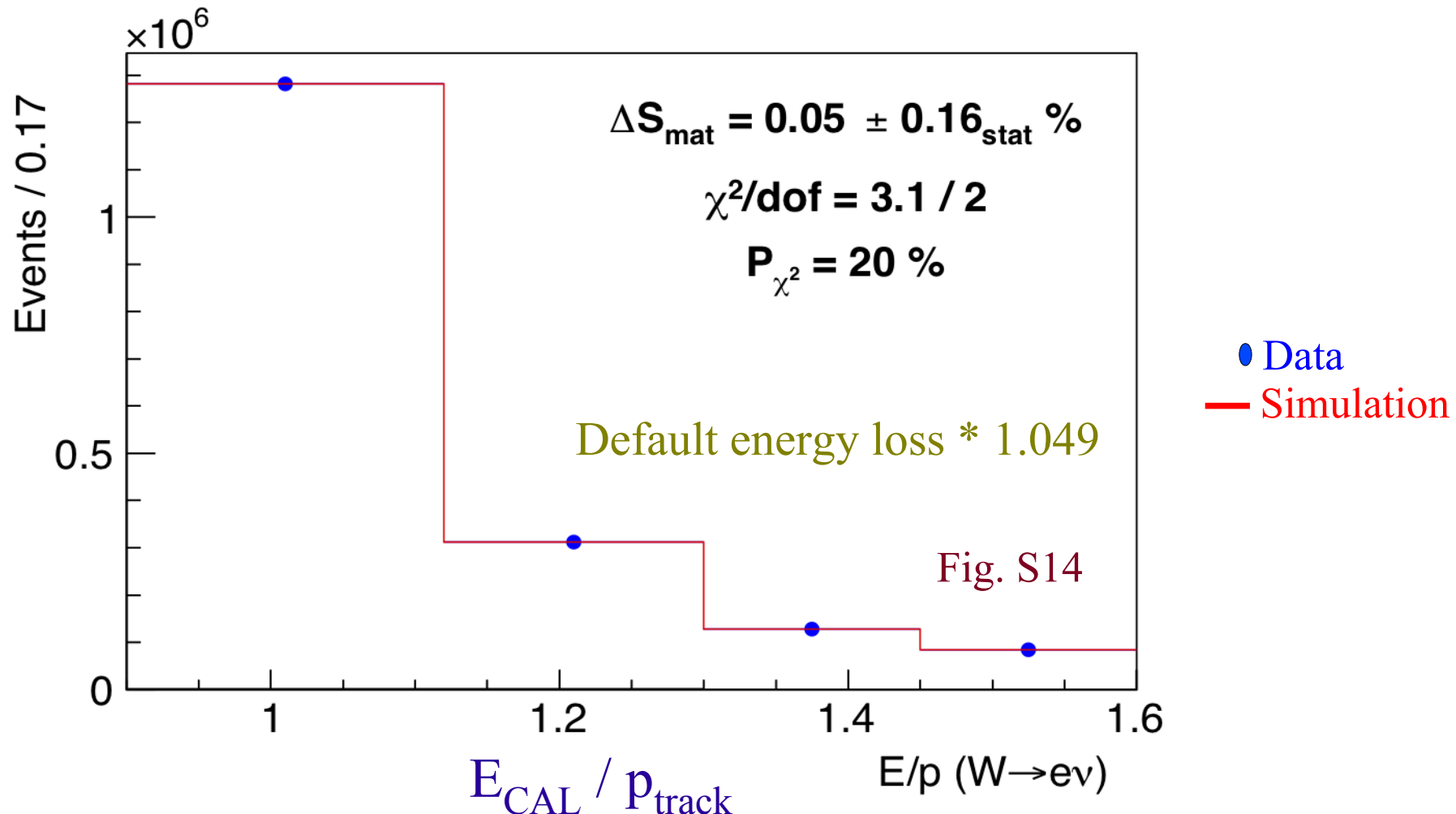
Measurement of EM Calorimeter Non-linearity

- Perform E/p fit-based calibration in bins of electron E_T

- GEANT-motivated parameterization of non-linear response:
$$S_E = 1 + \beta \log(E_T / 39 \text{ GeV})$$

- Tune on W and Z data: $\beta = (7.2 \pm 0.4_{stat}) \times 10^{-3}$

    => $\Delta M_W = 2$ MeV
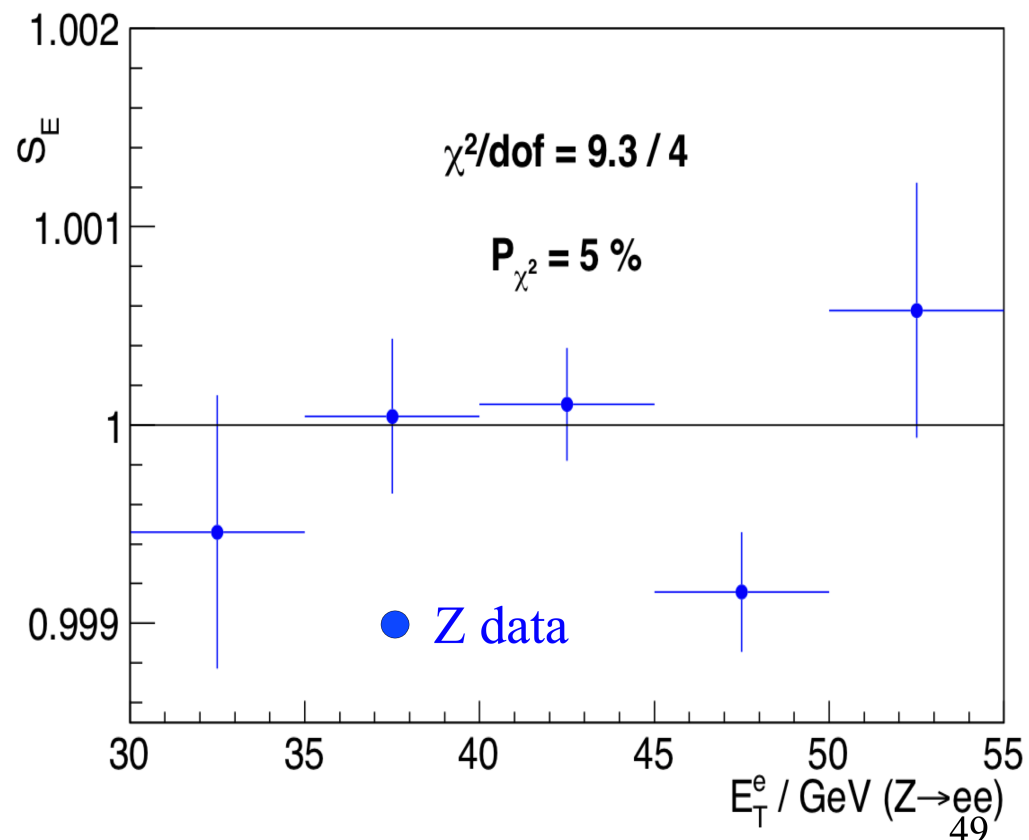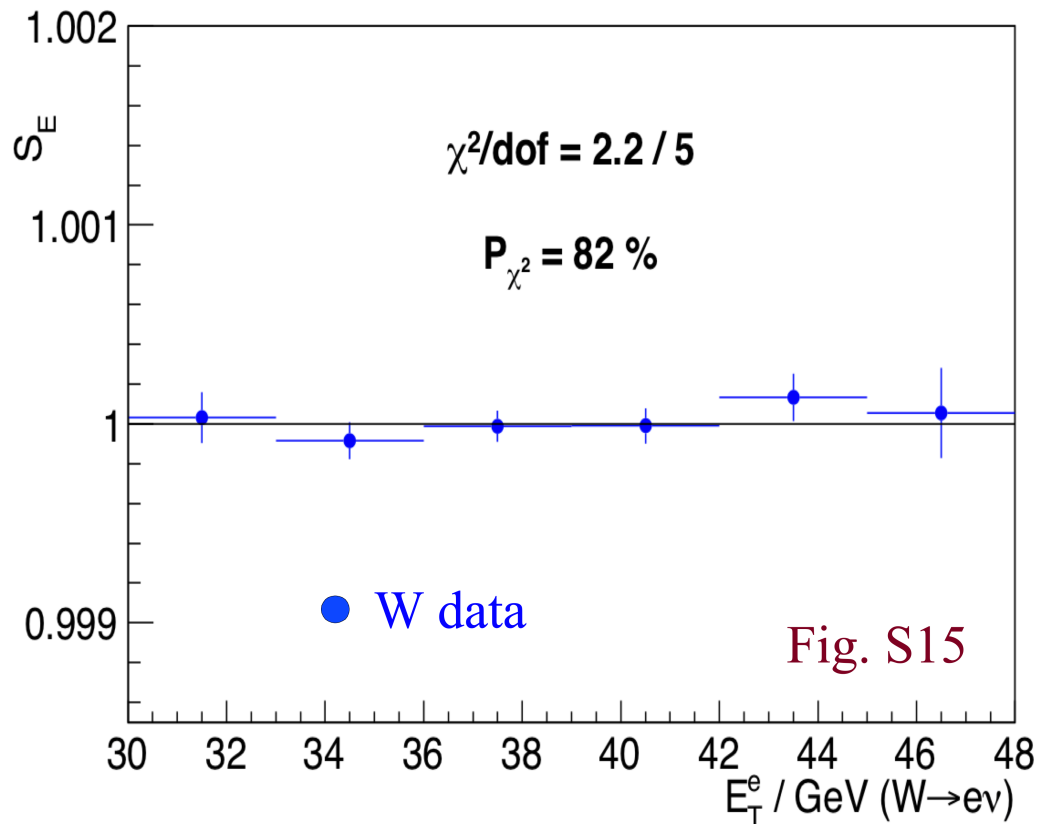
Fig. S15

EM Calorimeter Uniformity

- Checking uniformity of energy scale in bins of electron pseudo-rapidity

Fig. S13
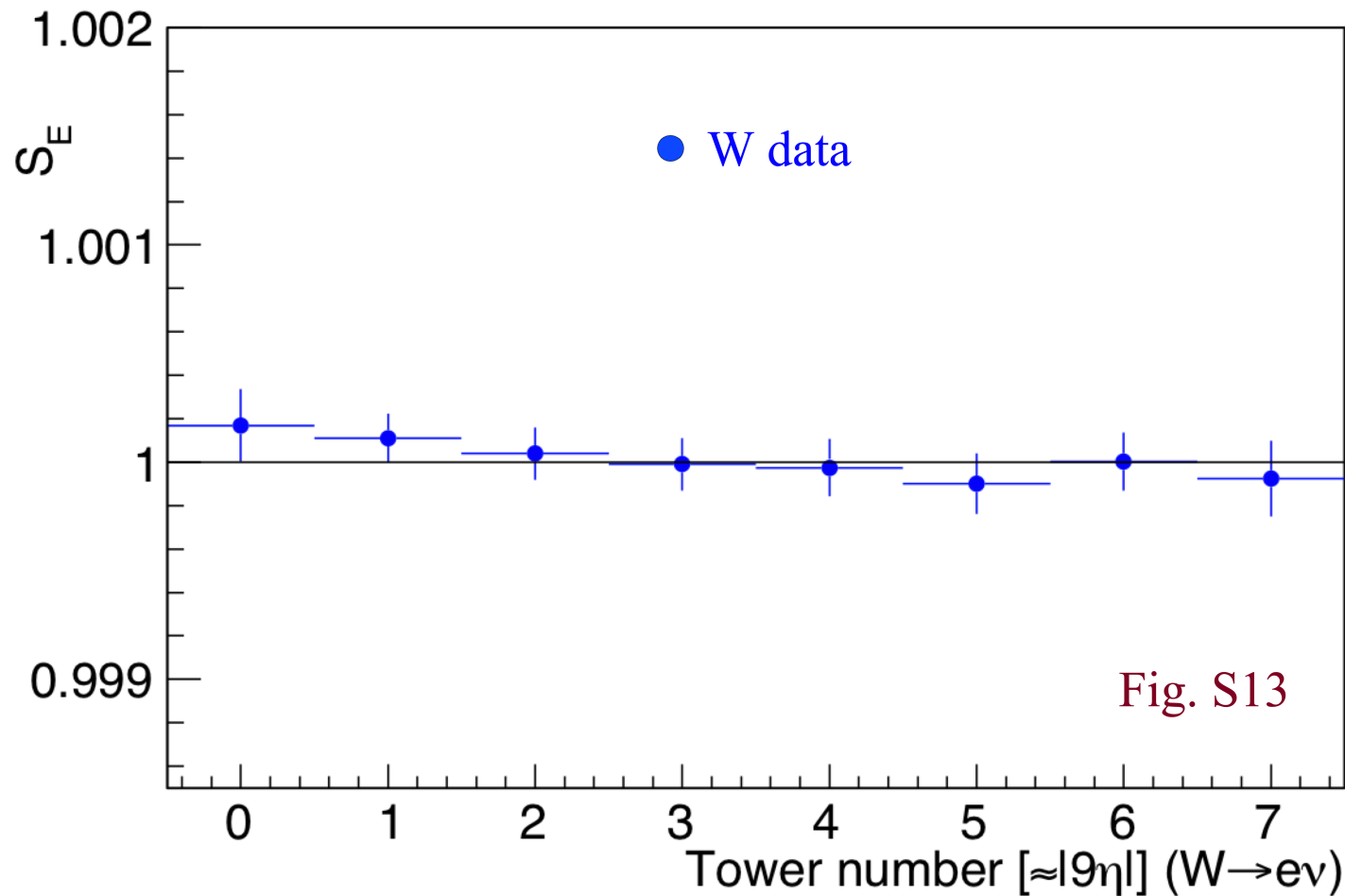
$Z \rightarrow ee$ Mass Cross-check and Combination

- Performed "blind" measurement of Z mass using E/p-based calibration

  - Consistent with PDG value (91188 MeV) within 0.5σ (statistical)

  - $M_Z = 91194.3 \pm 13.8_{stat} \pm 6.5_{calorimeter} \pm 2.3_{momentum} \pm 3.1_{QED} \pm 0.8_{alignment}$ MeV

- Combine E/p-based calibration with $Z \rightarrow ee$ mass for maximum precision

Fig. 3
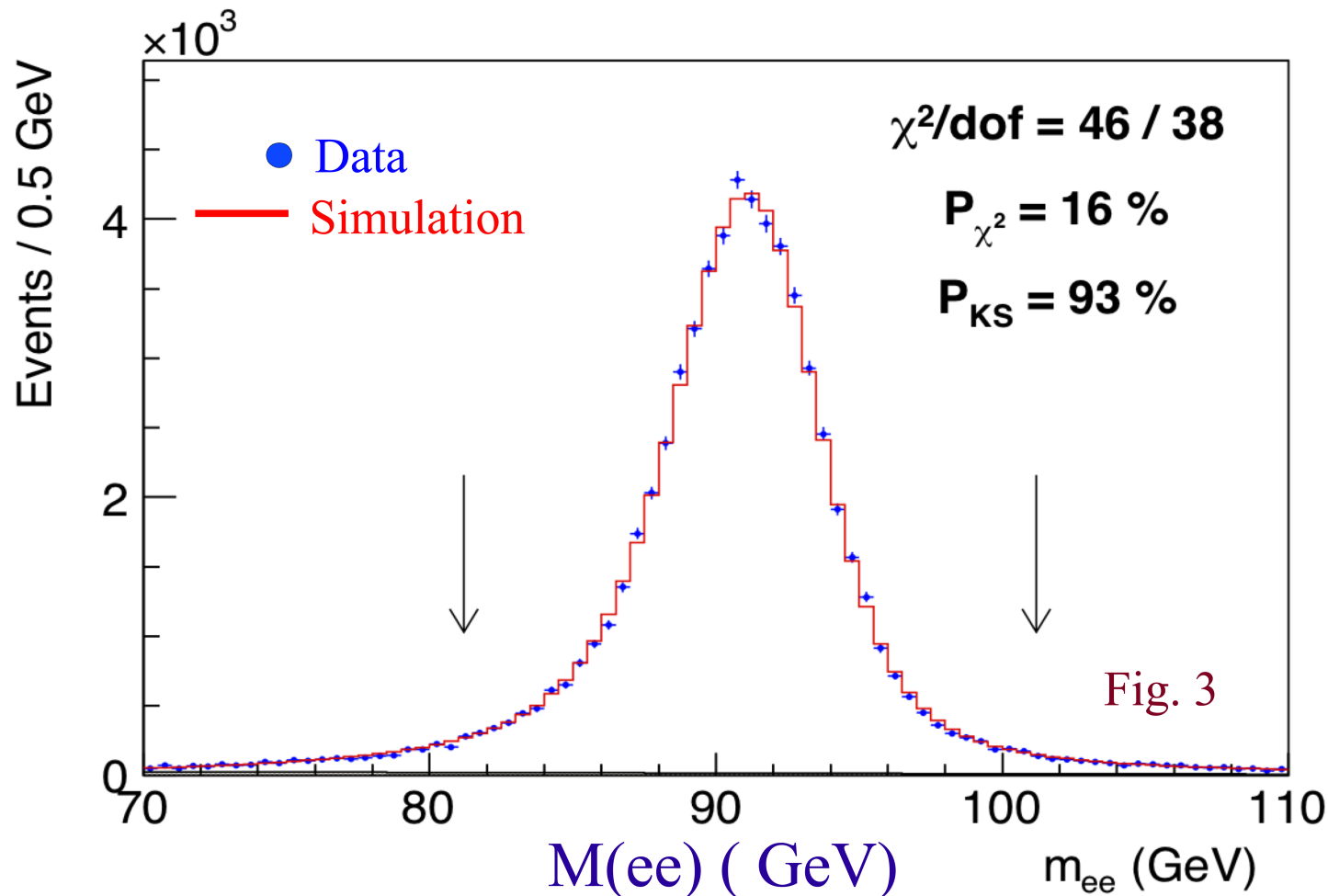
$\Delta M_W = 5.8$ MeV

$\Delta S_E = -14 \pm 72$ ppm

Z →ee Mass Cross-check using Electron Tracks

- Performed "blind" measurement of Z mass using electron tracks, separately for radiative/non-radiative pairs

  – Consistent with PDG value

- Checks tracking for electrons vs muons, and model of radiative energy loss

Fig. S16

$\chi^2/dof = 62 / 58$

$P_{\chi^2} = 31\ \%$

$P_{KS} = 95\ \%$

● Data
— Simulation

$(E/p)_1 < 1.1$ &
$(E/p)_2 > 1.1$

Track M(ee) (GeV)   track m_{ee} (GeV)

$Z \rightarrow ee$ Mass Cross-check using Electrons

- Performed "blind" measurement of Z mass using electron clusters and tracks, separately for radiative/non-radiative pairs

  - Consistent with PDG value

- Checks tracking for electrons vs muons, and model of radiative energy loss

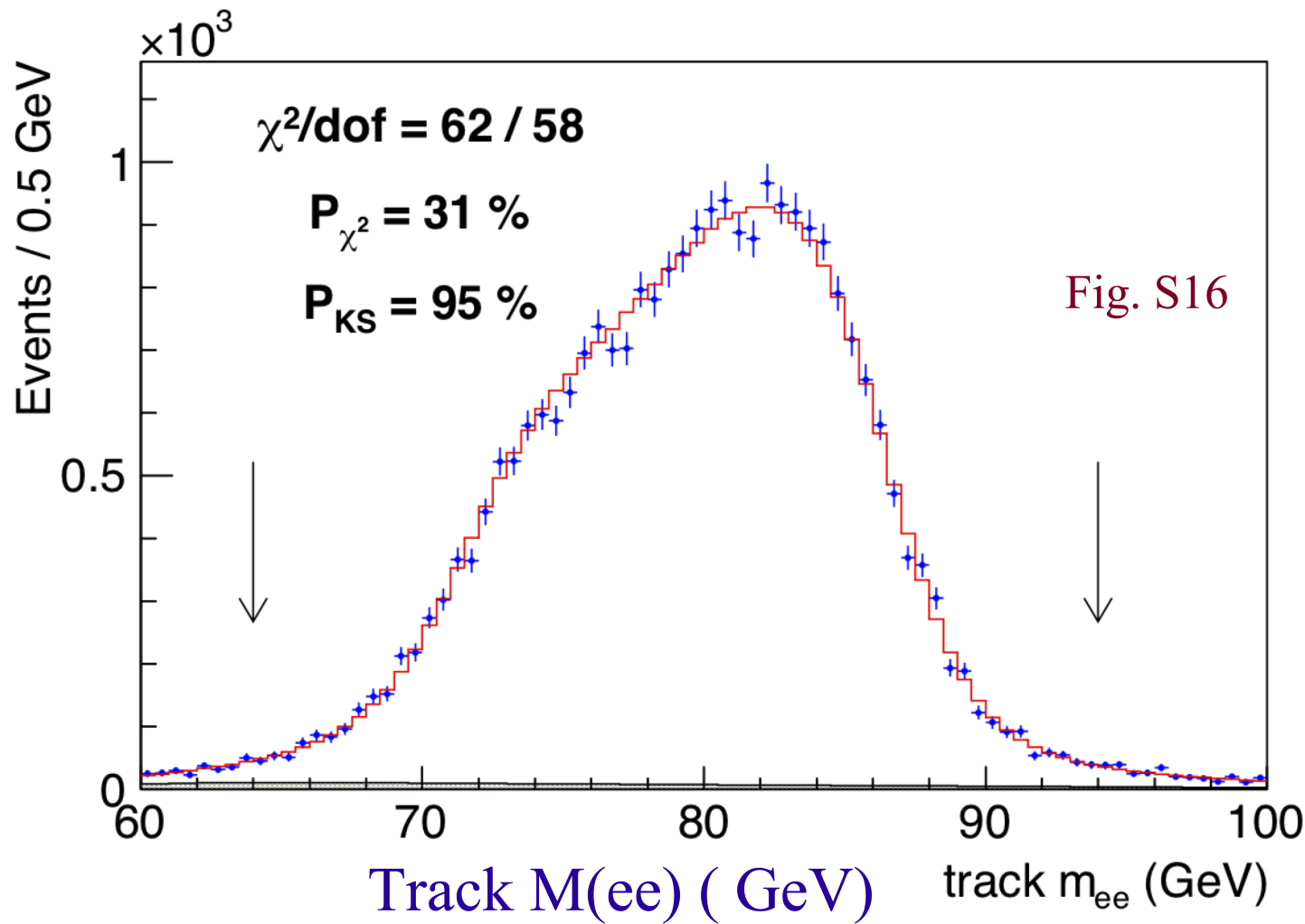| Electrons	Calorimeter	Track
$E/p < 1.1$ only	$91\,190.9 \pm 19.7$	$91\,215.2 \pm 22.4$
$E/p > 1.1$ and $E/p < 1.1$	$91\,201.1 \pm 21.5$	$91\,259.9 \pm 39.0$
$E/p > 1.1$ only	$91\,184.5 \pm 46.4$	$91\,167.7 \pm 109.9$

Table S4

Lepton Resolutions

- Tracking resolution parameterized in the custom simulation by

  - Radius-dependent drift chamber hit resolution $\sigma_h \sim (150 \pm 1_{stat})\ \mu m$

  - Beamspot size $\sigma_b = (36.0 \pm 0.5_{stat})\ \mu m$

  - Tuned on the widths of the $Z \rightarrow \mu\mu$ (beam-constrained) and $\Upsilon \rightarrow \mu\mu$ (both beam constrained and non-beam constrained) mass peaks

    $$\Rightarrow \Delta M_W = 0.3\ \text{MeV (muons)}$$

- Electron cluster resolution parameterized in the custom simulation by

  - $12.6\% / \sqrt{E_T}$ (sampling term)

  - constant term $\kappa = (0.73 \pm 0.02_{stat})\ \%$

  - Tuned on the widths of the E/p peak and the $Z \rightarrow ee$ peak (selecting radiative electrons)

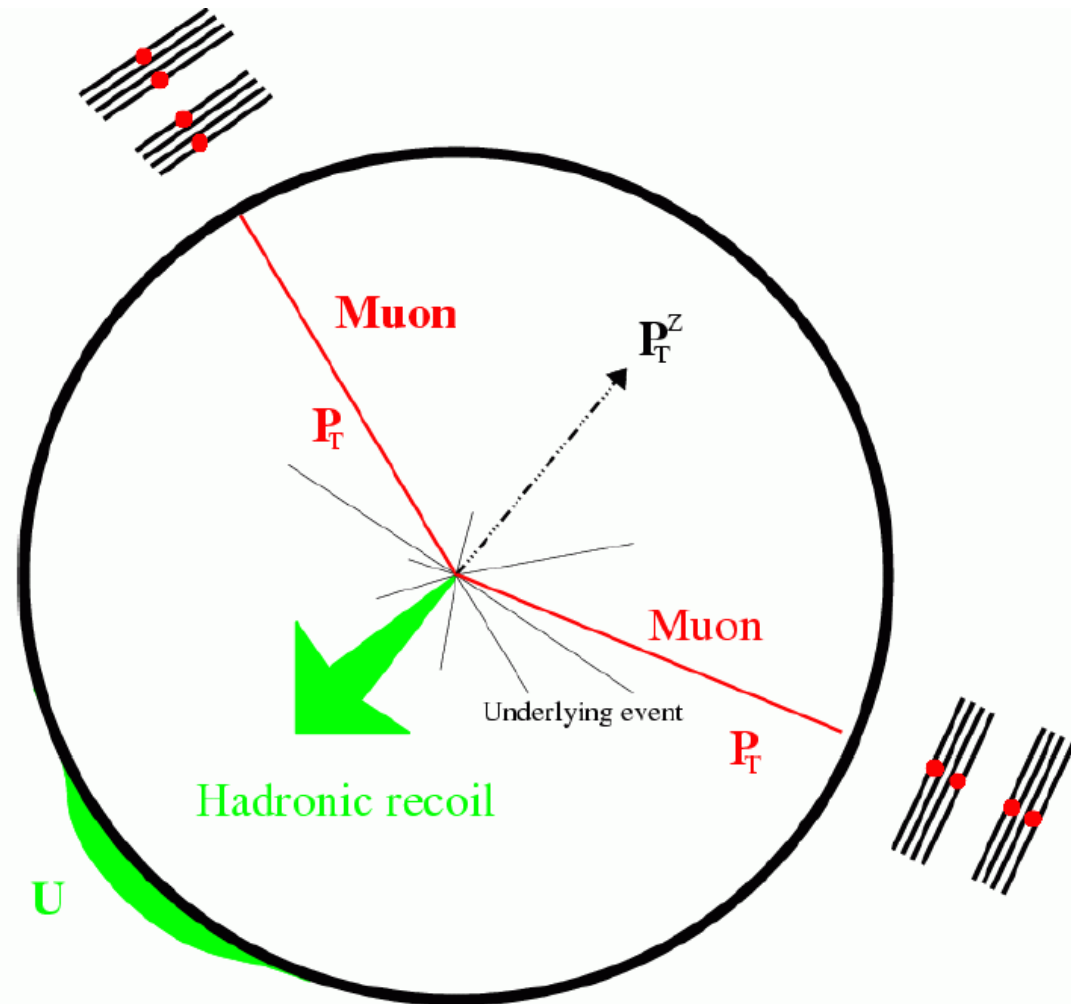 $$\Rightarrow \Delta M_W = 0.9\ \text{MeV (electrons)}$$

Hadronic Recoil Model

Constraining the Hadronic Recoil Model

Exploit similarity in production and decay of *W* and *Z* bosons

Detector response model for hadronic recoil tuned using p_T-balance in $Z \longrightarrow ll$ events

Transverse momentum of Hadronic recoil (***u***) calculated as 2-vector-sum over calorimeter towers

Lepton Tower Removal

Lepton

Lepton towers
(excluded from
recoil)

Recoil

- We remove the calorimeter towers containing lepton energy from the hadronic recoil calculation

  – Lost underlying event energy is measured in φ-rotated windows in W boson data

$$\Delta M_W = 1 \text{ MeV}$$

Figs. S17 & S18

Electron Electromagnetic E_T (MeV)

Tower Δη						
3	61	61	62	63	62	61	61
2	62	61	62	69	64	62	61
1	63	63	66	1227	90	64	63
0	63	66	79	38534	176	68	64
-1	61	61	62	178	67	61	61
-2	61	61	61	63	62	61	61
-3	60	61	61	61	61	61	61

Tower Δφ: -3 -2 -1 0 1 2 3

Muon Electromagnetic E_T (MeV)

Tower Δη						
3	60	60	60	61	60	60	60
2	59	59	60	62	61	59	59
1	61	61	62	82	66	61	61
0	61	61	63	378	70	62	61
-1	59	60	61	67	62	60	60
-2	59	59	60	61	61	60	59
-3	60	60	60	61	61	60	60

Tower Δφ: -3 -2 -1 0 1 2 3
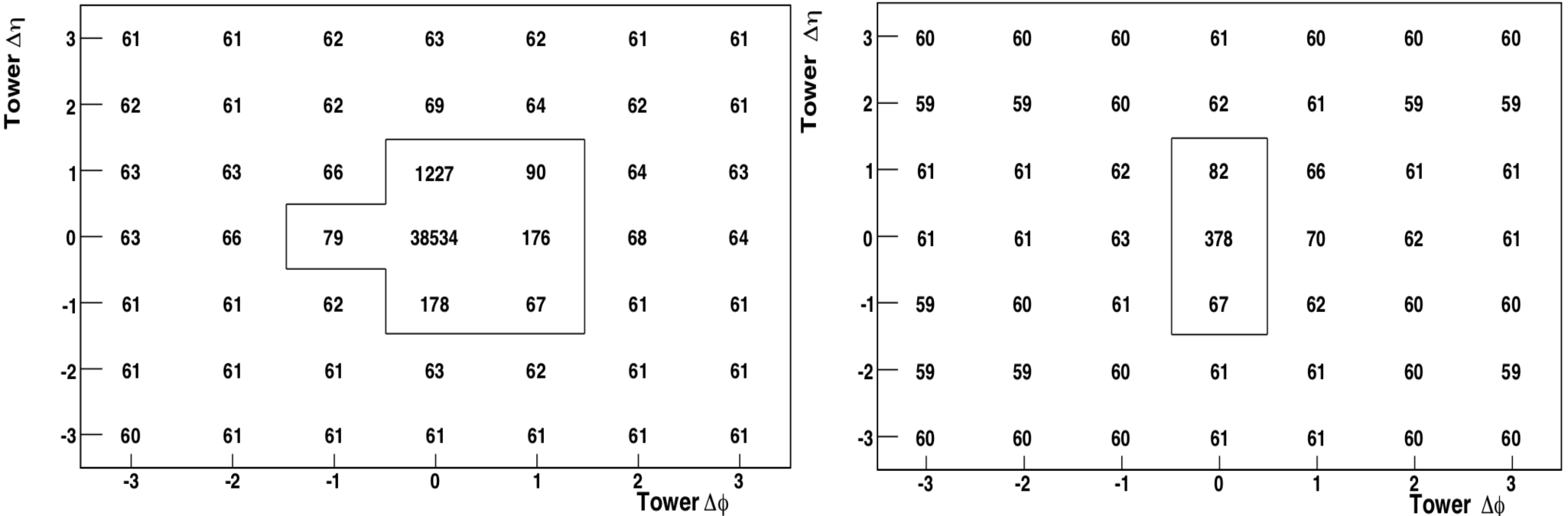
Lepton Tower Removal
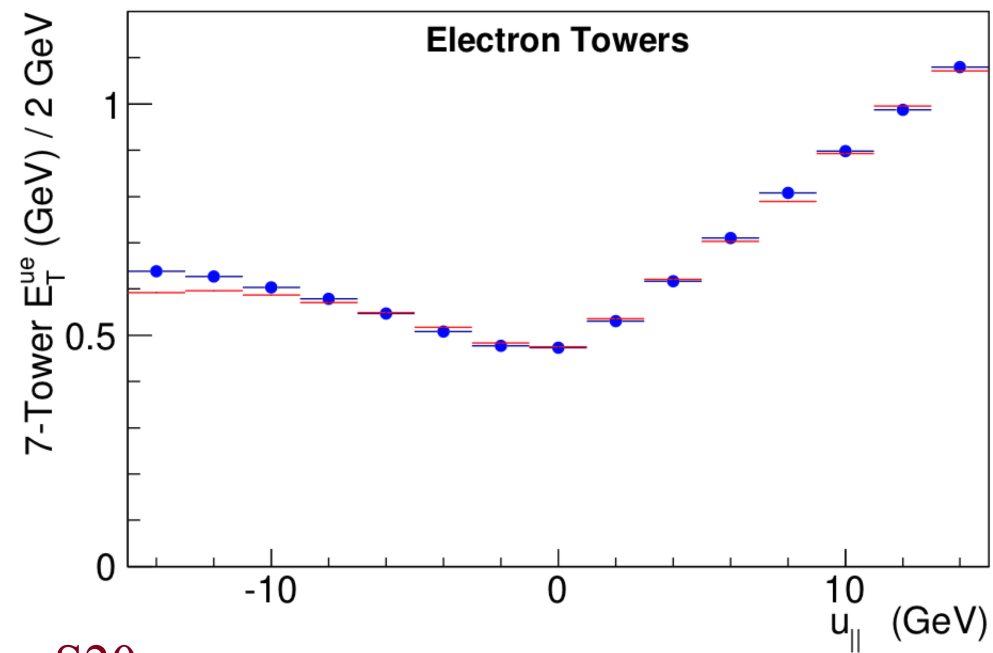
Fig. S20

Constraining the Hadronic Recoil Model

Exploit similarity in production and decay of *W* and *Z* bosons

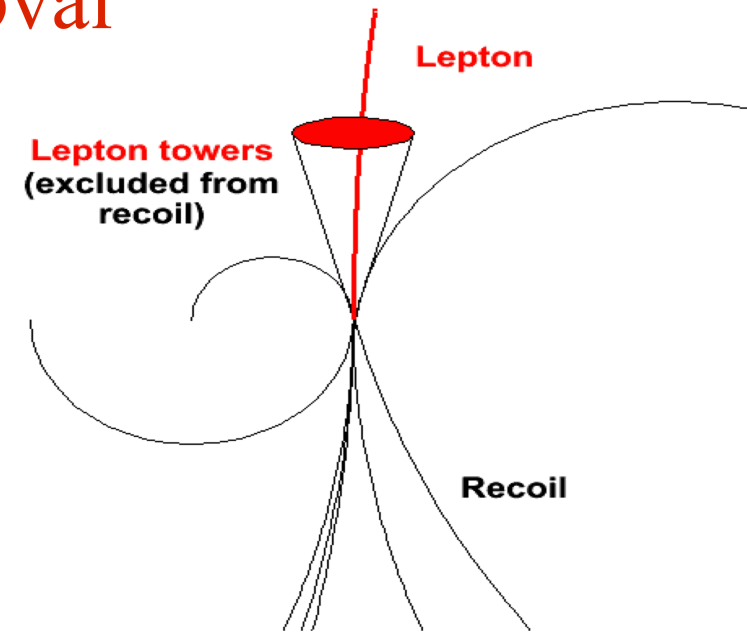Detector response model for hadronic recoil tuned using p_T-balance in $Z \rightarrow ll$ events

Transverse momentum of Hadronic recoil (***u***) calculated as 2-vector-sum over calorimeter towers
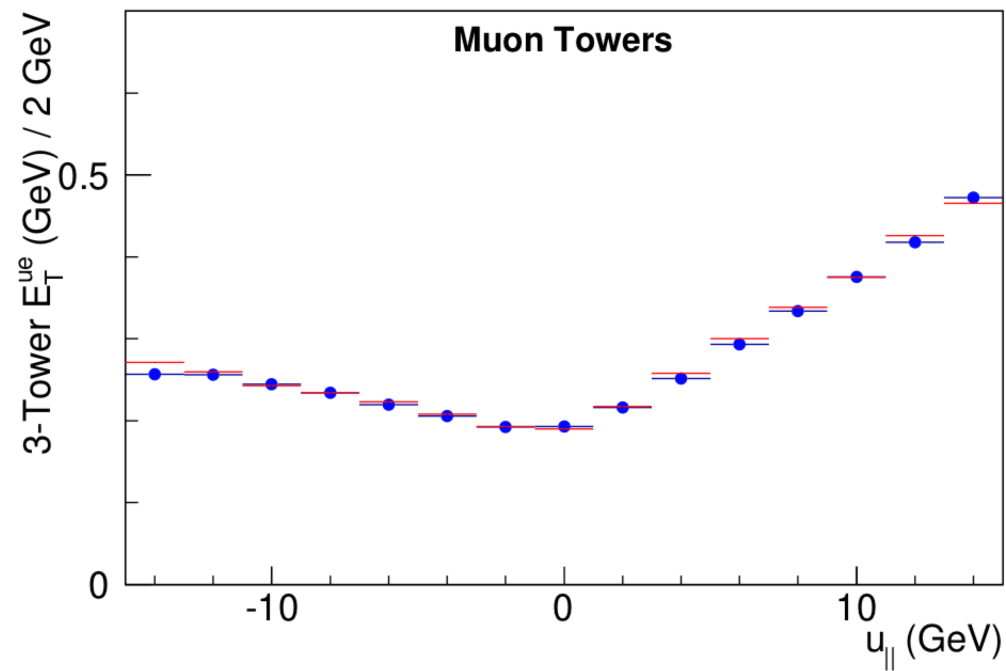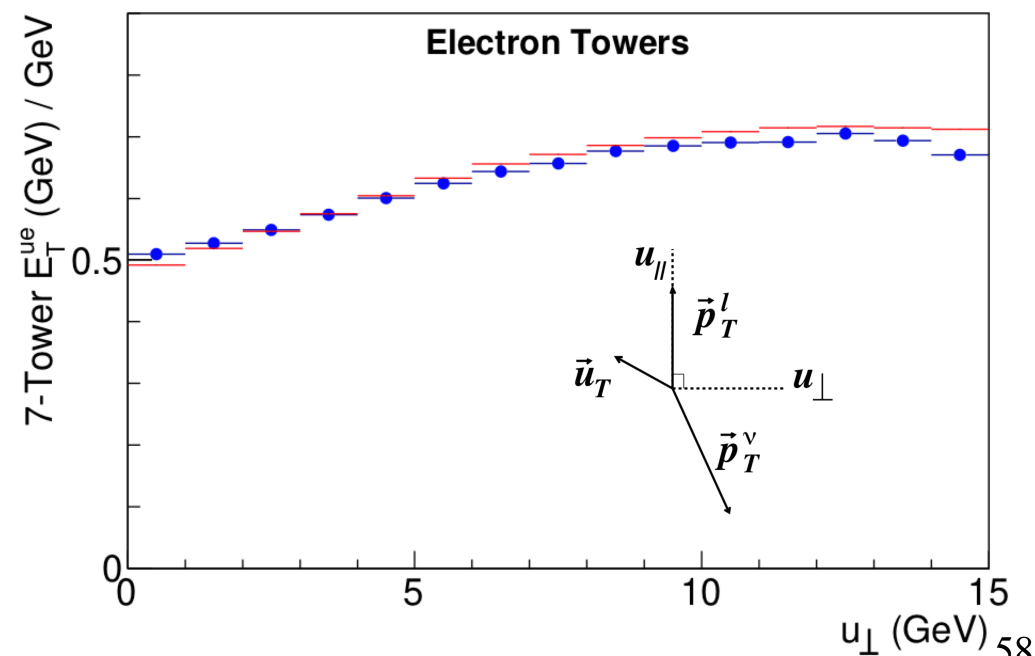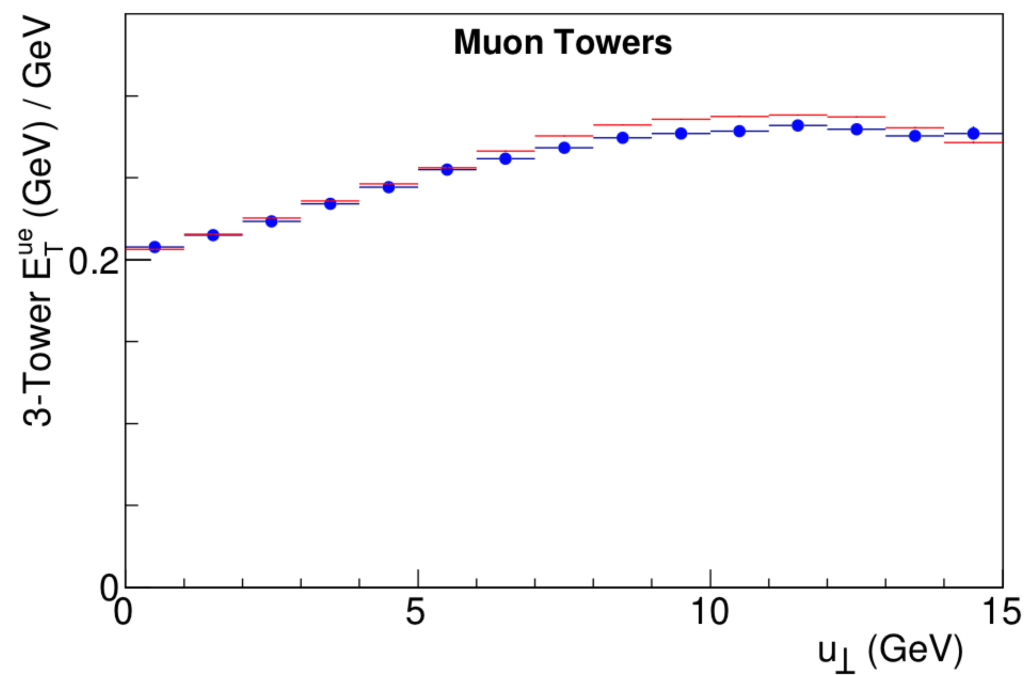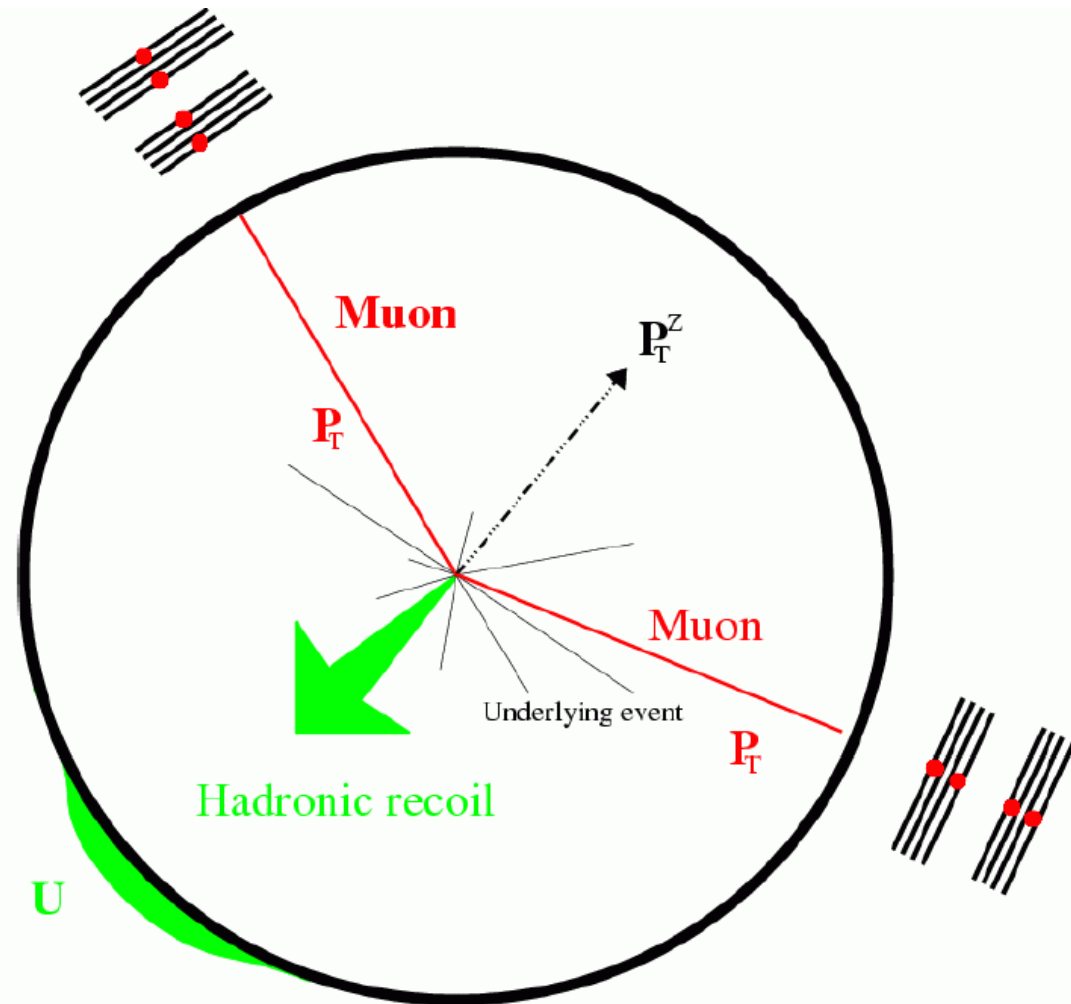
Hadronic Recoil Simulation

Recoil momentum 2-vector $\boldsymbol{u}$ has

- a soft 'spectator interaction' component, randomly oriented
  - Modeled using minimum-bias data with tunable magnitude
- A hard 'jetty' component, directed opposite the boson p_T

  - P_T-dependent response and resolution parameterizations

  - Hadronic response $R = \boldsymbol{u}_{\text{reconstructed}} / \boldsymbol{u}_{\text{true}}$ parameterized as a logarithmically increasing function of boson p_T motivated by Z boson data

Fig. S22

Project the vector sum of $p_T(ll)$ and $\boldsymbol{u}$ on a set of orthogonal axes defined by boson p_T

Mean and rms of projections as a function of $p_T(ll)$ provide information on hadronic model parameters

FIG. S3: (left) Sketches of typical transverse vectors associated to quantities reconstructed in a W-boson event, with the recoil hadron momentum $(\vec{u}_T)$ separated into axes parallel $(u_{||})$ and perpendicular $(u_\perp)$ to the charged lepton. (right) Illustration of the η and ξ axes in Z boson events.

Tuning Recoil Response Model with *Z* events

Project the vector sum of $p_T(ll)$ and **u** on a set of orthogonal axes defined by boson p_T

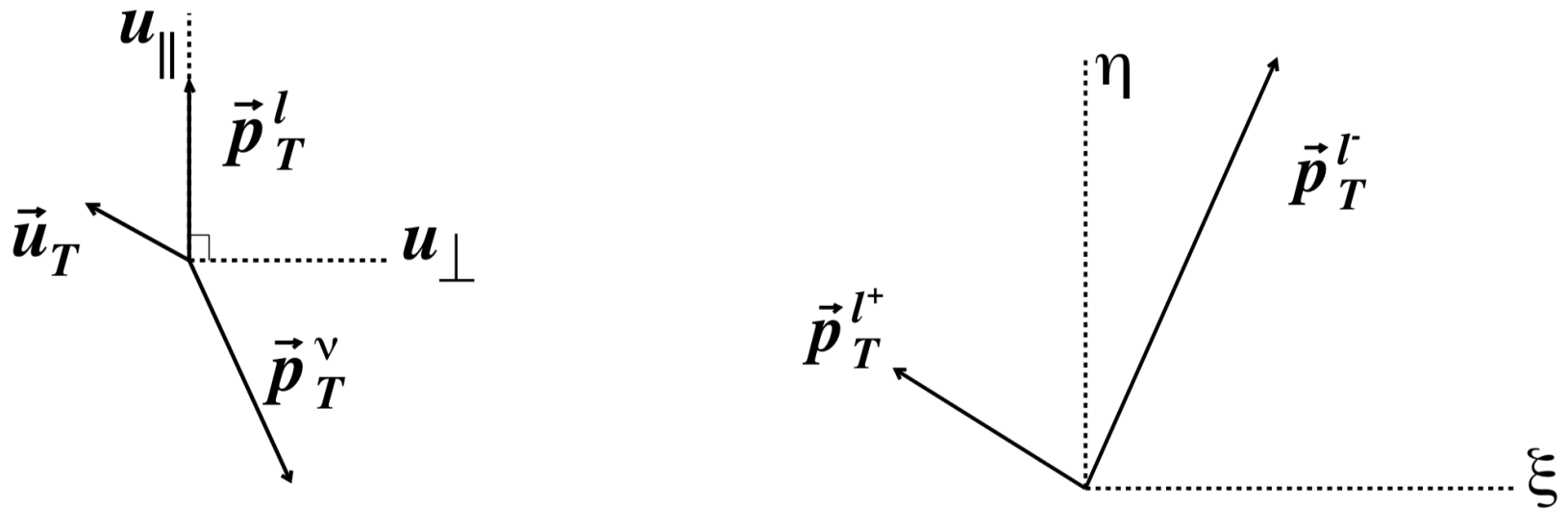Mean and rms of projections as a function of $p_T(ll)$ provide information on hadronic model parameters

Fig. S23

$\chi^2 / \text{dof} = 14 / 14$
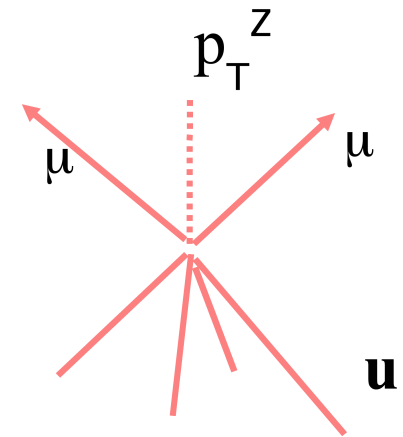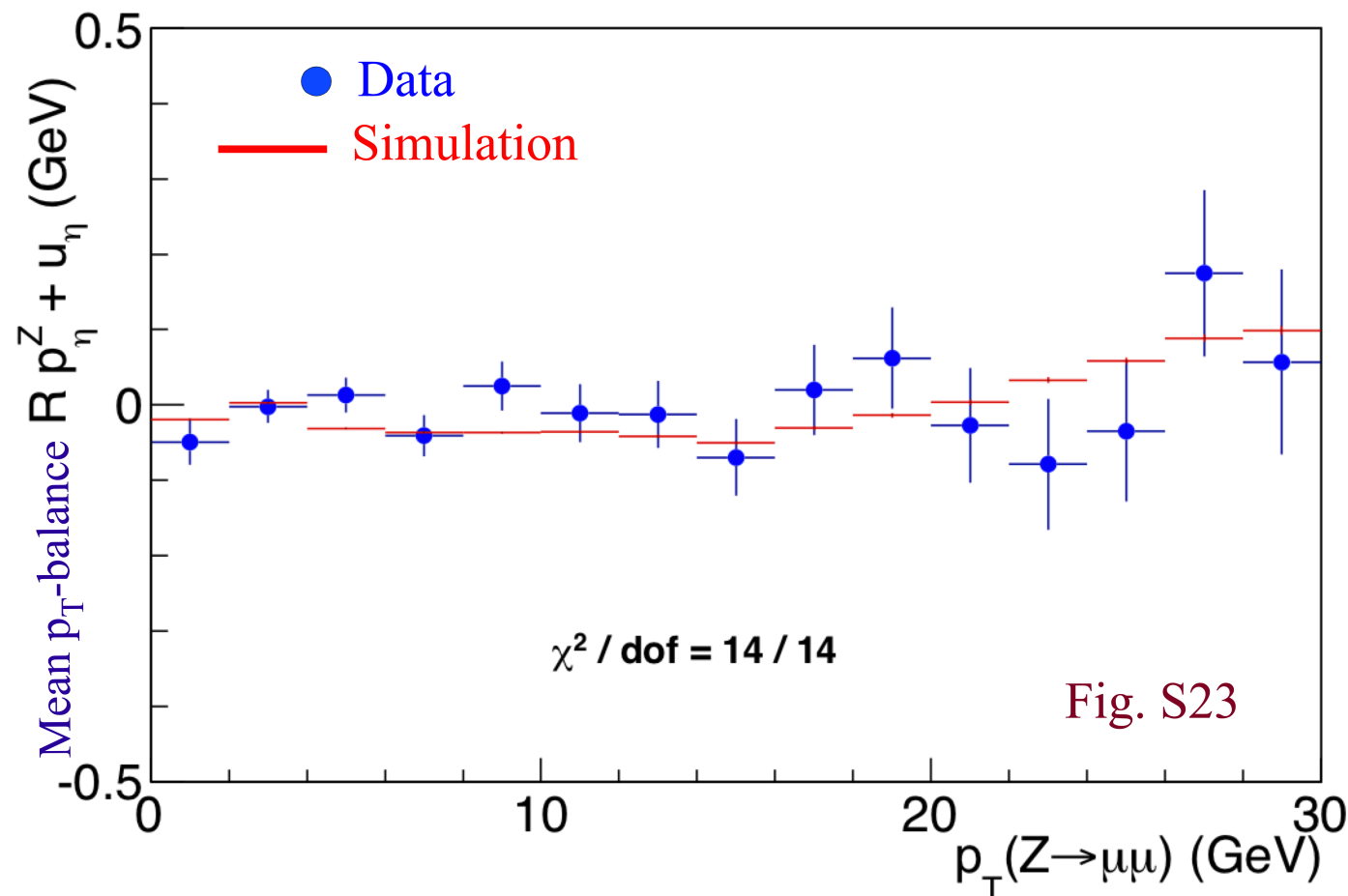
Hadronic model parameters tuned by minimizing χ^2 between data and simulation

$\Delta M_W = 2$ MeV

Tuning Recoil Resolution Model with *Z* events

At low $p_T(Z)$, p_T-balance constrains hadronic resolution due to underlying event

Fig. S24

$\chi^2 / dof = 18 / 14$

p_T^Z

ι μ

u

● Data
— Simulation
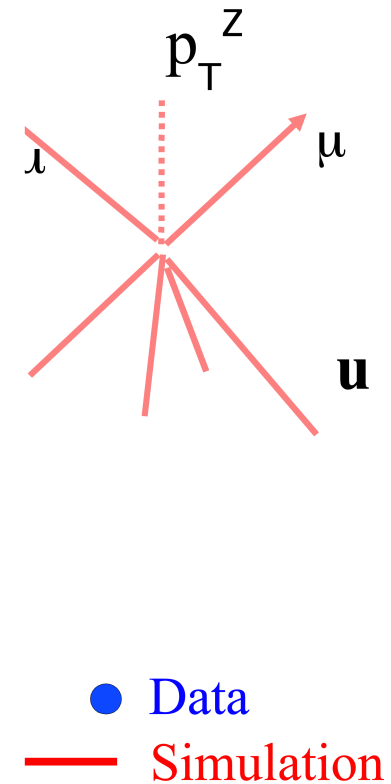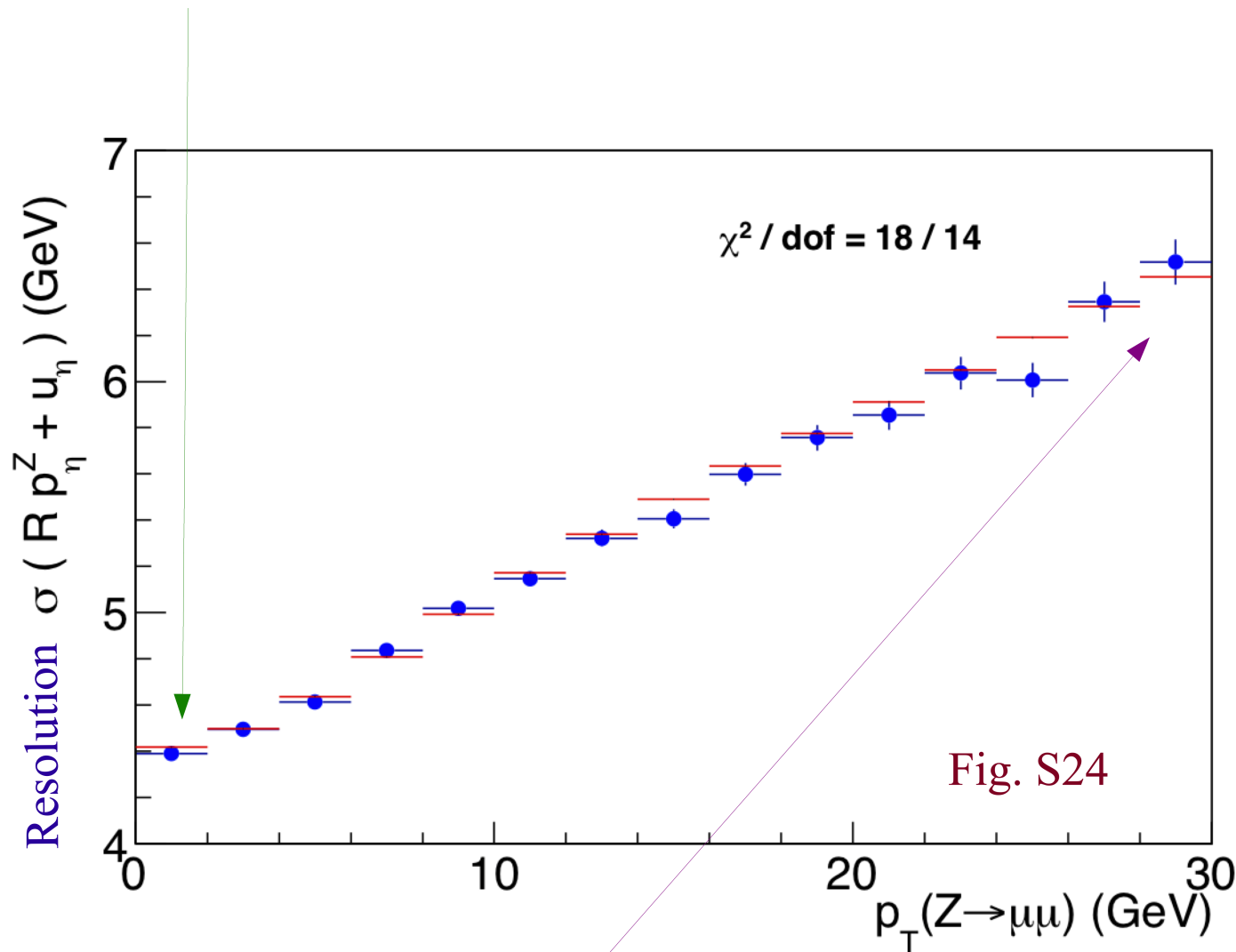
At high $p_T(Z)$, p_T-balance constrains jet resolution

Tuning Recoil Resolution Model with *Z* events

NEW: model of boson + dijet events

χ^2 / dof = 12 / 14

Fig. S27

- Data
- Simulation
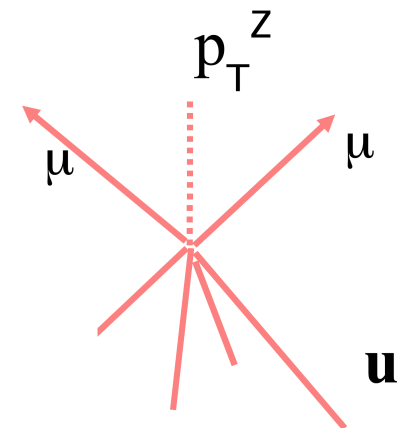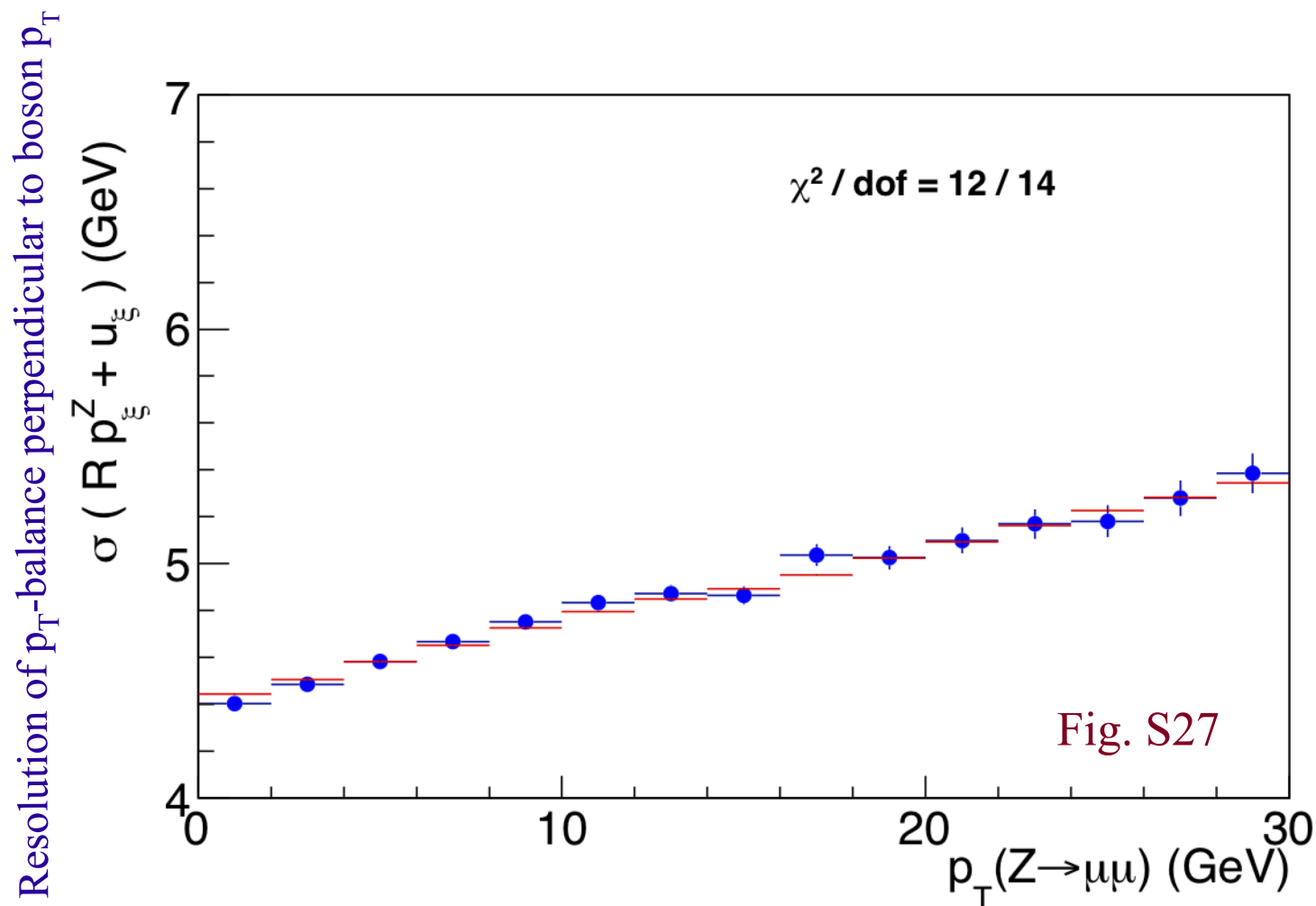
$\Delta M_W = 1.8$ MeV

As a function of $p_T(Z)$, dijet event fraction varies between 0.4 % & 1.2 %

Tuning Recoil Resolution Model with *Z* events
Model of p_T-dependent collimation of jet(s) recoiling against boson
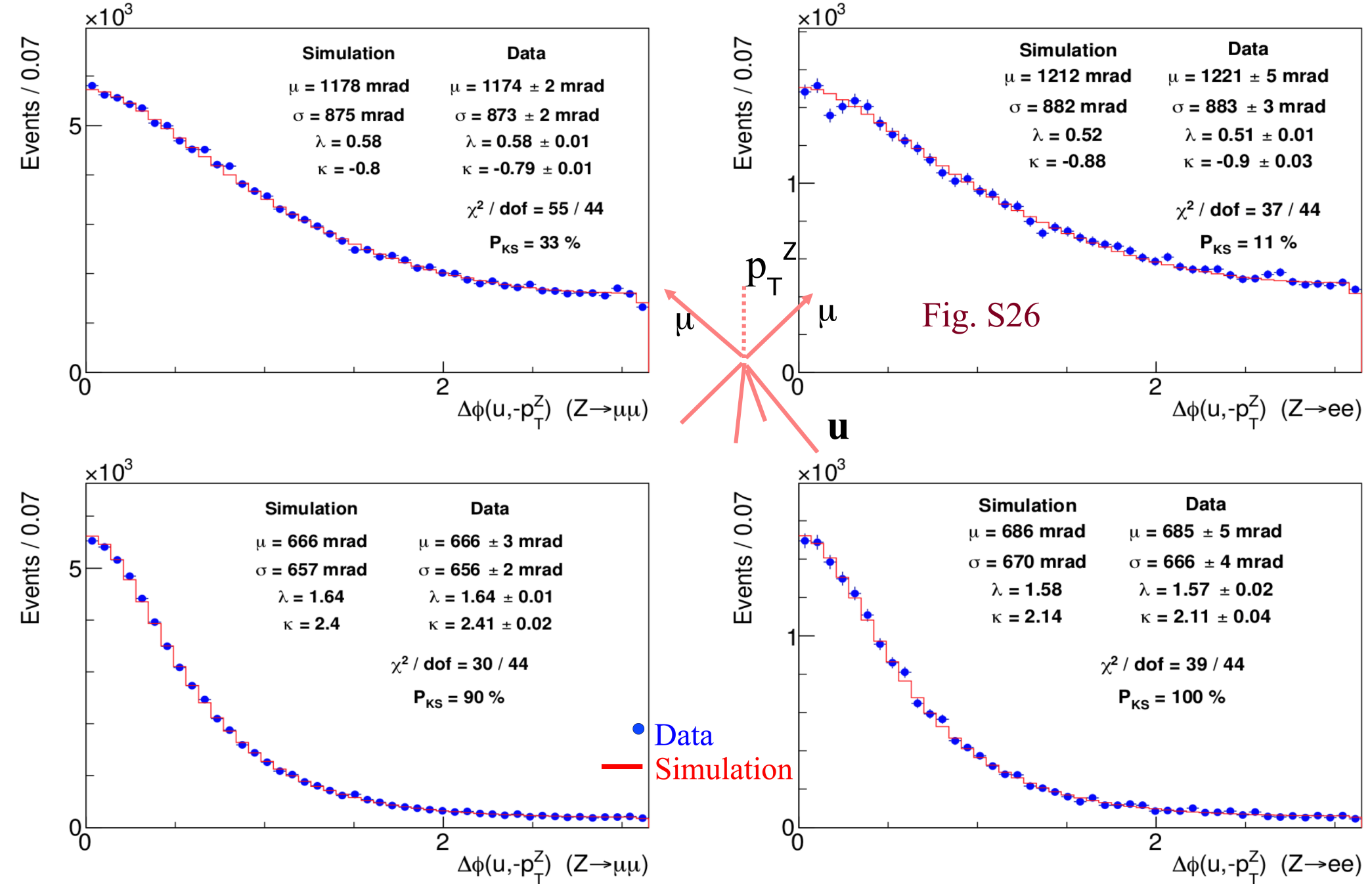
Fig. S26

Tuning Recoil Resolution Model with *Z* events
NEW: Fine-tuning model for resolution along p$_T$(Z) axis
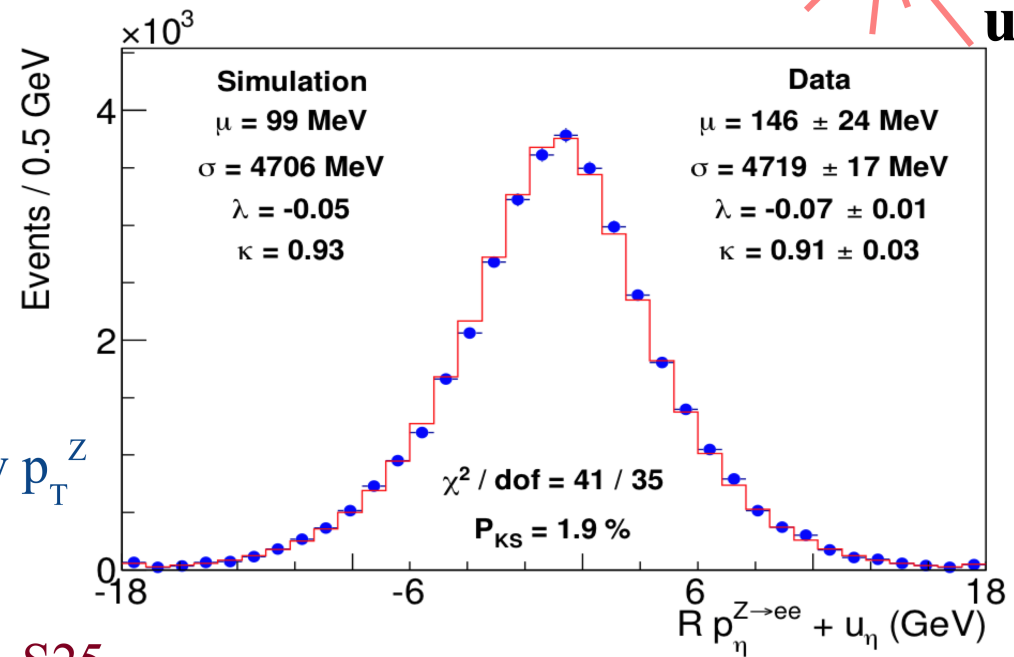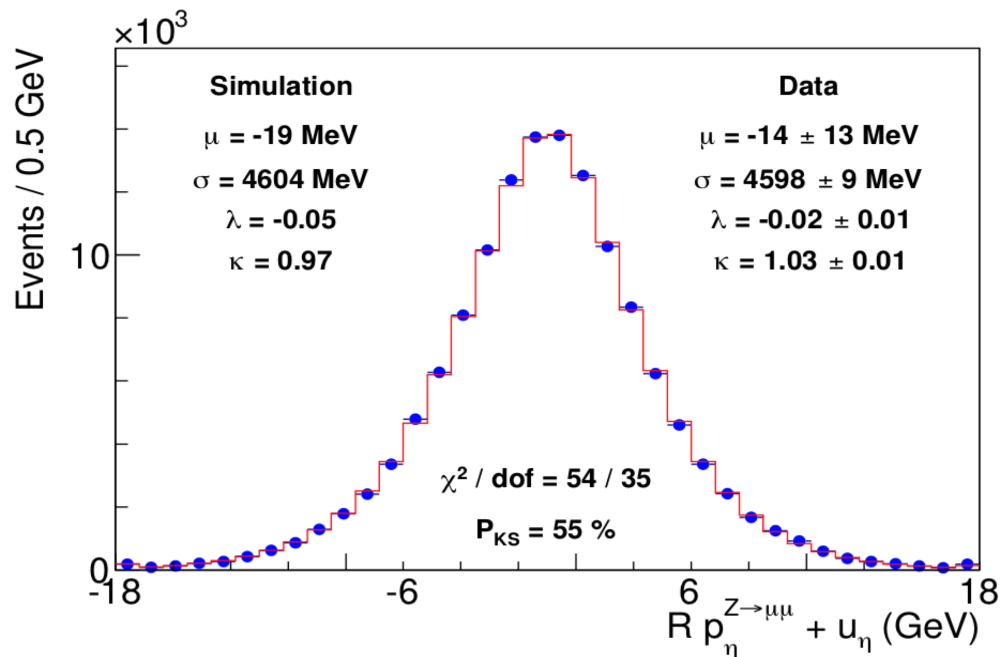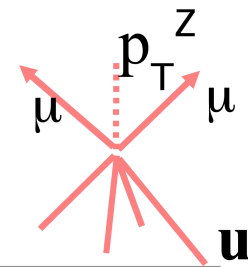
Fig. S25
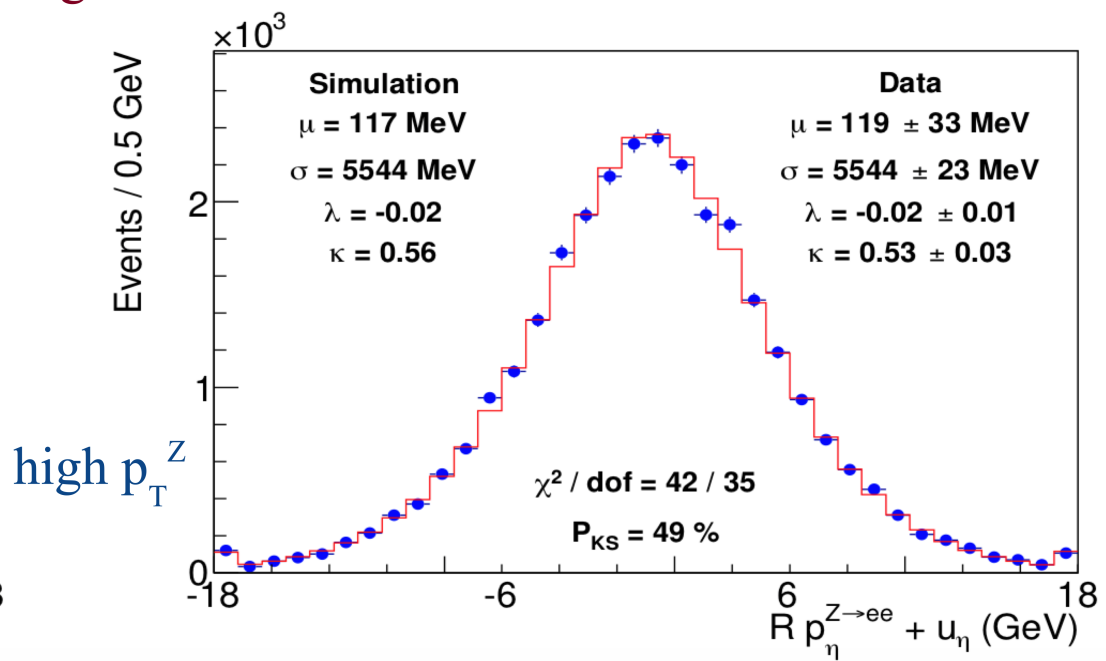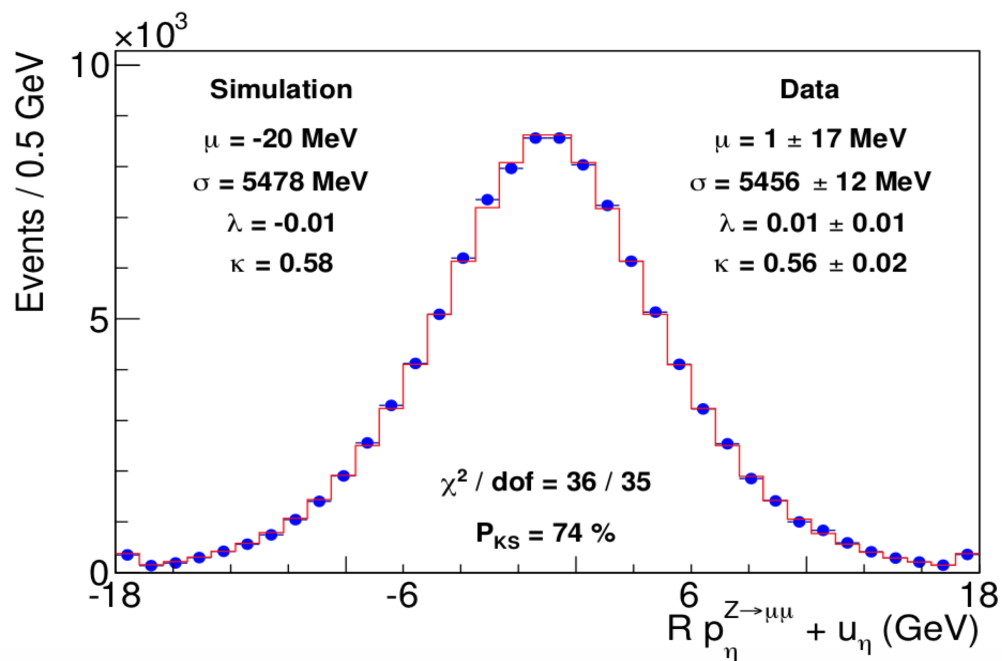
Tuning Recoil Resolution Model with *Z* events

NEW: Fine-tuning model for resolution perpendicular to $p_T(Z)$ axis
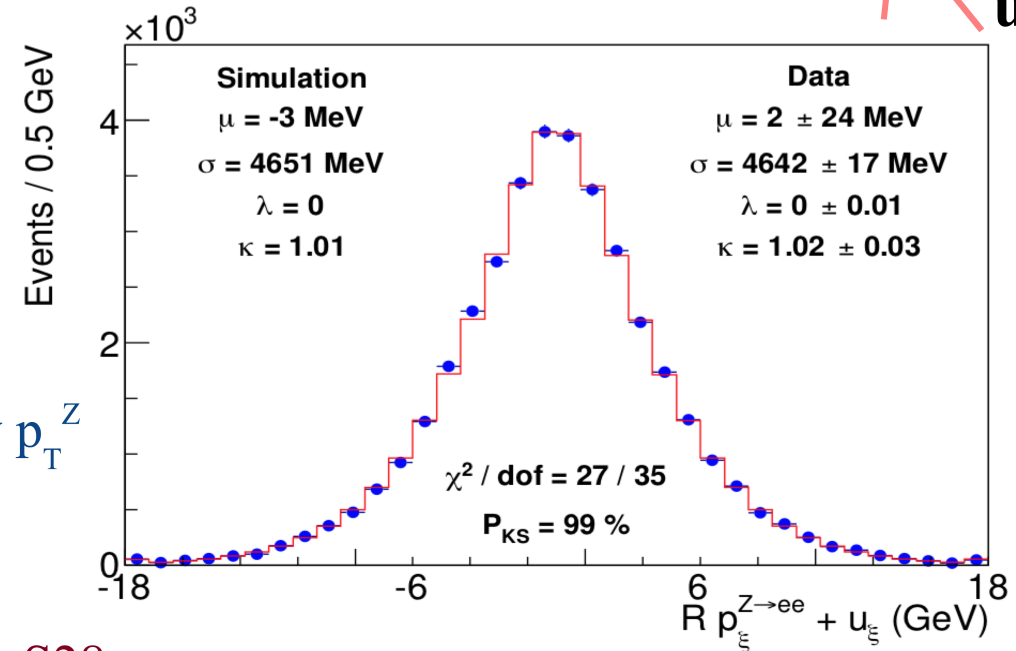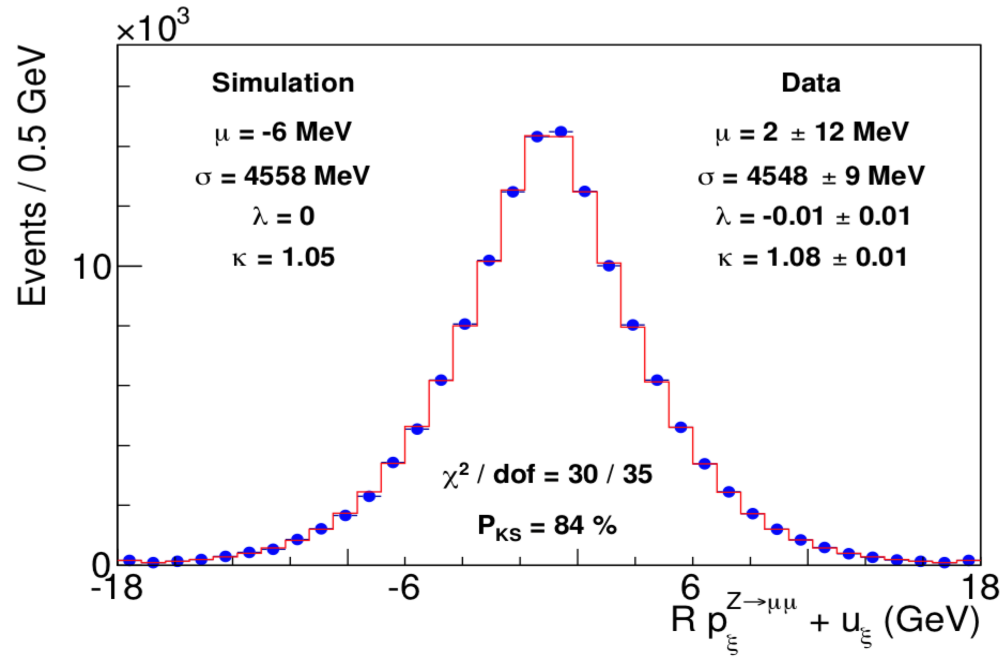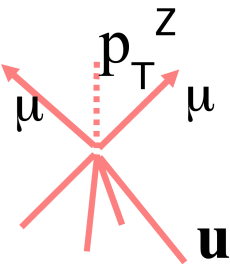
Fig. S28
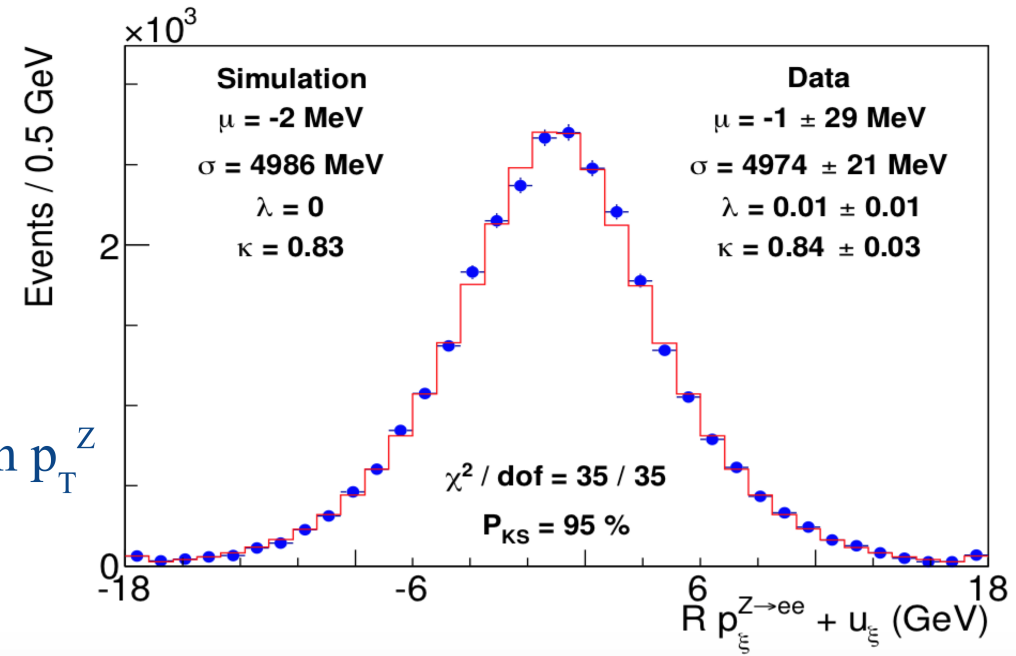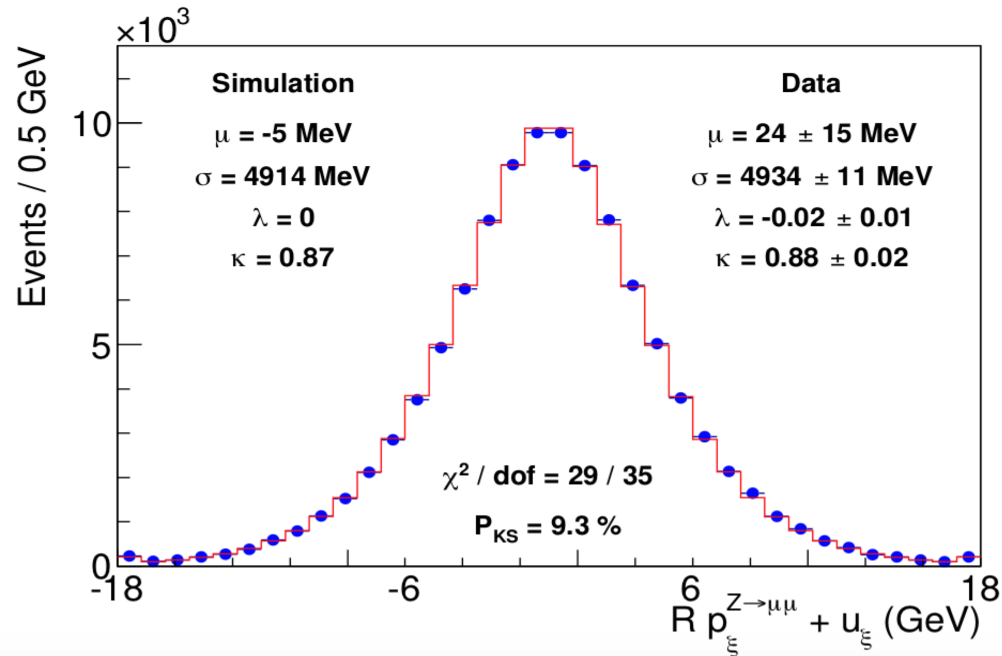
Testing Hadronic Recoil Model with *W* boson events

u(recoil)

l

Simulation
$\mu = -198 \pm 4$ MeV
$\sigma = 4928 \pm 3$ MeV
$\lambda = 0$
$\kappa = 0.1$

Data
$\mu = -202 \pm 3$ MeV
$\sigma = 4927 \pm 2$ MeV
$\lambda = 0$
$\kappa = 0.18$

$\chi^2 / \text{dof} = 18 / 14$
$P_{KS} = 44$ %

Events / 2 GeV

$u_{\parallel}(W \to \mu\nu)$ (GeV)

Simulation
$\mu = -291 \pm 4$ MeV
$\sigma = 4906 \pm 3$ MeV
$\lambda = 0.01$
$\kappa = 0.1$

Data
$\mu = -297 \pm 4$ MeV
$\sigma = 4890 \pm 3$ MeV
$\lambda = 0.01$
$\kappa = 0.19$

$\chi^2 / \text{dof} = 53 / 14$
$P_{KS} = 14$ %

Events / 2 GeV

$u_{\parallel}(W \to e\nu)$ (GeV)
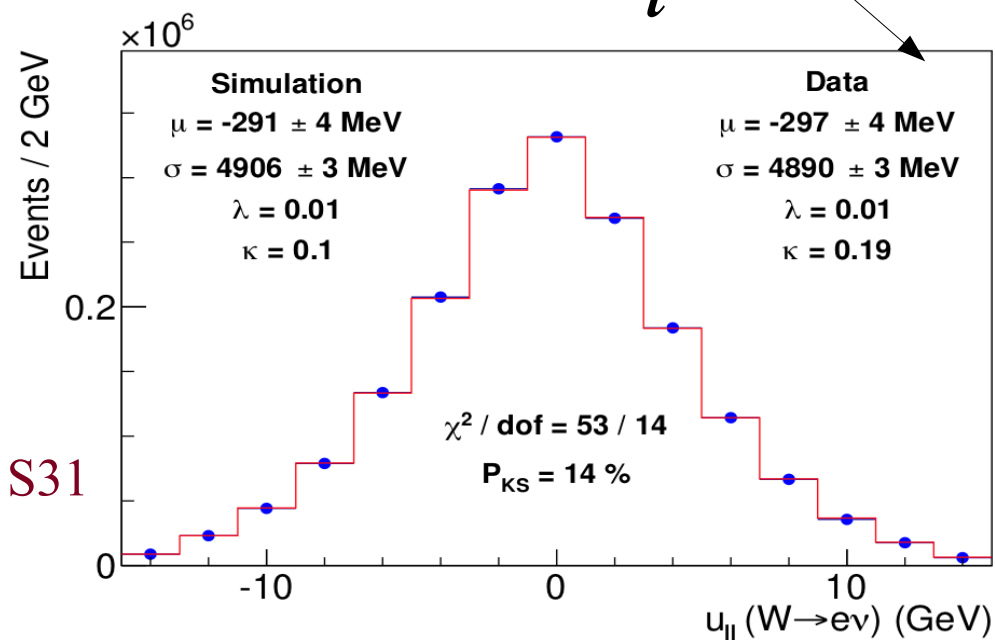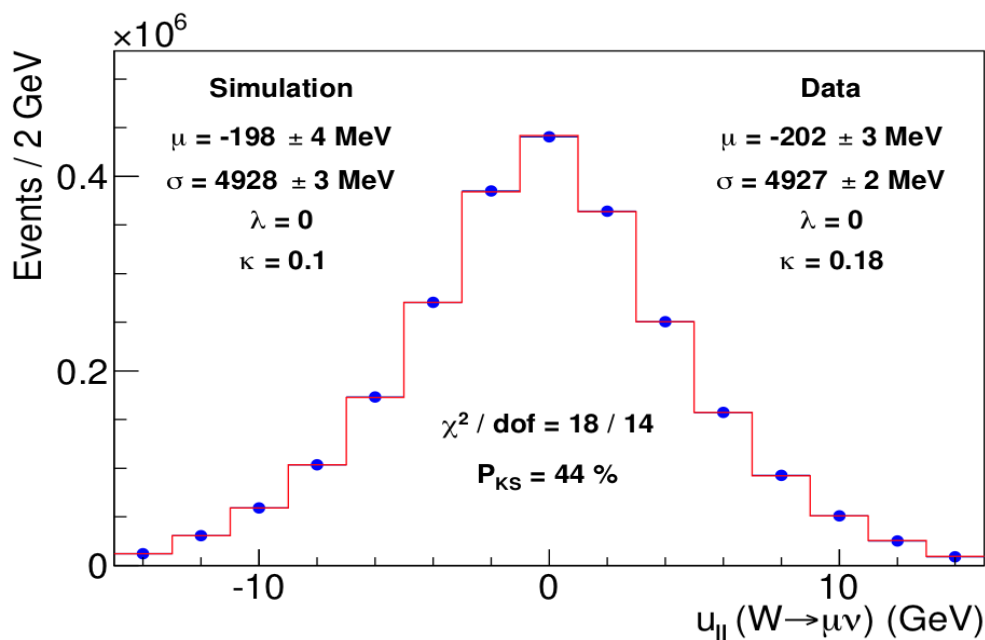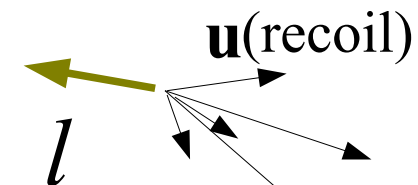
Fig. S31

Recoil projection (GeV) on lepton direction

Simulation
$\mu = 1 \pm 2$ MeV
$\sigma = 5398 \pm 3$ MeV
$\lambda = 0$
$\kappa = -0.09$

Data
$\mu = 11 \pm 3$ MeV
$\sigma = 5398 \pm 2$ MeV
$\lambda = 0$
$\kappa = -0.03$

$\chi^2 / \text{dof} = 24 / 14$
$P_{KS} = 8.3$ %

Events / 2 GeV

$u_{\perp}(W \to \mu\nu)$ (GeV)

Simulation
$\mu = 1 \pm 2$ MeV
$\sigma = 5434 \pm 3$ MeV
$\lambda = 0$
$\kappa = -0.11$

Data
$\mu = 3 \pm 4$ MeV
$\sigma = 5432 \pm 3$ MeV
$\lambda = 0$
$\kappa = -0.05$

$\chi^2 / \text{dof} = 11 / 14$
$P_{KS} = 76$ %

Events / 2 GeV

$u_{\perp}(W \to e\nu)$ (GeV)
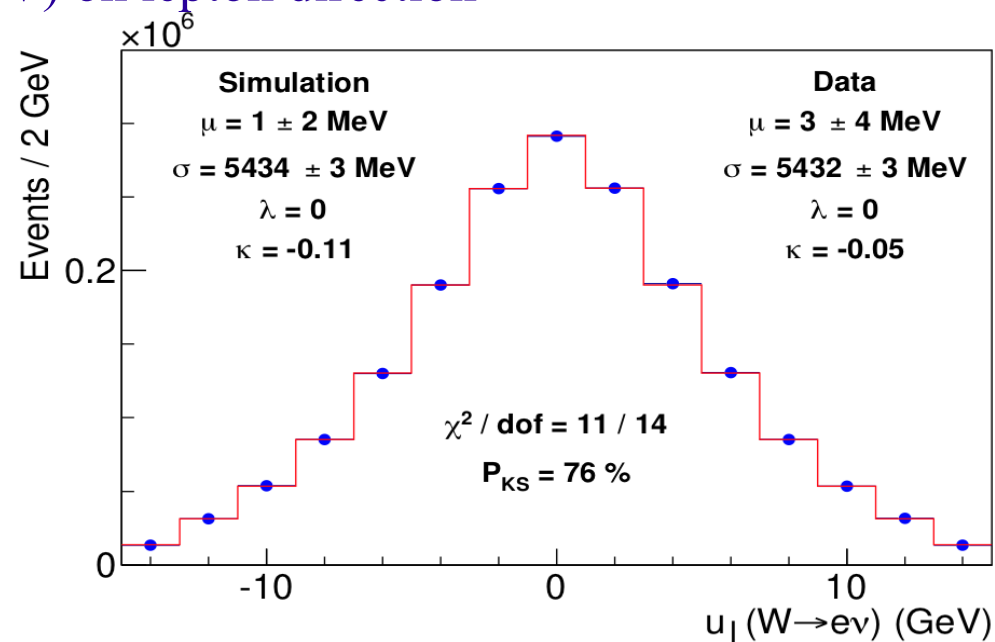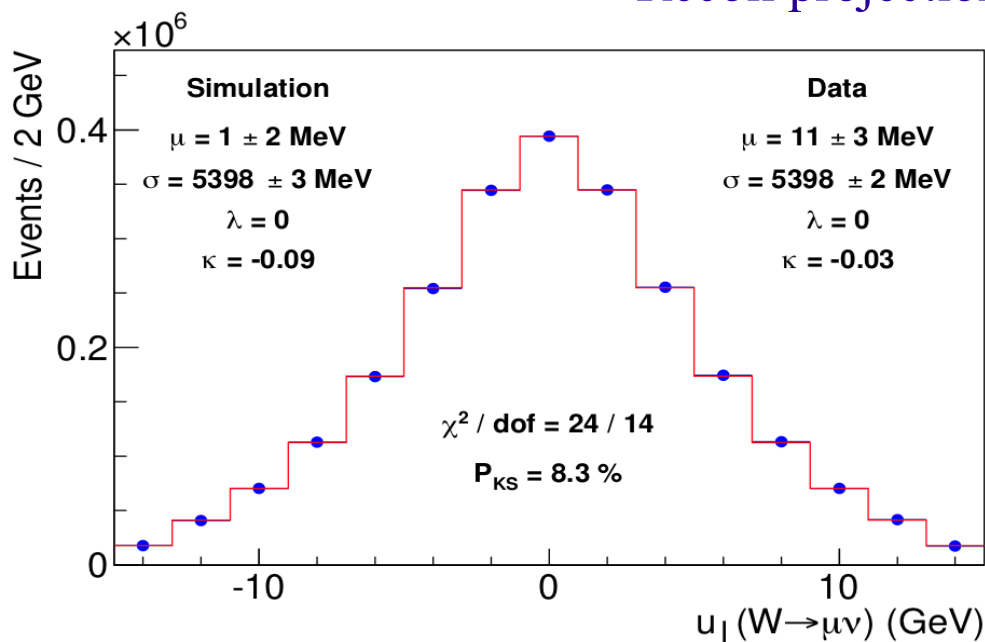
Recoil projection (GeV) perpendicular to lepton

Additional Constraint on $p_T(W)$ Model with *W* boson events

- NEW: In addition to the $p_T(Z)$ data constrain on the boson p_T spectrum, the ratio of the $p_T(W)$ / $p_T(Z)$ spectra is also constrained from the $p_T(W)$ data

  - DyqT : triple-differential cross section calculation at NNLO-QCD used to model scale variation of ratio

  - $p_T(W)$ data is used as constraint on ratio model

  - correlation with hadronic recoil model is taken into account

Fig. S32

$p_T(W)$, muon channel

$p_T(W)$, electron channel

• Data
— Simulation
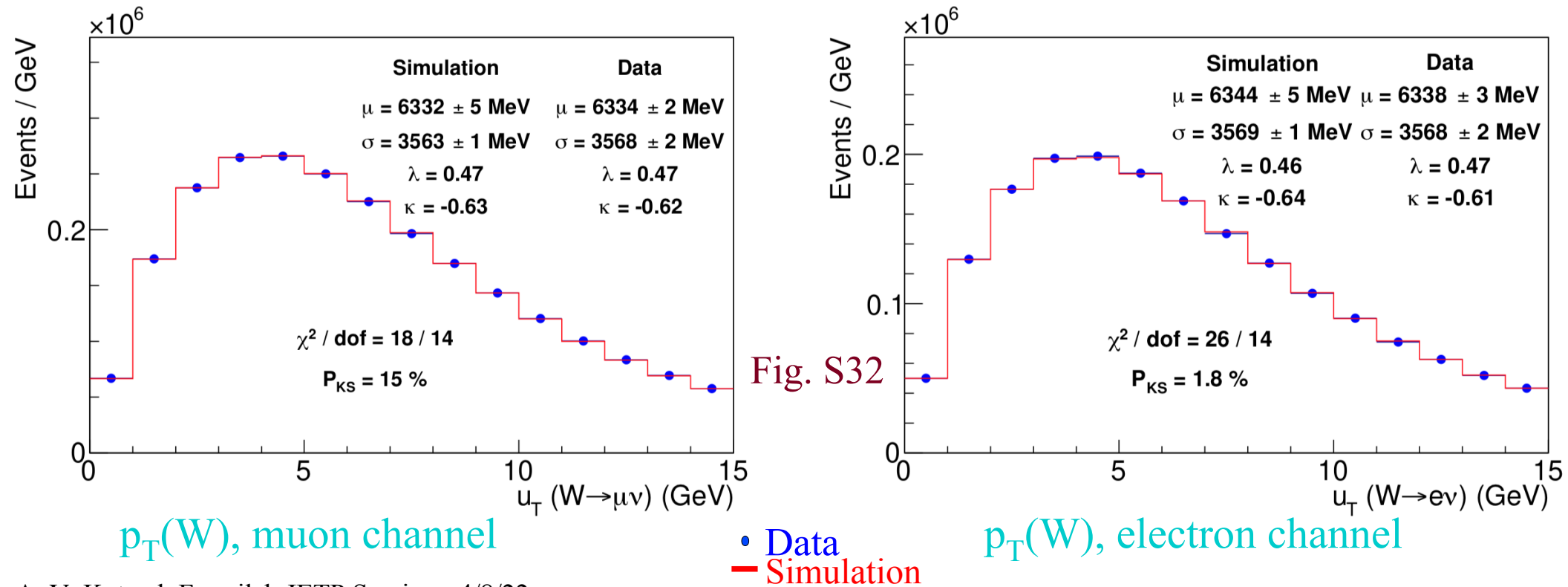
Parton Distribution Functions and Backgrounds

Parton Distribution Functions

- Affect W boson kinematic line-shapes through acceptance cuts

- We use NNPDF3.1 as the default NNLO PDFs

- Use ensemble of 25 'uncertainty' PDFs => 3.9 MeV

  - Represent variations of eigenvectors in the PDF parameter space

  - compute δM_W contribution from each error PDF

- Central values from NNLO PDF sets CT18, MMHT2014 and NNPDF3.1 agree within 2.1 MeV of their midpoint

- As an additional check, central values from NLO PDF sets ABMP16, CJ15, MMHT2014 and NNPDF3.1 agree within 3 MeV of their midpoint

- Missing higher-order QCD effects estimated to be 0.4 MeV

  - varying the factorization and renormalization scales

  - comparing two event generators with different resummation and non-perturbative schemes.

Backgrounds in the *W* boson sample

- *Z → ll* events with only one reconstructed leptons:
  - efficiency and calorimeter response mapped using control samples of $Z → ll$ data, and modeled in the custom simulation
  - background estimates validated using a full GEANT-based CDF detector simulation
  - the only large background is $Z → \mu\mu$ with geometrical acceptance loss of forward muons

- $W → \tau\upsilon → l\upsilon\bar{\upsilon}\upsilon$ background estimated using custom simulation

- QCD jet background estimated using control samples of data, anti-selected on lepton quality requirements

- Pion and kaon decays-in-flight to mis-reconstructed muons
  - Estimated using control samples of data, anti-selected on muon track-quality requirements

- Cosmic ray muons estimated using a dedicated track-finding algorithm

Backgrounds in the *W* boson sample

Muon channel

Source	Fraction (%)	m_T fit	p_T^μ fit	p_T^ν fit
$Z/\gamma^* \to \mu\mu$	7.37 ± 0.10	1.6 (0.7)	3.6 (0.3)	0.1 (1.5)
$W \to \tau\nu$	0.880 ± 0.004	0.1 (0.0)	0.1 (0.0)	0.1 (0.0)
Hadronic jets	0.01 ± 0.04	0.1 (0.8)	-0.6 (0.8)	2.4 (0.5)
Decays in flight	0.20 ± 0.14	1.3 (3.1)	1.3 (5.0)	-5.2 (3.2)
Cosmic rays	0.01 ± 0.01	0.3 (0.0)	0.5 (0.0)	0.3 (0.3)
Total	8.47 ± 0.18	2.1 (3.3)	3.9 (5.1)	5.7 (3.6)

Electron channel

Source	Fraction (%)	m_T fit	p_T^e fit	p_T^ν fit
$Z/\gamma^* \to ee$	0.134 ± 0.003	0.2 (0.3)	0.3 (0.0)	0.0 (0.6)
$W \to \tau\nu$	0.94 ± 0.01	0.6 (0.0)	0.6 (0.0)	0.6 (0.0)
Hadronic jets	0.34 ± 0.08	2.2 (1.2)	0.9 (6.5)	6.2 (-1.1)
Total	1.41 ± 0.08	2.3 (1.2)	1.1 (6.5)	6.2 (1.3)

Backgrounds are small (except Z → μμ with a forward muon)

W Mass Fits

Blind Analysis Technique

- All W and Z mass fit results were blinded with a random [-50,50] MeV offset hidden in the likelihood fitter

- Blinding offset removed after the analysis was declared frozen

- Technique allows to study all aspects of data while keeping Z boson mass and W boson mass result unknown within ±50 MeV

W Transverse Mass Fits
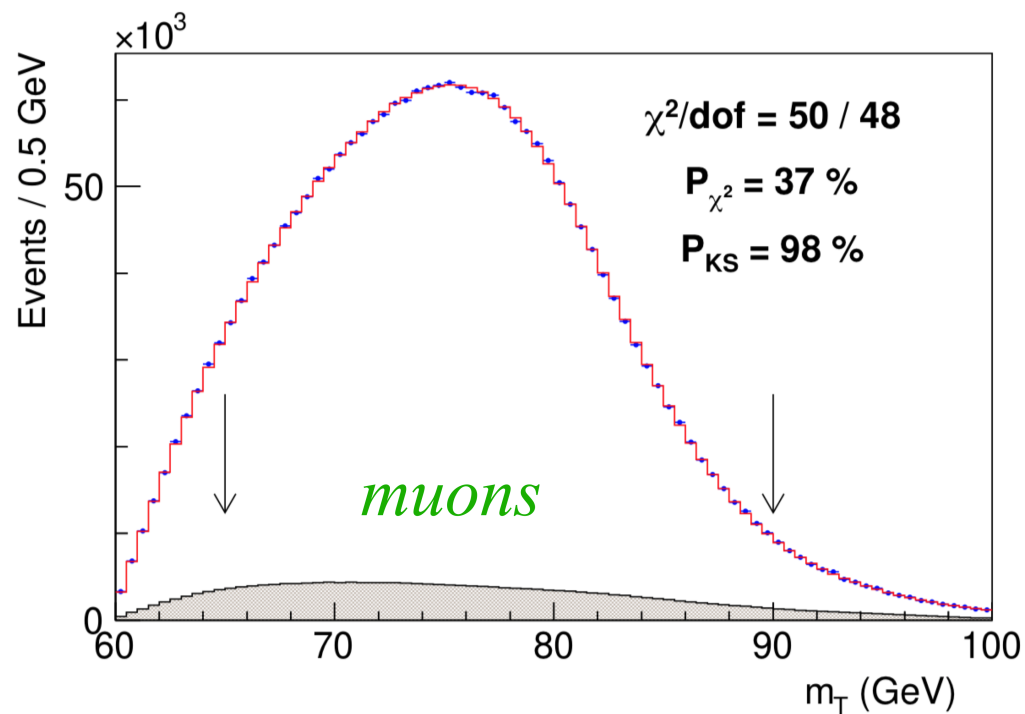
Fig. 4
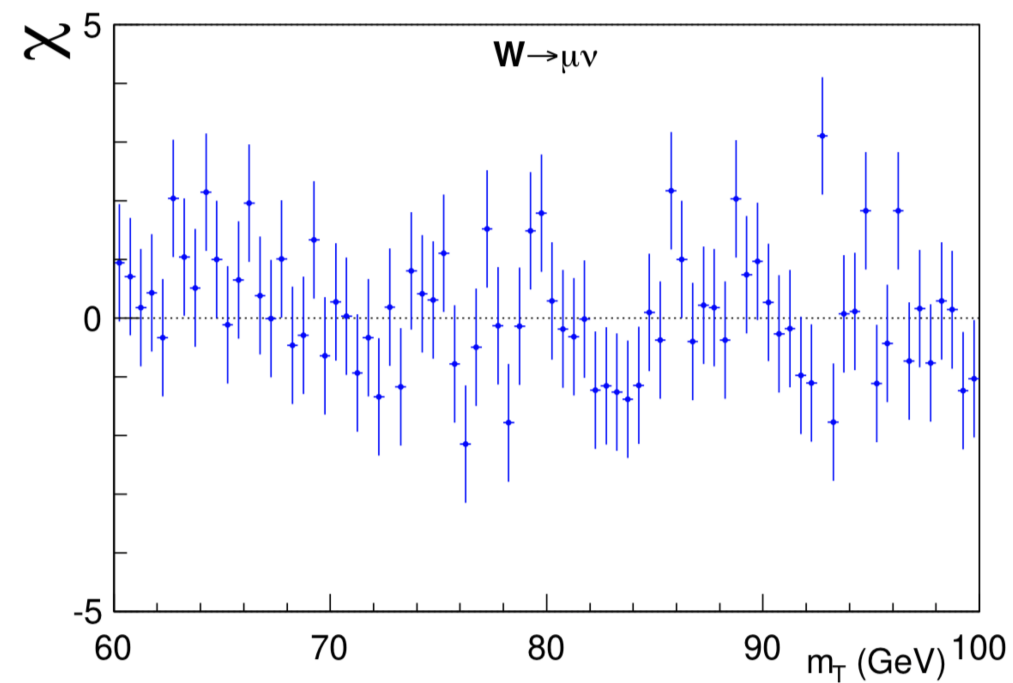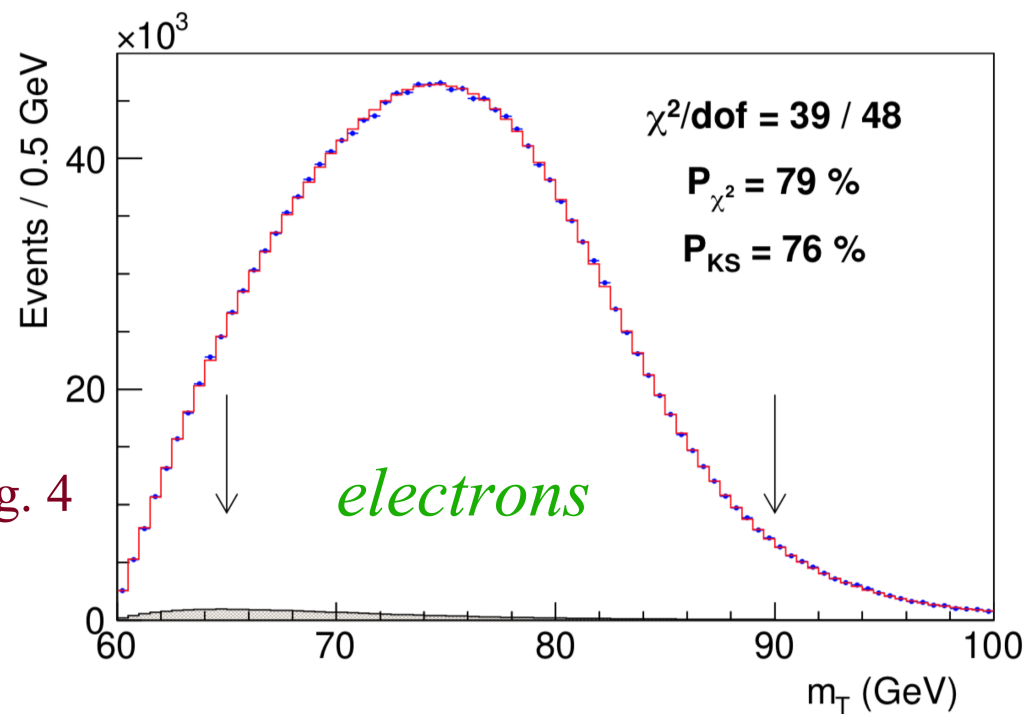
Fig. 36

W Charged Lepton p$_\text{T}$ Fits

$\chi^2/\text{dof} = 82 / 62$

$P_{\chi^2} = 4\ \%$

$P_{KS} = 89\ \%$

muons

Fig. 4

$\chi^2/\text{dof} = 83 / 62$

$P_{\chi^2} = 3\ \%$

$P_{KS} = 53\ \%$

electrons

$W \rightarrow \mu\nu$

$W \rightarrow e\nu$
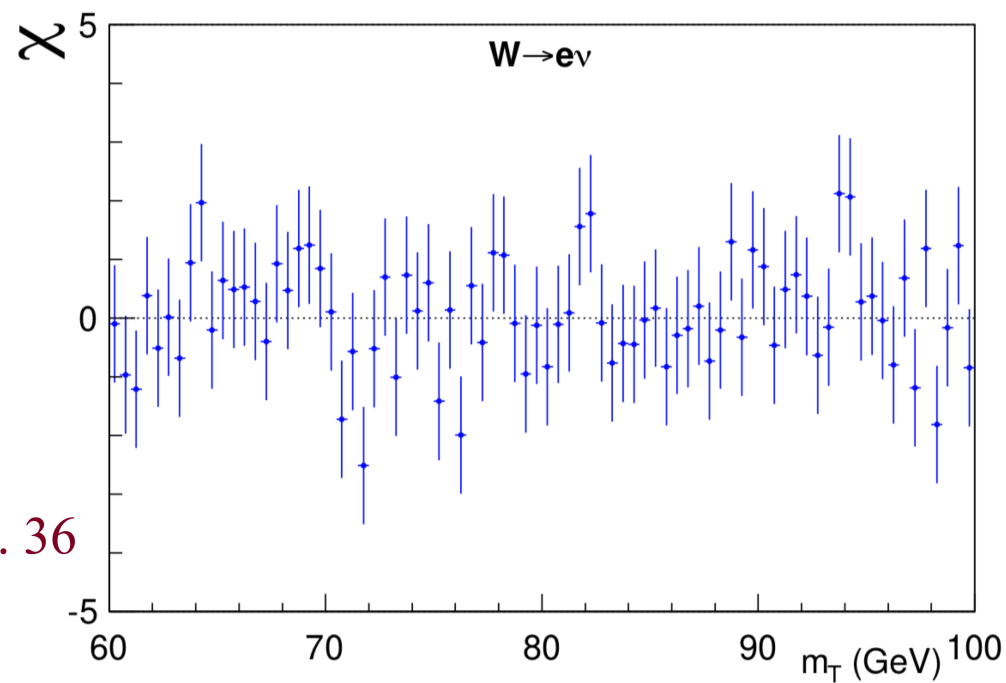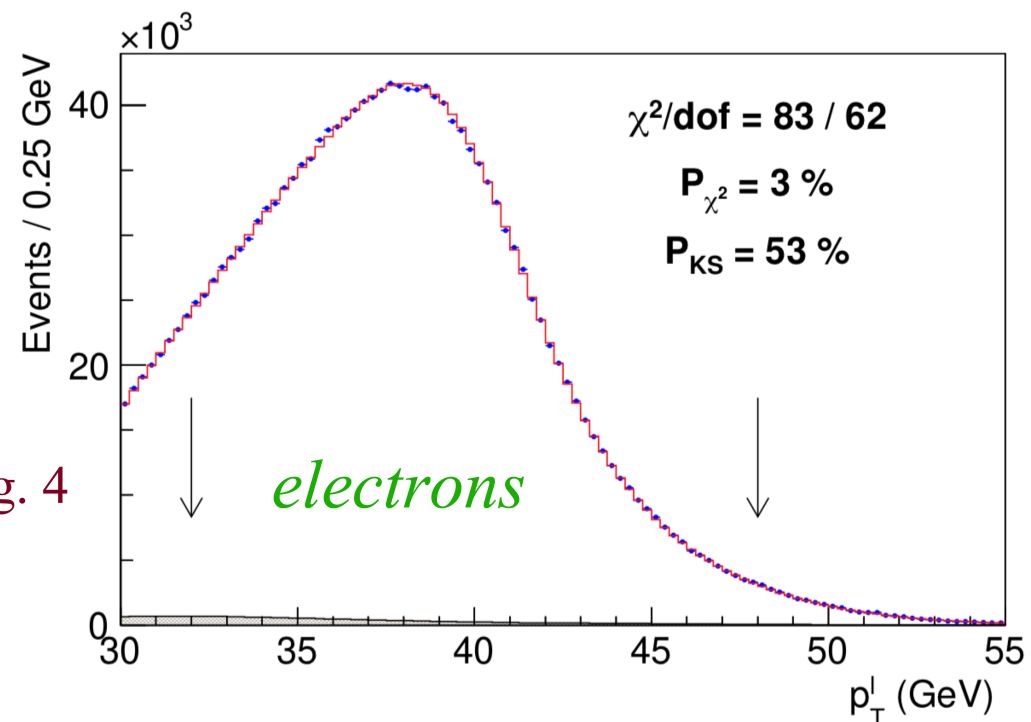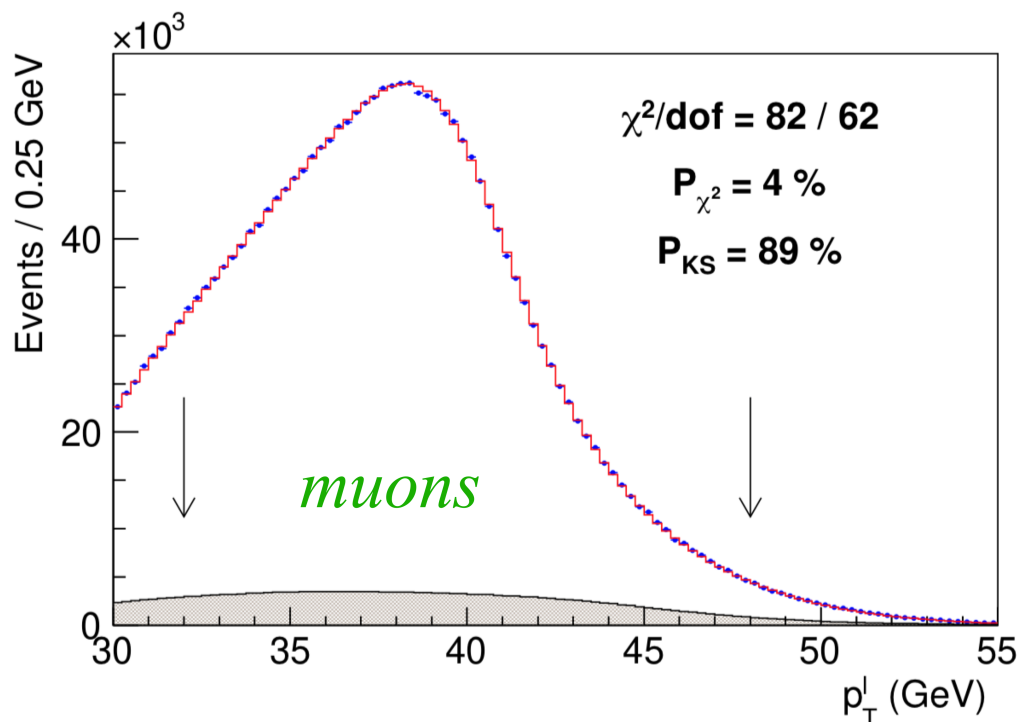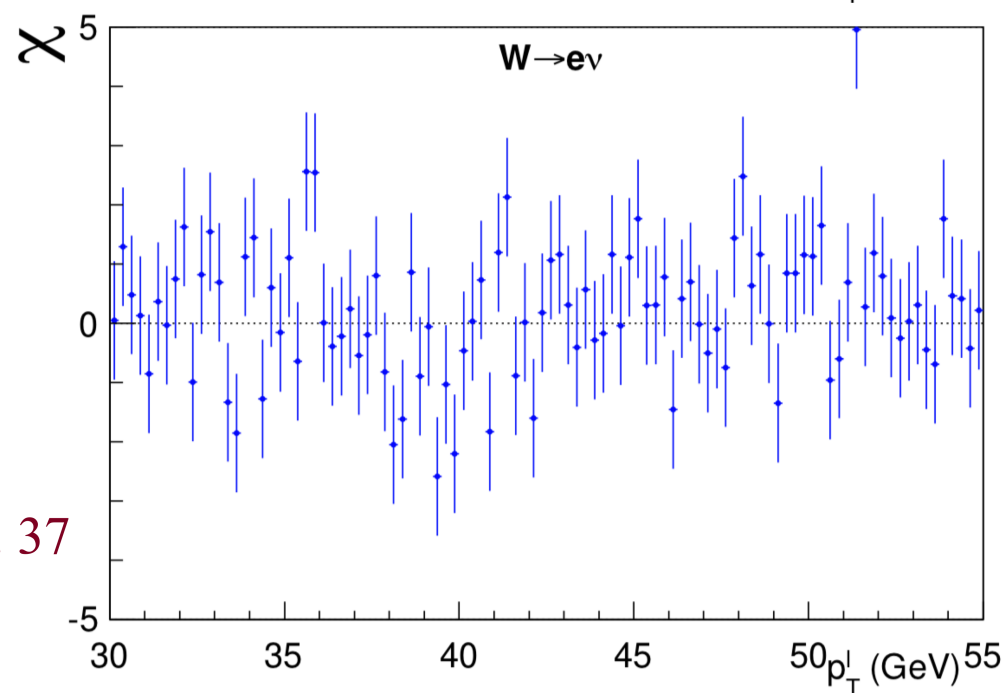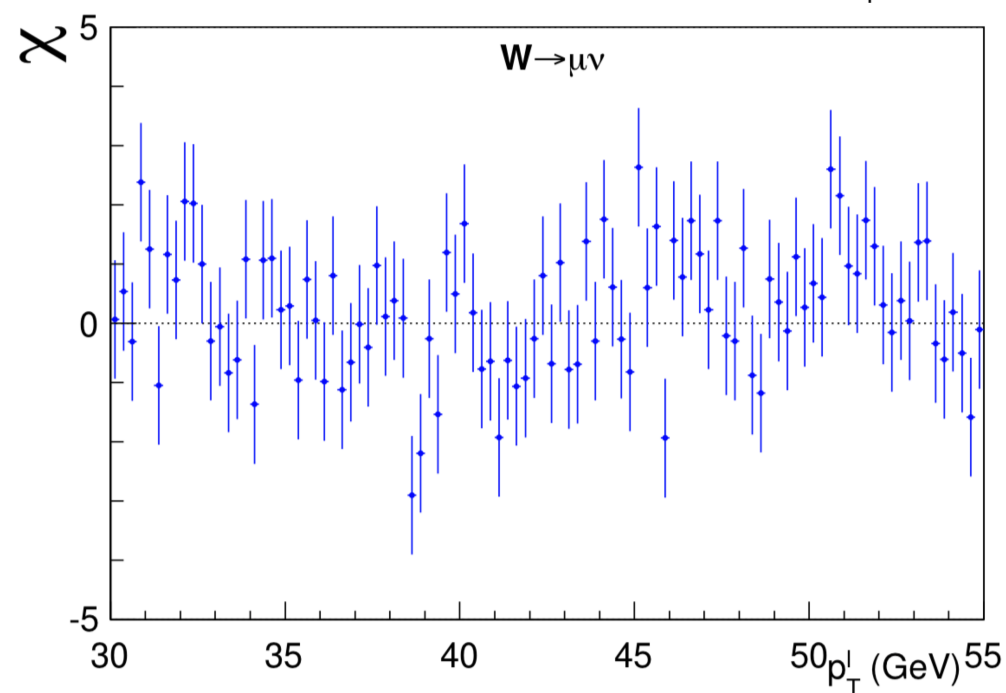
Fig. 37

W Neutrino p$_T$ Fits

Fig. 4

χ^2/dof = 63 / 62
P$_{\chi^2}$ = 43 %
P$_{KS}$ = 70 %

muons

χ^2/dof = 69 / 62
P$_{\chi^2}$ = 23 %
P$_{KS}$ = 96 %

electrons

Fig. 38

W→μν

W→eν
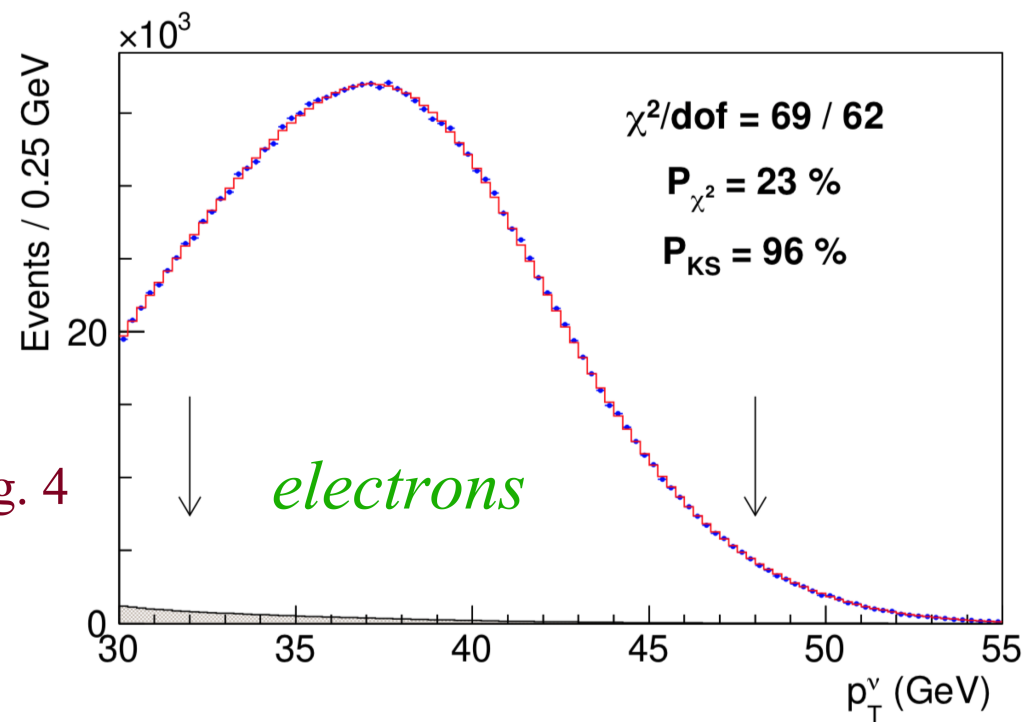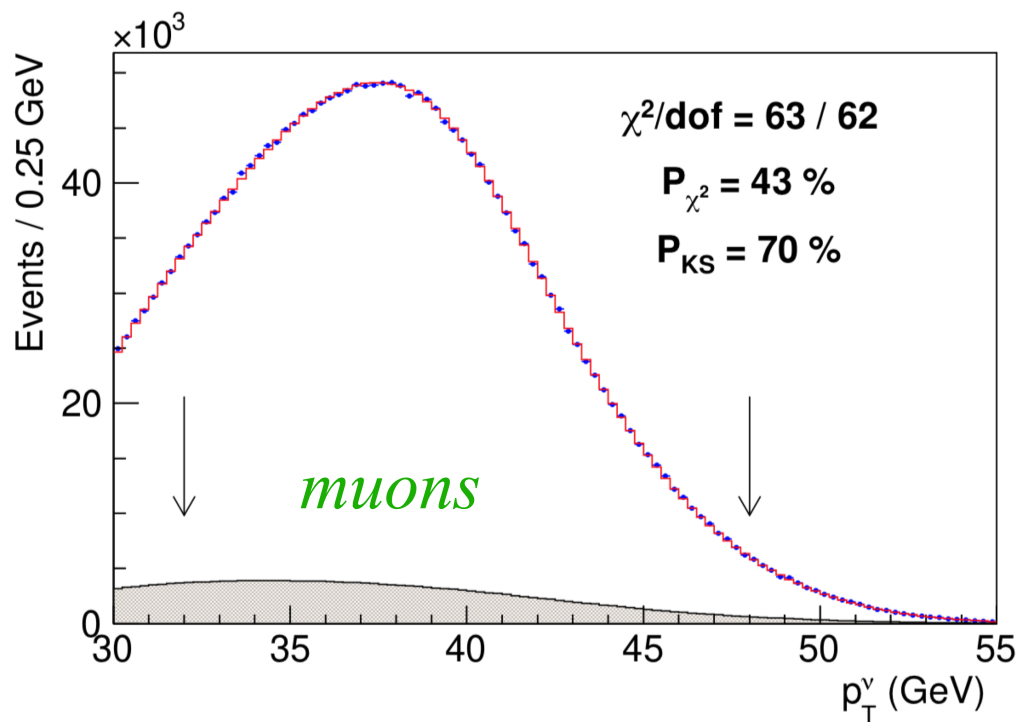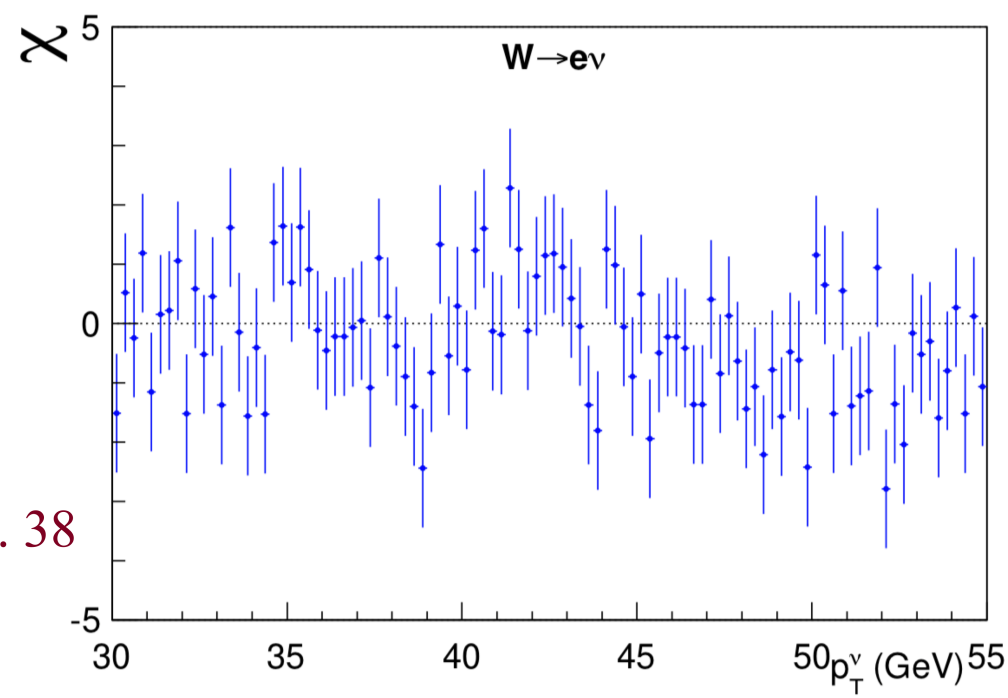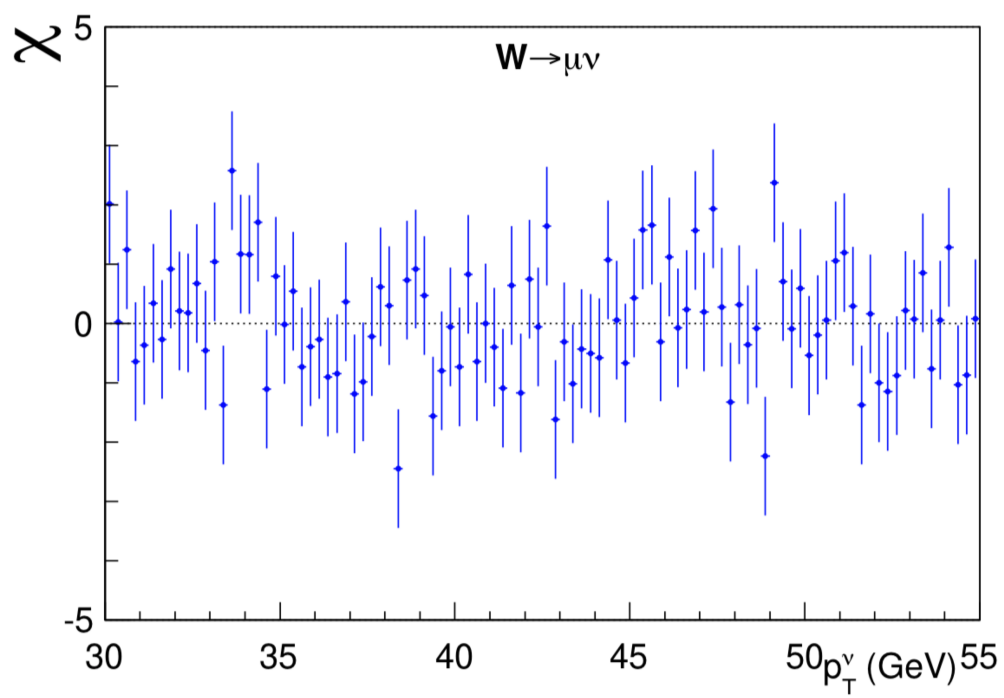
Summary of *W* Mass Fits

Distribution	W-boson mass (MeV)	χ^2/dof
$m_T(e,\nu)$	$80\ 429.1 \pm 10.3_{\mathrm{stat}} \pm 8.5_{\mathrm{syst}}$	$39/48$
$p_T^\ell(e)$	$80\ 411.4 \pm 10.7_{\mathrm{stat}} \pm 11.8_{\mathrm{syst}}$	$83/62$
$p_T^\nu(e)$	$80\ 426.3 \pm 14.5_{\mathrm{stat}} \pm 11.7_{\mathrm{syst}}$	$69/62$
$m_T(\mu,\nu)$	$80\ 446.1 \pm 9.2_{\mathrm{stat}} \pm 7.3_{\mathrm{syst}}$	$50/48$
$p_T^\ell(\mu)$	$80\ 428.2 \pm 9.6_{\mathrm{stat}} \pm 10.3_{\mathrm{syst}}$	$82/62$
$p_T^\nu(\mu)$	$80\ 428.9 \pm 13.1_{\mathrm{stat}} \pm 10.9_{\mathrm{syst}}$	$63/62$
combination	$80\ 433.5 \pm 6.4_{\mathrm{stat}} \pm 6.9_{\mathrm{syst}}$	$7.4/5$

Table 1

Consistency between two channels and three kinematic fits

Combinations of Fit Results

Combination	m_T fit Electrons	Muons	p_T^ℓ fit Electrons	Muons	p_T^ν fit Electrons	Muons	Value (MeV)	χ^2/dof	Probability (%)
m_T	✓	✓					80 439.0 ± 9.8	1.2 / 1	28
p_T^ℓ			✓	✓			80 421.2 ± 11.9	0.9 / 1	36
p_T^ν					✓	✓	80 427.7 ± 13.8	0.0 / 1	91
m_T & p_T^ℓ	✓	✓	✓	✓			80 435.4 ± 9.5	4.8 / 3	19
m_T & p_T^ν	✓	✓			✓	✓	80 437.9 ± 9.7	2.2 / 3	53
p_T^ℓ & p_T^ν			✓	✓	✓	✓	80 424.1 ± 10.1	1.1 / 3	78
Electrons	✓		✓		✓		80 424.6 ± 13.2	3.3 / 2	19
Muons		✓		✓		✓	80 437.9 ± 11.0	3.6 / 2	17
All	✓	✓	✓	✓	✓	✓	80 433.5 ± 9.4	7.4 / 5	20

Table S9

- Combined electrons (3 fits): M_W = 80424.6 ± 13.2 MeV, $P(\chi^2)$ = 19%

- Combined muons (3 fits): M_W = 80437.9 ± 11.0 MeV, $P(\chi^2)$ = 17%

- All combined (6 fits): M_W = 80433.5 ± 9.4 MeV, $P(\chi^2)$ = 20%

Previous CDF Result (2.2 fb⁻¹)
Transverse Mass Fit Uncertainties (MeV)

	electrons	*muons*	*common*
W statistics	19	16	0
Lepton energy scale	10	7	5
Lepton resolution	4	1	0
Recoil energy scale	5	5	5
Recoil energy resolution	7	7	7
Selection bias	0	0	0
Lepton removal	3	2	2
Backgrounds	4	3	0
pT(W) model	3	3	3
Parton dist. Functions	10	10	10
QED rad. Corrections	4	4	4
Total systematic	18	16	15
Total	26	23	

Systematic uncertainties shown in green: statistics-limited by control data samples

New CDF Result (8.8 fb^{-1})
Transverse Mass Fit Uncertainties (MeV)

	electrons	muons	common
W statistics	10.3	9.2	0
Lepton energy scale	5.8	2.1	1.8
Lepton resolution	0.9	0.3	-0.3
Recoil energy scale	1.8	1.8	1.8
Recoil energy resolution	1.8	1.8	1.8
Selection bias	0.5	0.5	0
Lepton removal	1	1.7	0
Backgrounds	2.6	3.9	0
pT(Z) & pT(W) model	1.1	1.1	1.1
Parton dist. Functions	3.9	3.9	3.9
QED rad. Corrections	2.7	2.7	2.7
Total systematic	8.7	7.4	5.8
Total	13.5	11.8	5.8

New CDF Result (8.8 fb⁻¹) All Fit Uncertainties (MeV)

Source of systematic uncertainty	m_T fit Electrons	Muons	Common	p_T^ℓ fit Electrons	Muons	Common	p_T^ν fit Electrons	Muons	Common
Lepton energy scale	5.8	2.1	1.8	5.8	2.1	1.8	5.8	2.1	1.8
Lepton energy resolution	0.9	0.3	-0.3	0.9	0.3	-0.3	0.9	0.3	-0.3
Recoil energy scale	1.8	1.8	1.8	3.5	3.5	3.5	0.7	0.7	0.7
Recoil energy resolution	1.8	1.8	1.8	3.6	3.6	3.6	5.2	5.2	5.2
Lepton $u_\parallel$ efficiency	0.5	0.5	0	1.3	1.0	0	2.6	2.1	0
Lepton removal	1.0	1.7	0	0	0	0	2.0	3.4	0
Backgrounds	2.6	3.9	0	6.6	6.4	0	6.4	6.8	0
p_T^Z model	0.7	0.7	0.7	2.3	2.3	2.3	0.9	0.9	0.9
p_T^W/p_T^Z model	0.8	0.8	0.8	2.3	2.3	2.3	0.9	0.9	0.9
Parton distributions	3.9	3.9	3.9	3.9	3.9	3.9	3.9	3.9	3.9
QED radiation	2.7	2.7	2.7	2.7	2.7	2.7	2.7	2.7	2.7
Statistical	10.3	9.2	0	10.7	9.6	0	14.5	13.1	0
Total	13.5	11.8	5.8	16.0	14.1	7.9	18.8	17.1	7.4

Table S8

Previous CDF Result (2.2 fb^{-1})
Combined Fit Systematic Uncertainties

Source	Uncertainty (MeV)
Lepton Energy Scale	7
Lepton Energy Resolution	2
Recoil Energy Scale	4
Recoil Energy Resolution	4
$u_{\parallel}$ efficiency	0
Lepton Removal	2
Backgrounds	3
$p_T(W)$ model	5
Parton Distributions	10
QED radiation	4
W boson statistics	12
Total	19

New CDF Result (8.8 fb^{-1})
Combined Fit Systematic Uncertainties

Source	Uncertainty (MeV)
Lepton energy scale	3.0
Lepton energy resolution	1.2
Recoil energy scale	1.2
Recoil energy resolution	1.8
Lepton efficiency	0.4
Lepton removal	1.2
Backgrounds	3.3
p_T^Z model	1.8
p_T^W/p_T^Z model	1.3
Parton distributions	3.9
QED radiation	2.7
W boson statistics	6.4
Total	9.4

Table 2

CDF M_W *vs* m_{top}
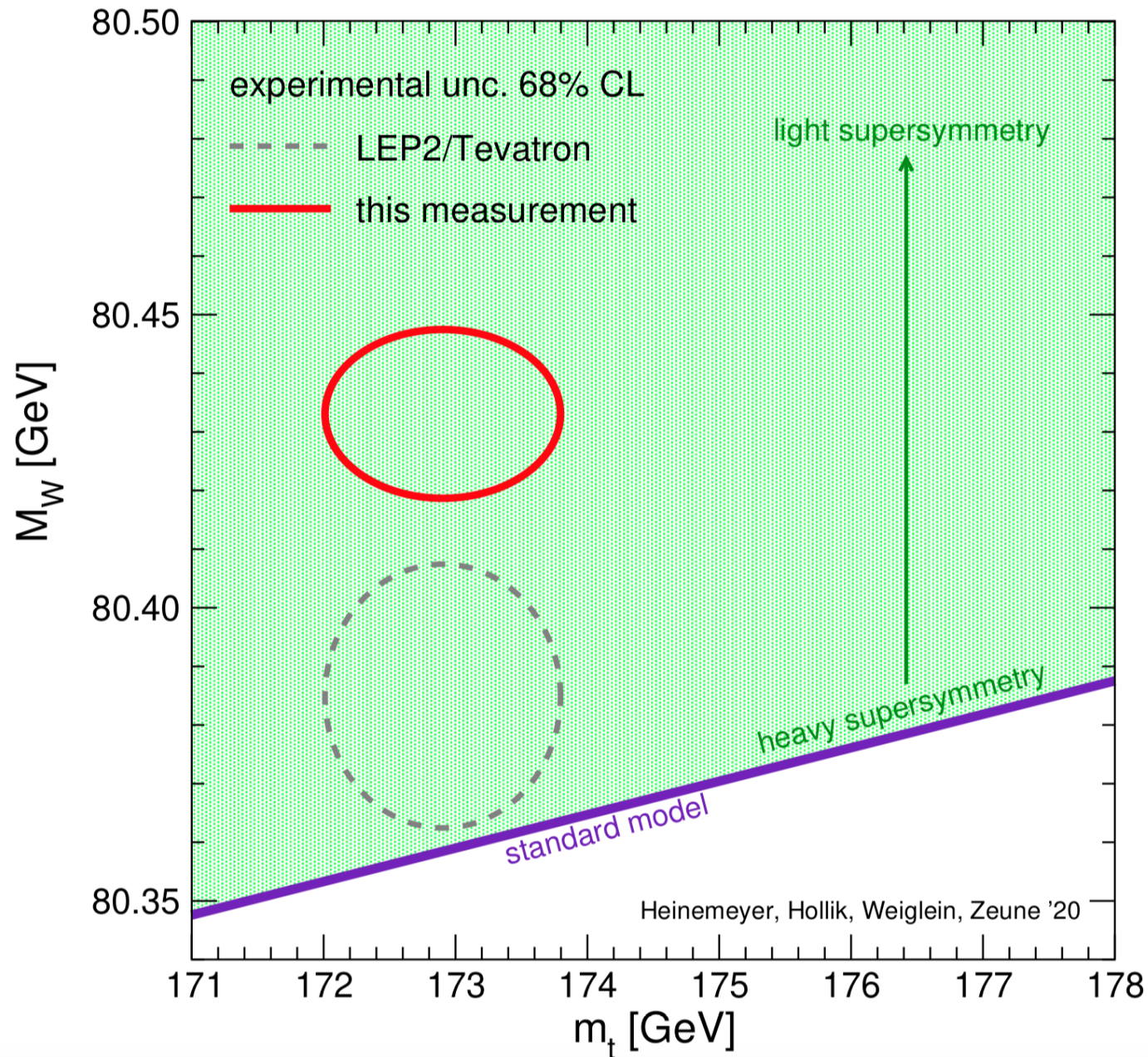
Fig. 1

Understanding Tevatron-LHC correlations and combination with ATLAS in progress

W Boson Mass Measurements from Different Experiments

	SM	
D0 I	80478 ± 83	
CDF I	80432 ± 79	
DELPHI	80336 ± 67	
L3	80270 ± 55	
OPAL	80415 ± 52	
ALEPH	80440 ± 51	
D0 II	80376 ± 23	
ATLAS	80370 ± 19	
CDF II	80433 ± 9	

W boson mass (MeV/c^2)

Fig. 5

SM expectation: $M_W = 80,357 \pm 4_{inputs} \pm 4_{theory}$ (PDG 2020)

LHCb measurement : $M_W = 80,354 \pm 23_{stat} \pm 10_{exp} \pm 17_{theory} \pm 9_{PDF}$ *[JHEP **2022,** 36 (2022)]*

Improvements over 2012 Analysis (Table S1 of Paper)

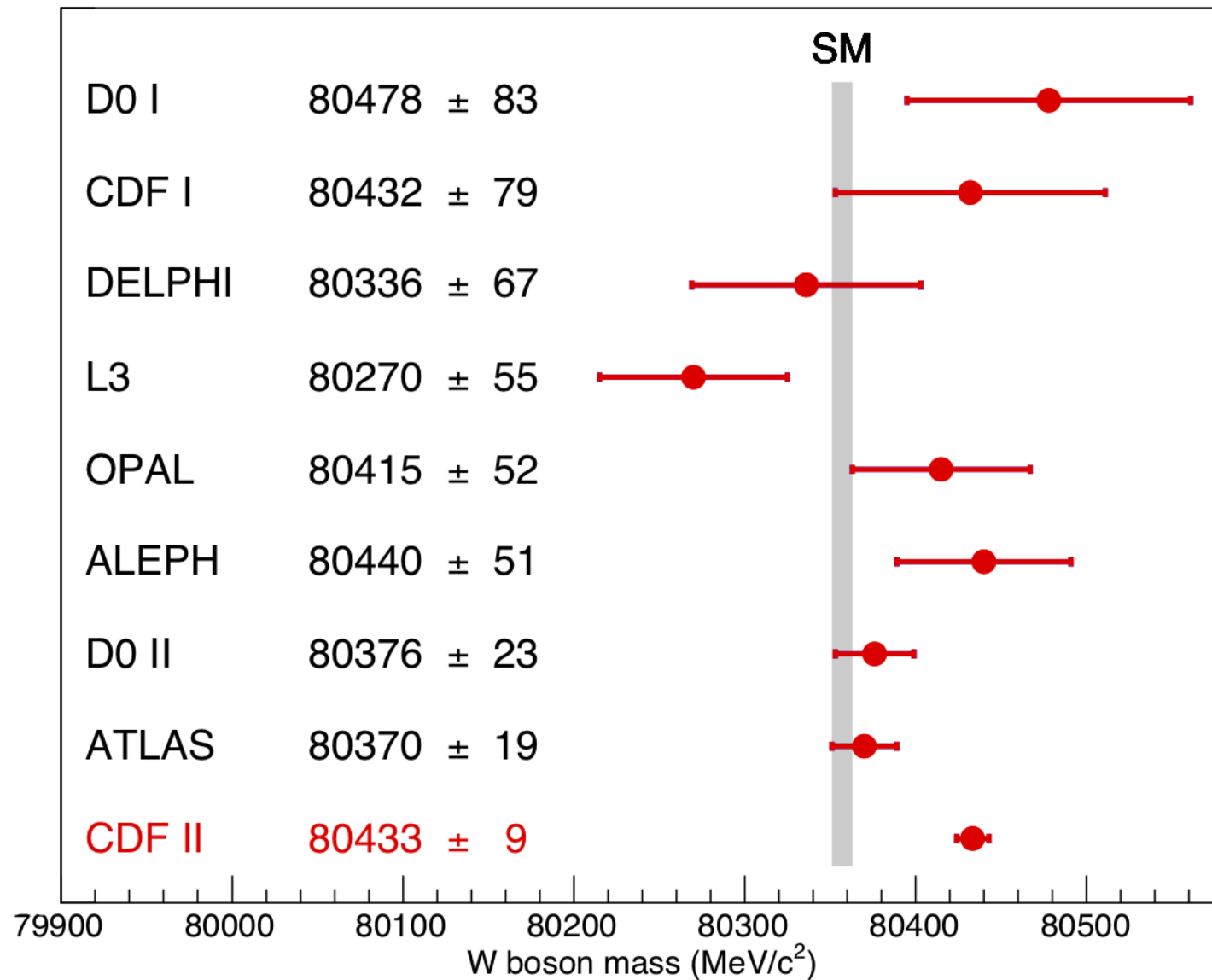| Method or technique	impact	section of paper
Detailed treatment of parton distribution functions	+3.5 MeV	IV A
Resolved beam-constraining bias in CDF reconstruction	+10 MeV	VI C
Improved COT alignment and drift model [65]	uniformity	VI
Improved modeling of calorimeter tower resolution	uniformity	III
Temporal uniformity calibration of CEM towers	uniformity	VII A
Lepton removal procedure corrected for luminosity	uniformity	VIII A
Higher-order calculation of QED radiation in J/ψ and Υ decays	accuracy	VI A & B
Modeling kurtosis of hadronic recoil energy resolution	accuracy	VIII B 2
Improved modeling of hadronic recoil angular resolution	accuracy	VIII B 3
Modeling dijet contribution to recoil resolution	accuracy	VIII B 4
Explicit luminosity matching of pileup	accuracy	VIII B 5
Modeling kurtosis of pileup resolution	accuracy	VIII B 5
Theory model of p_T^W/p_T^Z spectrum ratio	accuracy	IV B
Constraint from p_T^W data spectrum	robustness	VIII B 6
Cross-check of p_T^Z tuning	robustness	IV B

Table S1

Quantified shifts in 2012 result due to updates in PDF and track reconstruction

Improvements over 2012 Analysis

- The statistical precision of the measurement from the four times larger sample is improved by almost a factor of 2

- To achieve a commensurate reduction in systematic uncertainties, a number of analysis improvements have been incorporated

- These improvements are based on using cosmic-ray and collider data in ways not employed previously to improve

  - the COT alignment and drift model and the uniformity of the EM calorimeter response

  - the accuracy and robustness of the detector response and resolution model in the simulation

  - theoretical inputs to the analysis have been updated

- Upon incorporating the improved understanding of PDFs and track reconstruction, our previous measurement is increased by 13.5 MeV to 80,400.5 MeV

  - consistency of the latter with the new measurement is at the percent probability level

Summary

- The *W* boson mass is a very interesting parameter to measure with increasing precision

- New CDF result is twice as precise as previous measurements:

    - $M_W = 80433.5 \pm 6.4_{stat} \pm 6.9_{syst}$ MeV
      $= 80433.5 \pm 9.4$ MeV

- Difference from SM expectation of $M_W = 80,357 \pm 6$ MeV

    - significance of 7.0σ

    - suggests the possibility of improvements to the SM calculation or of extensions to the SM

Thank you for your attention !
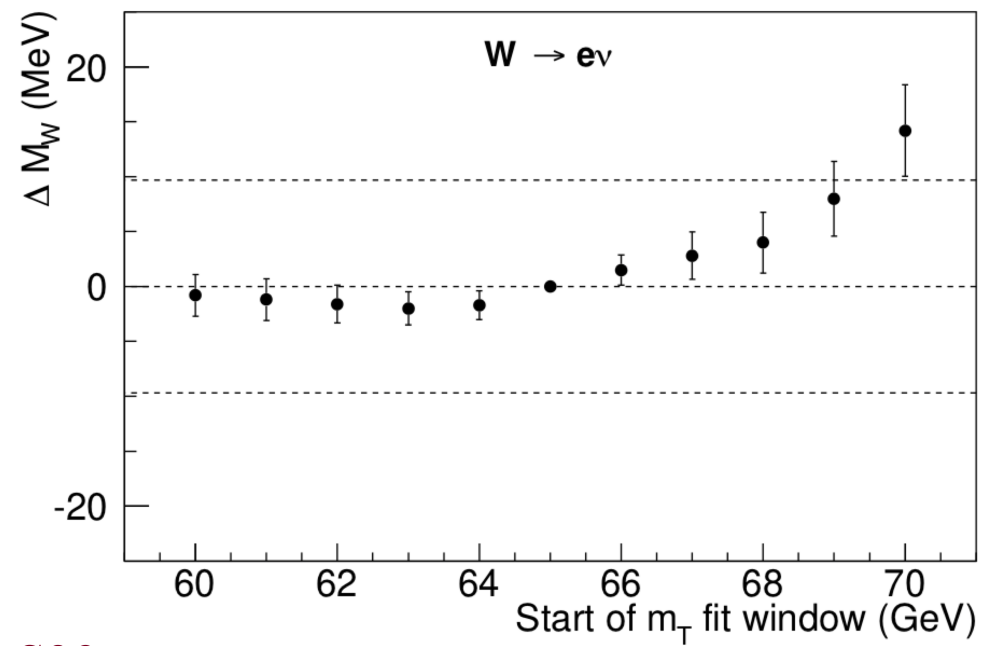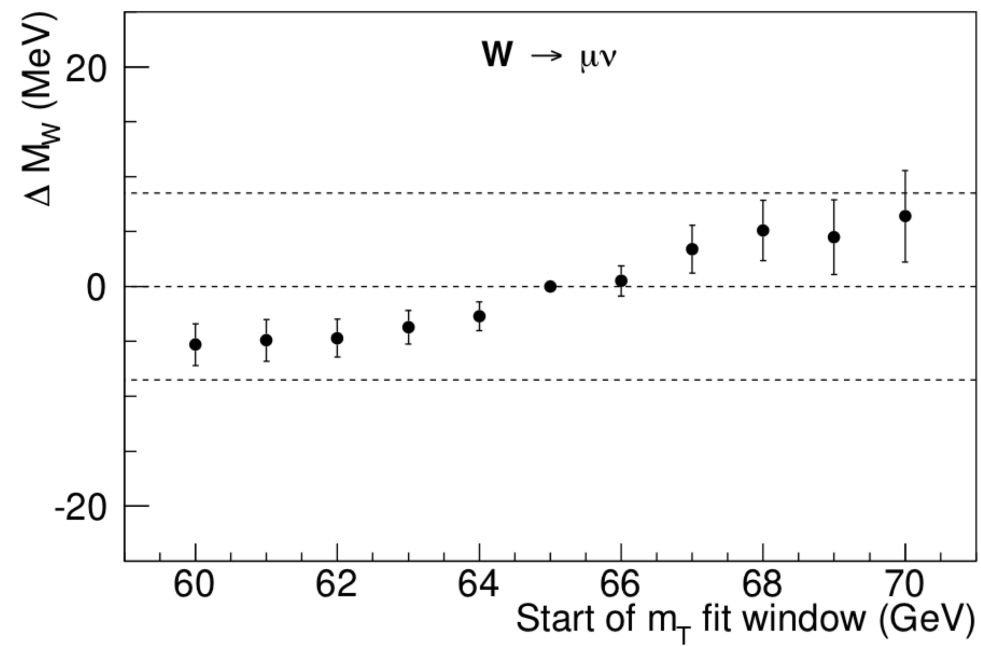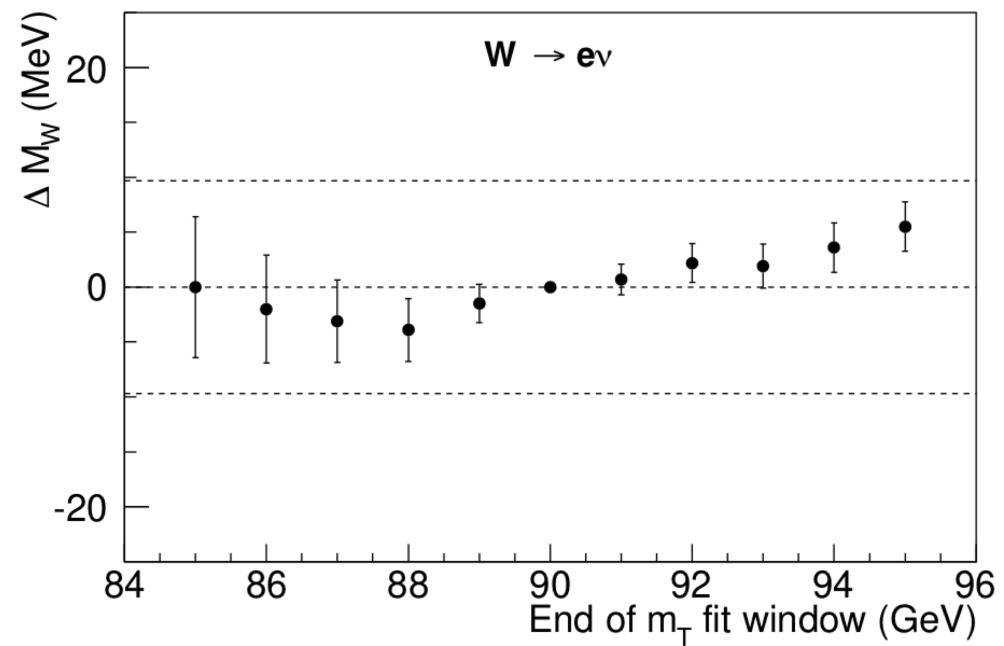
Backup slides
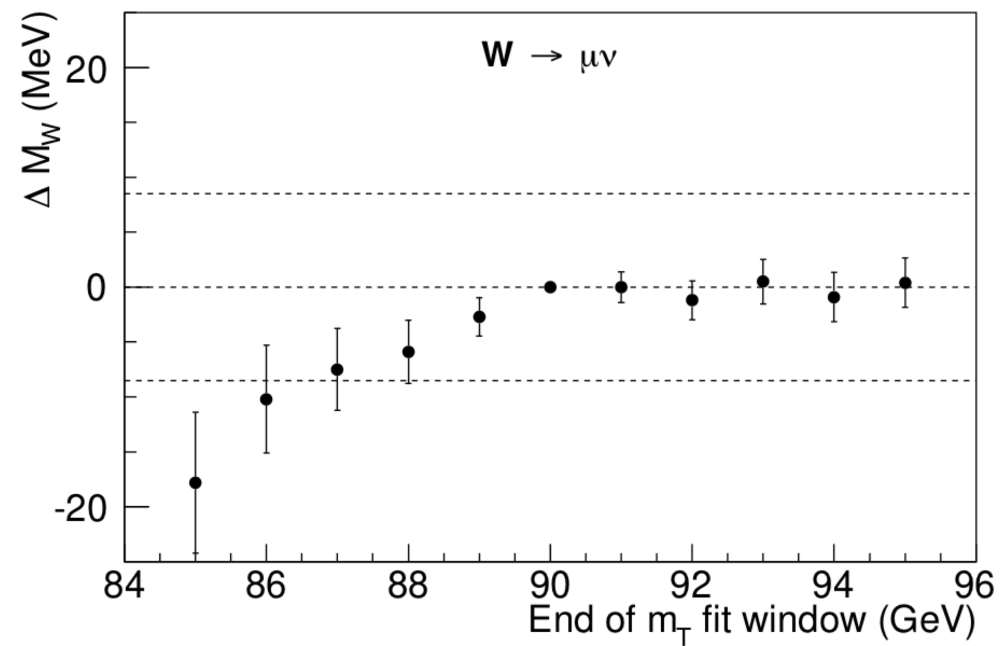
W Mass Fit Window Variation, m~T~ Fit
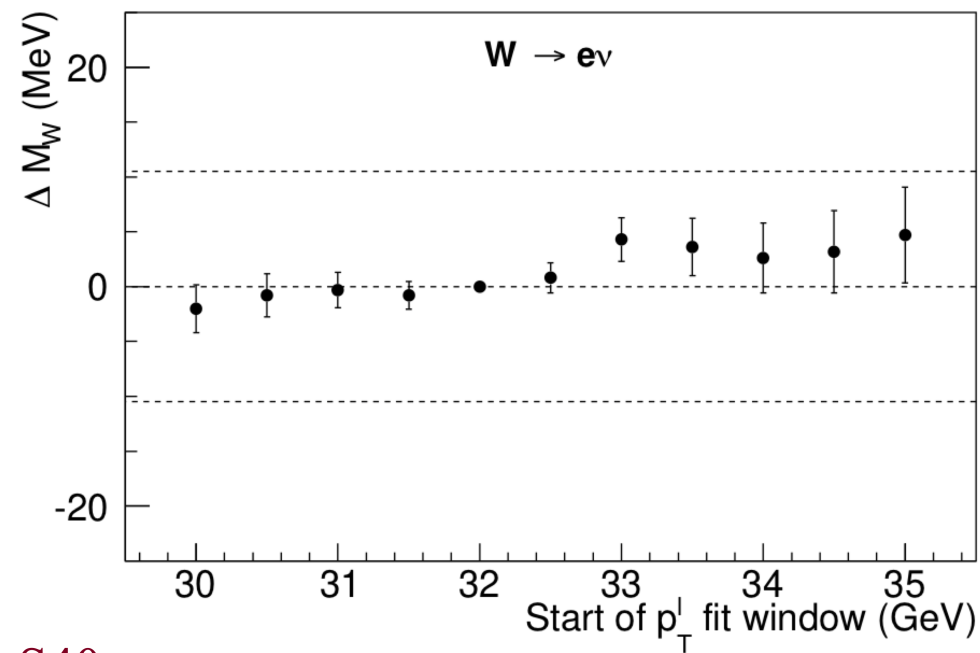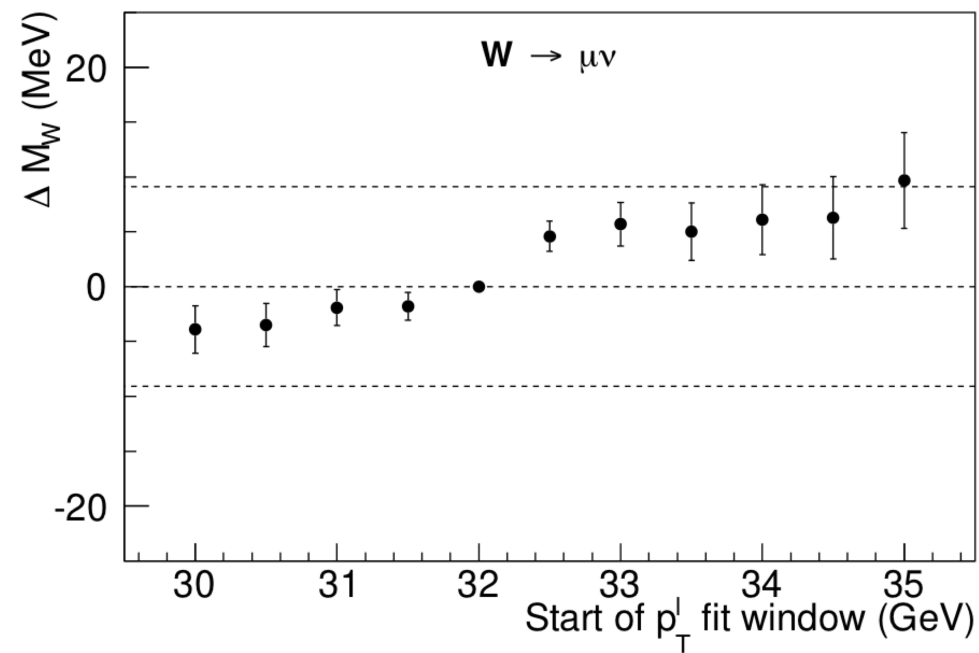

Fig. S39

W Mass Fit Window Variation, p$_T$(l) Fit

Fig. S40
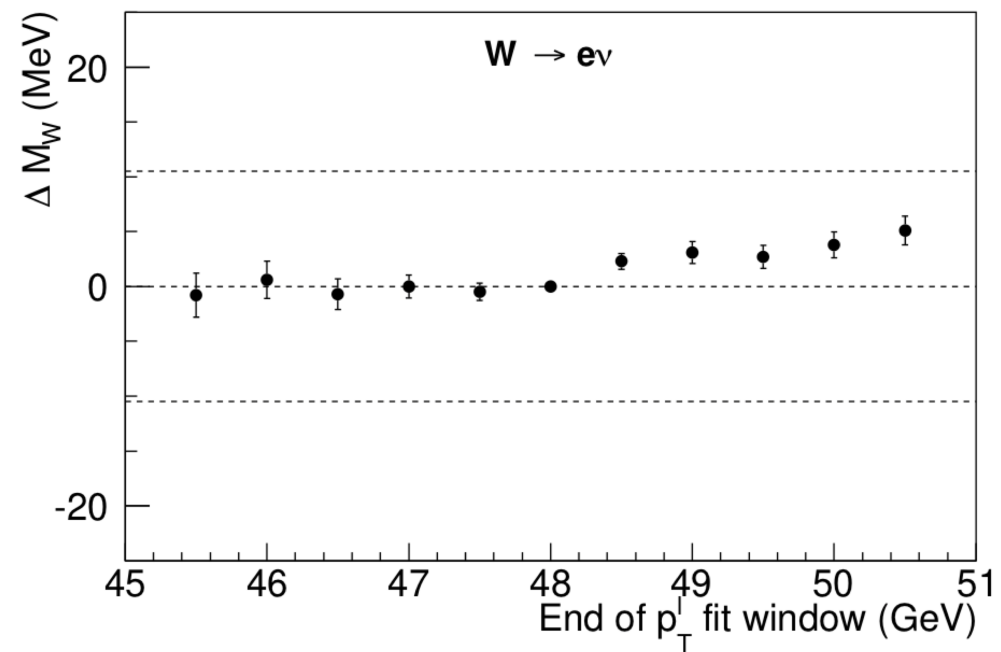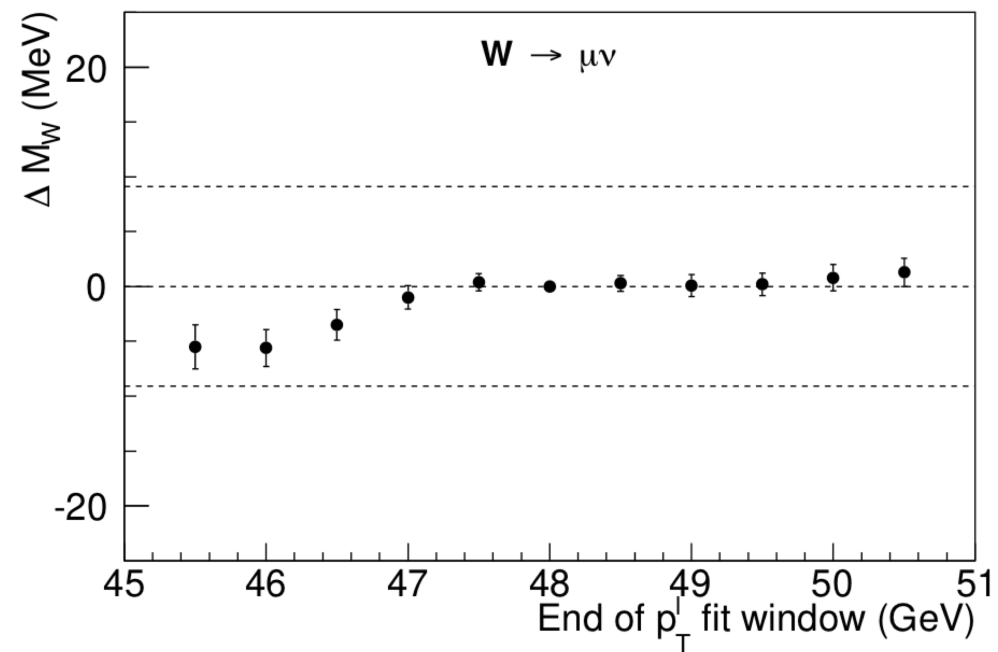
W Mass Fit Window Variation, $p_T(v)$ Fit
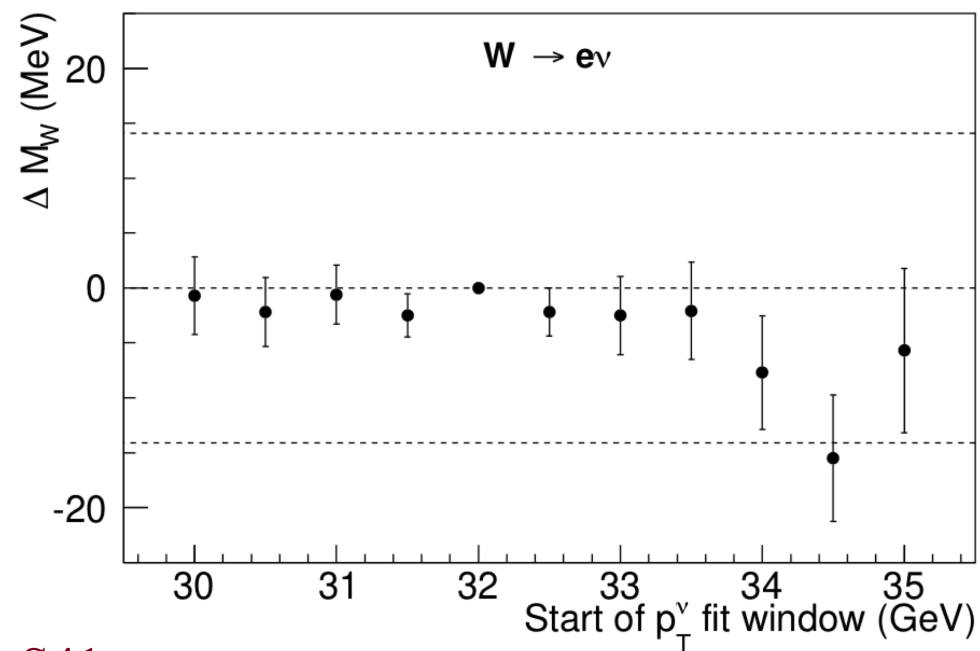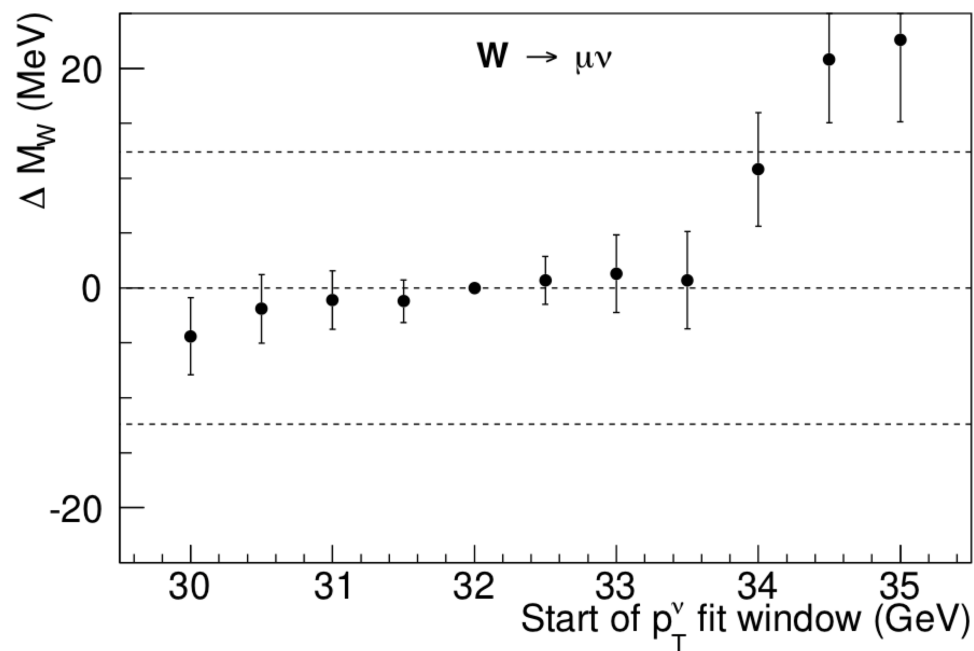
Fig. S41
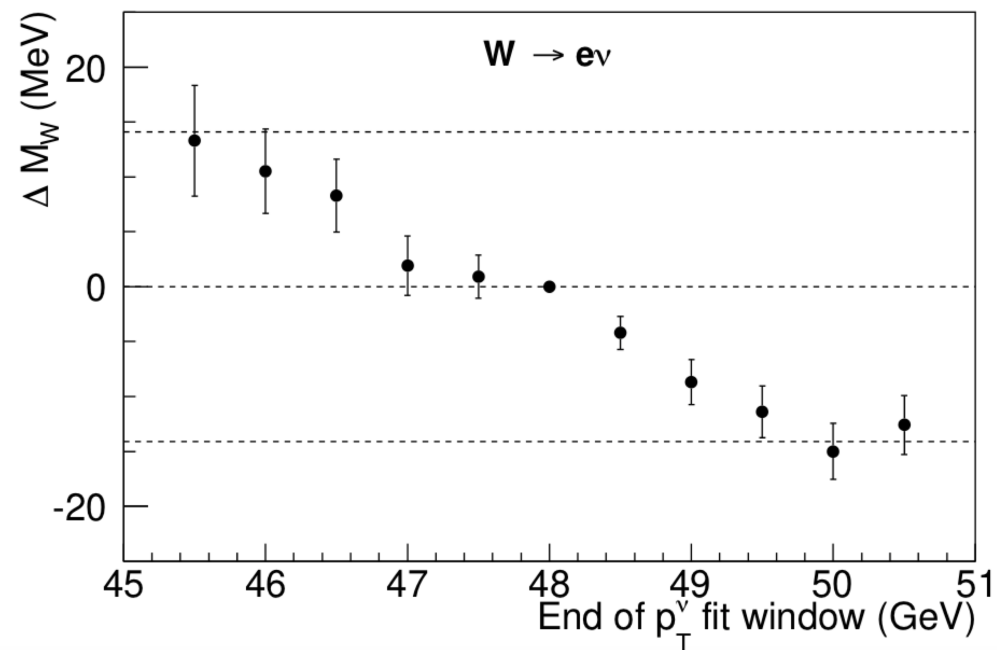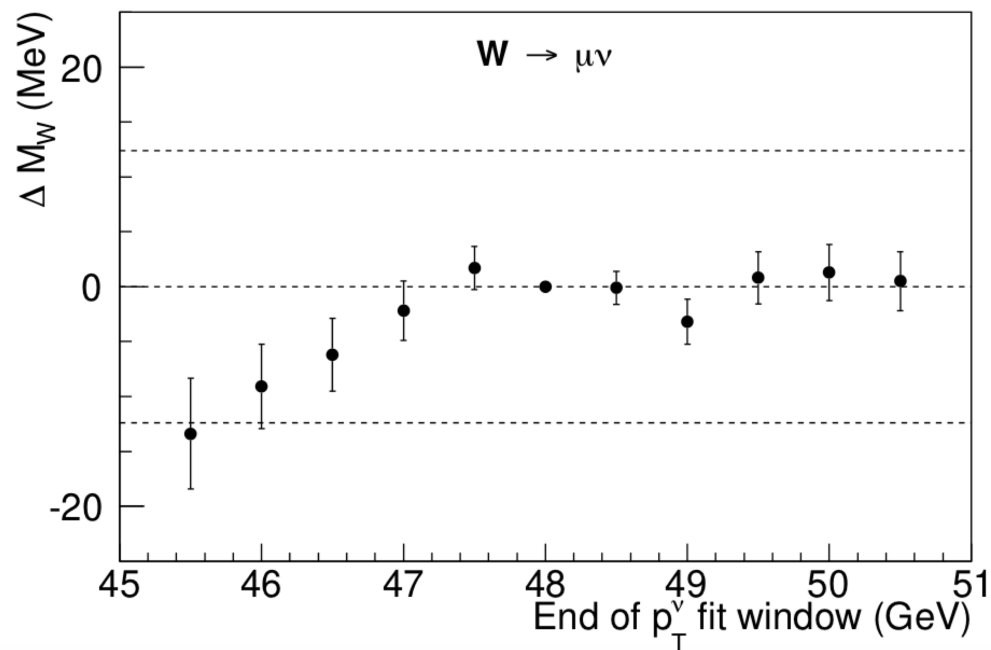
Radiative Corrections to W Boson Mass

All these corrections can be combined into relations among physical observables, e.g.:

$$m_W^2 = m_Z^2 \left[\frac{1}{2} + \frac{1}{2}\sqrt{1 - \frac{2\sqrt{2}\,\pi\alpha}{G_F\, m_Z^2}\,(1+\Delta r)} \right]$$

Δr can be parametrized in terms of two universal corrections and a remainder:

$$\Delta r = \Delta\alpha(m_Z) - \frac{c^2}{s^2}\Delta\rho + \Delta r_{\rm rem}$$

The leading corrections depend quadratically on m_t but only logarithmically on m_H:

$$\Delta\rho = \frac{\Pi_{ZZ}(0)}{m_Z^2} - \frac{\Pi_{WW}(0)}{m_W^2} \approx \frac{3\,\alpha}{16\pi c^2}\left(\frac{m_t^2}{s^2 m_Z^2} + \log\frac{m_H^2}{m_W^2} + \dots \right)$$

$$\frac{\delta m_W^2}{m_W^2} \approx \frac{c^2}{c^2 - s^2}\Delta\rho\,, \qquad \delta\sin^2\theta_{\rm eff} \approx -\frac{c^2 s^2}{c^2 - s^2}\Delta\rho$$

Parameters of Electro-Weak Interactions

At tree level, all of the observables can be expressed in terms of *three* parameters of the SM Lagrangian: v, g, g' or, equivalently, v, e, $s \equiv \sin\theta_W$ (also $c \equiv \cos\theta_W$)

$$\alpha = \frac{e^2}{4\pi}, \qquad G_F = \frac{1}{2\sqrt{2}v^2}, \qquad m_Z = \frac{e\,v}{\sqrt{2}sc}, \qquad m_W = \frac{e\,v}{\sqrt{2}s}, \qquad s_{\text{eff}}^2 = s^2,$$

Radiative corrections to the relations between physical observables and Lagrangian params:

$$m_Z^2 = \frac{e^2 v^2}{2\,s^2 c^2} + \Pi_{ZZ}(m_Z^2)$$

$$m_W^2 = \frac{e^2 v^2}{2\,s^2} + \Pi_{WW}(m_W^2)$$

$$\Pi_{VV}(q^2)$$

$$G_F = \frac{1}{2\sqrt{2}v^2}\left[1 - \frac{\Pi_{WW}(0)}{m_W^2} + \delta_{\text{VB}}\right]$$

Radiative Corrections to Electromagnetic Coupling

$$\alpha = \frac{e^2}{4\pi}\left[1 + \lim_{q^2 \to 0} \frac{\Pi_{\gamma\gamma}(q^2)}{q^2}\right]$$

this one is tricky: the hadronic contribution to $\Pi'_{\gamma\gamma}(0)$ cannot be computed perturbatively

We can however trade it for another experimental observable: $R_{\text{had}}(q^2) = \dfrac{\sigma_{\text{had}}(q^2)}{\sigma_{\ell^+\ell^-}(q^2)}$

$$\alpha(m_Z) = \frac{e^2}{4\pi}\left[1 + \frac{\Pi_{\gamma\gamma}(m_Z)}{m_Z}\right] = \frac{\alpha}{1 - \Delta\alpha(m_Z)}$$

$$\Delta\alpha(m_Z) = \underbrace{\Delta\alpha_\ell(m_Z) + \Delta\alpha_{\text{top}}(m_Z)}_{\text{calculable}} + \Delta\alpha^{(5)}_{\text{had}}(m_Z)$$

$$\Delta\alpha^{(5)}_{\text{had}}(m_Z) = -\frac{m_Z^2}{3\pi}\int_{4m_\pi^2}^{\infty} \frac{R_{\text{had}}(q^2)\,dq^2}{q^2\,(q^2 - m_Z^2)} = 0.02758 \pm 0.00035$$

(This hadronic contribution is one of the biggest sources of uncertainty in EW studies)

Updates to 2012 Result (2.2 fb^{-1})

- Shift from CTEQ6 to NNPDF3.1 PDF used for central value = +3.5 MeV

- In the 2.2 fb^{-1} analysis, an additional systematic uncertainty was quoted to cover an inconsistency between the NBC and BC Y $\rightarrow$ $\mu\mu$ mass fits.

- In this analysis we resolve the inconsistency caused by the beam-constraining procedure, eliminating the additional systematic uncertainty and increasing the measured M$_W$ value by $\approx$ 10 MeV.

- The beam-constraining procedure in the CDF track reconstruction software extrapolates the tracks found in the COT inward to the transverse position of the beamline. This extrapolation can and should take into account the energy loss in the material inside the inner radius of the COT (the beampipe, the silicon vertex detector and its services) to infer and update the track parameters at the beam position before applying the beam constraint.

- This update had been deactivated in the reconstruction software used for the previous analysis. By activating this updating feature of the extrapolator, the flaw in the BC Y $\rightarrow$ $\mu\mu$ mass is corrected, which changes the momentum scale derived from it.

Q & A

Q: Measurement of the W boson mass as a function of running period.

A: Historically, the analysis has been designed as an inclusive analysis. In its current form, measuring the W mass for subsamples of the data requires repeating almost the entire data analysis for each subsample.

For this analysis we invested two years in completely redoing the alignment of the COT, making substantial improvements in both the procedures and the alignment quality metrics, and including dependence on running period (NIM A 762, (2014)).

Compared to the previous analysis, we also invested in improving the uniformity and stability of the EM calorimeter by performing an E/p-based calibration for individual φ-wedges as a function of running period.

However, many aspects of the analysis, including all calibrations related to the hadronic calorimeter and all the backgrounds, cannot yet be performed for subsamples of the data, other than by brute-force repetition. The latter would be a tedious and multi-year process. We plan on improving the functionality of the analysis to handle subsamples, which also improves our understanding of the fundamentals.

Subsample Fit Stability

TABLE S10: Differences (in MeV) between W-mass p_T^ℓ-fit results and Z-mass fit results obtained from subsamples of our data with equal statistics. For the spatial and time dependence of the electron channel fit result, we show the dependence with (without) the corresponding cluster energy calibration using the subsample E/p fit.

Fit difference	Muon channel	Electron channel
$M_W(\ell^+) - M_W(\ell^-)$	$-7.8 \pm 18.5_{\text{stat}} \pm 12.7_{\text{COT}}$	$14.7 \pm 21.3_{\text{stat}} \pm 7.7_{\text{stat}}^{\text{E/p}}$ $(0.4 \pm 21.3_{\text{stat}})$
$M_W(\phi_\ell > 0) - M_W(\phi_\ell < 0)$	$24.4 \pm 18.5_{\text{stat}}$	$9.9 \pm 21.3_{\text{stat}} \pm 7.5_{\text{stat}}^{\text{E/p}}$ $(-0.8 \pm 21.3_{\text{stat}})$
$M_Z(\text{run} > 271100) - M_Z(\text{run} < 271100)$	$5.2 \pm 12.2_{\text{stat}}$	$63.2 \pm 29.9_{\text{stat}} \pm 8.2_{\text{stat}}^{\text{E/p}}$ $(-16.0 \pm 29.9_{\text{stat}})$

$\Upsilon \longrightarrow \mu\mu$ mass fit – stability w.r.t. time and instantaneous luminosity

Table S2. The BC $\Upsilon \to \mu\mu$ sample is divided into two equal size sub-samples to check the stability of the momentum scale versus time and versus instantaneous luminosity. The momentum scales are consistent within the statistical uncertainty; the difference between the later and earlier datasets is $(\frac{\Delta p}{p})_{\text{later}} - (\frac{\Delta p}{p})_{\text{earlier}} = (23 \pm 22_{\text{stat}})$ ppm and the difference between the higher and lower instantaneous-luminosity datasets is $(\frac{\Delta p}{p})_{\text{higher}} - (\frac{\Delta p}{p})_{\text{lower}} = (22 \pm 22_{\text{stat}})$ ppm (the later dataset has a higher average instantaneous luminosity).

- The use of a single ``constant term'' for the EM calorimeter resolution is improved in this analysis by making the constant term a linear function of the absolute value of pseudorapidity. This modification takes into account the observed degradation of the EM calorimeter resolution with pseudorapidity

  - The measured width of the $Z{\to}ee$ peak is found to be consistent with this resolution mode. In the past, there was an inconsistency which had to be resolved by introducing another resolution parameter with an additional systematic uncertainty.

- Uniformity of the COT calibration is significantly enhanced by an alignment of the COT wire-positions using cosmic-ray data. A number of improvements were incorporated in the latest (separately published) alignment procedure compared to the procedure presented in the previous analysis

  - Residual biases that were not resolved in the previous iteration of the alignment were eliminated in this iteration.

- A temporal uniformity calibration of the EM calorimeter is introduced in this analysis. The calorimeter response in each longitudinal tower is studied as functions of experiment operational time, and the time-dependence is corrected for.
  - In the previous analysis the time dependence of the EM response was not studied or corrected for, beyond the standard uniformity calibration applied globally within CDF.

- The procedure of tuning the recoil angular smearing model on the distributions of the azimuthal angle difference between the recoil vector and the dilepton p_T vector in $Z \rightarrow l\,l$ data is a new feature that incorporates additional information from the data compared to the previous analysis.

Description of Analysis Changes since 2012 (Table S1 of Paper)

- The procedure of tuning the kurtosis of the recoil energy resolution on the distributions of p_T-balance in the $Z \to ll$ data is a new feature that incorporates additional information compared to the previous analysis.
  - Higher moments of the recoil resolution (beyond the first two moments) were not considered in past analyses
  - This enhancement of the analysis is incorporated independently for the parallel and the perpendicular components of the recoil.

- As another refinement to the previous analysis, which only considered the first two moments of the fluctuations of energy flow from multiple interactions, we also examine the skewness and excess kurtosis of the fluctuations as functions of $\sqrt{\Sigma E_T}$
  - To better model the resolution function arising from multiple interactions, we include these measurements as functions of $\sqrt{\Sigma E_T}$ in the simulation

- The fluctuations in the energy flow from spectator parton interactions and additional proton-antiproton collisions contribute to the recoil resolution. These fluctuations are measured from zero-bias data; the luminosity profile of these data must be matched to the triggered data
    - In the past, this matching was performed ``by hand'', and a single distribution was used for both the electron and muon channels

- The new procedure for matching the luminosity profiles uses a 2D histogram look-up technique which performs the matching by construction, separately for each channel
    - This automated procedure is more robust than the ``by hand'' matching of the previous analysis

- Confirmed by comparing the data and simulated distributions of $\sqrt{\Sigma E_T}$ for the W and Z boson data in each channel. This comparison was not shown in the previous analysis

- The use of a theoretical calculation of the p_T^W / p_T^Z spectrum ratio to study its QCD scale variation is a new feature of this analysis compared to the previous analysis.
  - We use the **DYqT** program for this purpose.

- The constraint from the p_T^W data spectrum is another new feature that incorporates additional information compared to the previous analysis.
  - In the past, only the p_T^Z data spectrum was used to constrain the production model. In the new analysis we use both spectra.

- Comparisons between the recoil distributions of the W- and Z-boson data and simulation were shown in the past, but the shapes were not compared, only the first two moments were compared.
  - In this analysis we quantify the quality of the shape comparisons and we also compare the values of the first four moments.

M_W from the 2012 Subset of Data using the 2022 Analysis

- The 2022 analysis has been performed for the full dataset and most of the inputs are data-driven (other than PDFs & electroweak radiative corrections)

- All data-driven inputs need to be re-derived for 2012 subset of data. This requires repeating the entire analysis except for the $J/\psi \rightarrow \mu\mu$ and the $\Upsilon \rightarrow \mu\mu$ analysis

- More useful to split the dataset into subsets of equal integrated luminosity and repeat on each subset independently

- Our priority has consistently been to improve the analysis, rather than retracing previous analyses, since the latter is unlikely to yield useful or actionable knowledge

Reduction of systematic uncertainty to 6.9 MeV from 15 MeV

- The lepton and recoil energy scale and resolution uncertainties are data-driven and expected to scale by statistics.
  - The elimination of the inconsistency between the beam-constrained and non-beam-constrained $\Upsilon \rightarrow \mu\mu$ analysis mass fits removed the additional uncertainty.
  - The recoil response and resolution model now extracts more information from the data than in the 2012 analysis

- The uncertainties due to lepton efficiency and lepton removal are data-driven.
  - The improvement in the modeling of the EM calorimeter resolution eliminated an additional source of uncertainty in the 2012 analysis

- The uncertainties due to backgrounds, though data-driven, contain contributions obtained from comparing different methods of background determination - not expected to reduce with statistics

Reduction of systematic uncertainty to 6.9 MeV from 15 MeV

- The systematic uncertainty due to PDFs is reduced by switching from the CTEQ6 set to the much newer NNPDF3.1 set and using the mathematically well-defined ``replica'' method of obtaining uncertainties from the latter set.

- The constraint on the boson p_T spectrum from the p_T^Z data are expected to scale with statistics. The additional constraint from the p_T^W data was not applied in the 2012 analysis and further reduces the current uncertainty

The Future of the M_W Measurement

- The experiments at the LHC have collected and are collecting a lot of data.
  - While W bosons are produced slightly differently at the LHC (*pp* collider) than the Tevatron (*pp̄* collider), the LHC experiments have the opportunity to make this measurement.

- If built, a new electron-positron collider can also measure the W boson mass very precisely.

- The LHC as well as smaller, specialized experiments are sensitive to the kinds of new particles and interactions that can influence the W boson mass.
  - If there is new physics which could explain the tension of our result with the SM expectation, this new physics could show up directly in these experiments.

- CDF has analyzed and published on the full dataset. We have incorporated a lot of new ideas in this round of analysis. If we get more ideas, we will pursue them systematically.